CONSTRAINTS ON THE MAGMATIC EVOLUTION OF THE LOWER MAIN ZONE AND PLATREEF ON THE NORTHERN LIMB OF THE BUSHVELD COMPLEX AS INFERRED FROM THE MOORDKOPJE DRILL CORE.

Frederick Roelofse

A thesis submitted to the Faculty of Science, University of the Witwatersrand, Johannesburg, in fulfillment of the requirements for the degree of Doctor of Philosophy.

Johannesburg, 2010

Declaration

I declare that this thesis is my own, unaided work. It is being submitted for the degree of Doctor of Philosophy in the University of the Witwatersrand, Johannesburg. It has not been submitted for any degree or examination in any other University.

_____
Frederick Roelofse

_____ day of _____ 20____

Dedication

Vir Tiani, Carlyn & Rainhard

ACKNOWLEDGEMENTS

This study would not have been possible if it were not for the generosity showed by the Council for Geoscience in supporting my studies both financially and for allowing me ample time to pursue my research. The culture fostered by the Council for Geoscience (CGS) towards the development of their staff members is highly commendable and it is hoped that this culture will survive despite future changes and challenges affecting the organization. I would in particular like to acknowledge the manager of the Laboratory Unit of the CGS, Dr Thinus Cloete, for his involvement and support of this project, from its inception right to its completion. Prof Lew Ashwal, my research supervisor, is also thanked for his involvement in the project and for suggesting a suitable topic, something that eluded me at the time. Without his support and suggestions, this thesis would not have evolved to the extent that it has.

This thesis would also not have been possible if it were not for Anglo Platinum, who not only allowed access to and sampling of the Moordkopje drill core, but who also contributed generously towards the down-the-hole geophysical measurements conducted by QuikLog Geophysics. Gordon Chunnett is thanked in particular for his assistance in this regard.

Numerous staff members of the CGS assisted with analytical work and if it were not for their contributions, this thesis would undoubtedly have taken significantly longer to complete than it has. Stella Burger and Corlien Cloete are thanked for their assistance with the whole-rock X-Ray Fluorescence analyses, Hilde Maritz for her contributions with respect to the rare-earth element analyses and Leonie Mare for her contributions with respect to the laboratory geophysical property measurements. Annabe Walliser is thanked for her assistance with the microprobe work conducted at the CGS and her patience with an instrument that more often than not was not giving its full co-operation. My thanks also to Dr Jürgen Reinhardt of the University of Kwazulu-Natal for his assistance with the microprobe work conducted there and for his efforts to make my stay in Durban an enjoyable one.

The staff members at the Radiogenic Isotope Facility of the University of Cape Town (UCT) are thanked for their efforts in providing me with “numbers” despite an earlier disappointment. My thanks in this regard go to Prof Anton le Roex, Dr Petrus le Roux, Shireen Govender and Fayrooza Rawoot. The generous financial support towards the work conducted at UCT by the AG Bain Fund of the Geological Society of South Africa is also greatly acknowledged.

Numerous other people have contributed to this study and to my development over the course of the more than half a decade it occupied my thoughts and as such it would be impossible to acknowledge each and every contribution. To these “unknown” contributors, my thanks nevertheless.

To my parents who supported me throughout my life and who allowed me to pursue my various interests without hindrance, I do hope that I have made you proud. Also to my parents-in-law, many thanks for the support that you have given during undoubtedly the most trying time of my life, which just happened to coincide with the time at which I was busy with this study. My thanks also to my brother, Johan and his wife, Joce in this regard.

Particular gratitude also to my wife Tiani, who not only assisted with the X-Ray Diffraction analyses forming part of this study, but who also supported the completion of this work in more ways than can possibly be mentioned. I sincerely hope that our efforts towards the completion of this study would somehow lead to a better life for you, me, Carlyn and Rainhard.

Soli Deo Gloria.

ABSTRACT

This thesis reports the results of a detailed petrographic, geochemical, geophysical and isotopic study of the lower part of the Main Zone, the Platreef and its footwall as exposed by the 1563.02 m deep Moordkopje (MO-1) drill hole situated on the Northern Limb of the Bushveld Complex, where the footwall to the Platreef is granitic. A total of 179 samples were collected as part of the study, with the Main Zone being represented by 156 samples. The Main Zone of the Northern Limb shares a broad similarity with that as known from the Eastern and Western limbs, but differs from the latter in a number of pertinent points. Well-known marker horizons of the Eastern and Western limbs are lacking in the Northern Limb, which hosts an anomalous troctolite layer not known from the other limbs. The lower Main Zone of the Northern Limb shows very limited differentiation as exemplified by paramaters such as the An% of plagioclase, the Mg# of mafic silicates and the modified differentiation index and also lacks the presence of inverted pigeonite, which is locally a major constituent of the Main Zone in the Eastern and Western limbs. The lower Main Zone of the Northern Limb also shows abundant evidence for the decoupling of differentiation trends of plagioclase and pyroxene, a feature that is only locally observed within the main body of the intrusion. Very importantly, the lower Main Zone also exhibits significant isotopic disequilibrium between co-existing plagioclase (Sr_i ~0.708) and orthopyroxene (Sr_i up to ~0.711) in certain samples, a feature that has not been described for the Main Zone as present in the main body of the intrusion.

Many of the features of the lower Main Zone in the Northern Limb may be explained if it was intruded not as repeated influxes of magmas, but instead by the repeated intrusion of crystal mushes from a deep-seated staging chamber. The staging chamber, situated roughly at the boundary between the upper and lower crust, is proposed to have consisted of two sub-compartments connected at depth, with the wall rocks of the sub-compartments differing in terms of their isotopic compositions. Plagioclase crystallized within the staging chamber is deemed to have floated to the tops of the sub-compartments with mafic minerals settling to their bases. As such, magmas entering the Bushveld Complex may host plagioclase derived from the one sub-compartment and mafic silicates

derived from the other. Isotopic models using Vredefort crust suggest that the sub-compartment that contributed mostly plagioclase to the Bushveld Complex may have been contaminated by ~25% of a melt dominated by lower crustal material (70-80%) with a smaller contribution from upper crustal material (20-30%), whereas the sub-compartment from which the mafic silicates were derived, was contaminated by similar amounts of a melt richer in upper crustal material (30-40%) and poorer in lower crustal material (60-70%).

In support of a model whereby the lower Main Zone was formed by the intrusion of crystal mushes rather than by in-situ fractional crystallization, is the fact that the bulk compositions of the cumulates of the Main and Upper zones of the Northern Limb do not appear to be of a suitable composition to allow for the co-crystallization of plagioclase + 2 pyroxenes.

The Platreef as present in the MO-1 drill core consists from top to bottom of about 140 m of orthopyroxene-rich cumulates, followed by a package of hybridized rocks in which interstitial quartz-feldspar intergrowths abound, which is in turn followed by what was termed ‘pyroxene hornfels’ and then the granitic footwall. Comparison of the REE data for Platreef samples along the strike of the Northern Limb allowed for the identification of those Platreef cumulates least affected by footwall interaction, typically being those rocks occurring in the vicinity of the hangingwall contact of the Platreef. Incompatible trace element abundances and ratios suggest a B-1 magmatic lineage for the Platreef, which is supported by the Sr isotopic composition of early formed orthopyroxene within the Platreef (Sr_i ~0.706). Other parameters such as the Nd isotopic composition of orthopyroxene (εNd = -7.8), however, suggest affiliations with the Main Zone, highlighting the need for additional study.

TABLE OF CONTENTS

1. INTRODUCTION

1.1 Necessary background to the Bushveld Complex

The term 'Bushveld Igneous Complex' was coined by Hatch & Corstorphine (1905) to describe the granitic to ultramafic plutonic rocks of the central Transvaal, including the considerably younger and unrelated Pilanesberg Complex. The Complex, which covers an area of nearly 66 000 km^2 (Van der Merwe, 1978), is the largest preserved layered intrusion in the world (Cawthorn, 2005) and occurs in 5 limbs or lobes (Figure 1). The Western Limb occurs as a 200 km long arcuate body with an easterly dip stretching from Thabazimbi in the north to north of Pretoria in the south. The Far Western Limb stretches from the west of the Pilanesberg Complex towards the border of Botswana in the west and consists of two areas underlain by considerable thickness of Bushveld rocks, the first immediately west of Pilanesberg and the second ~60 km further to the west (Biesheuvel, 1970). The Eastern Limb occurs as a 200 km, westerly dipping arcuate body stretching from Chuniespoort in the north to Stoffberg in the south. The Bethal Limb, known only from drill core and geophysical measurements forms the southernmost extension of the Bushveld Complex.

The Northern Limb (Figure 2), also known as the Potgietersrus or Mokopane Limb, part of which forms the focus of this study, follows a north-south oriented sinuous outcrop (Kinnaird et al., 2005), which is partially covered by younger rocks, with outcrop confined to its eastern edge and near Villa Nora. Van der Merwe (1978) describes the Northern Limb as being triangular in outline with a central felsic portion, much of which is covered by the sediments of the Waterberg Supergroup, and an outer layered rim of mafic to ultramafic rocks. The westerly dipping layered succession crops out over a strike length of 110 km (Kinnaird et al., 2005) and is terminated against the Zebediela fault in the south, where it is juxtaposed against basalts of the Karoo Supergroup, and in the north it is covered by Waterberg Supergroup sediments approximately 20 km east of Steilloopbrug. The Villa Nora fragment, which strikes east-west and dips south, outcrops approximately 60 km west of the northernmost visible extension of the main part of the Northern Limb, where it is terminated in the north by the Abbotspoort fault and covered

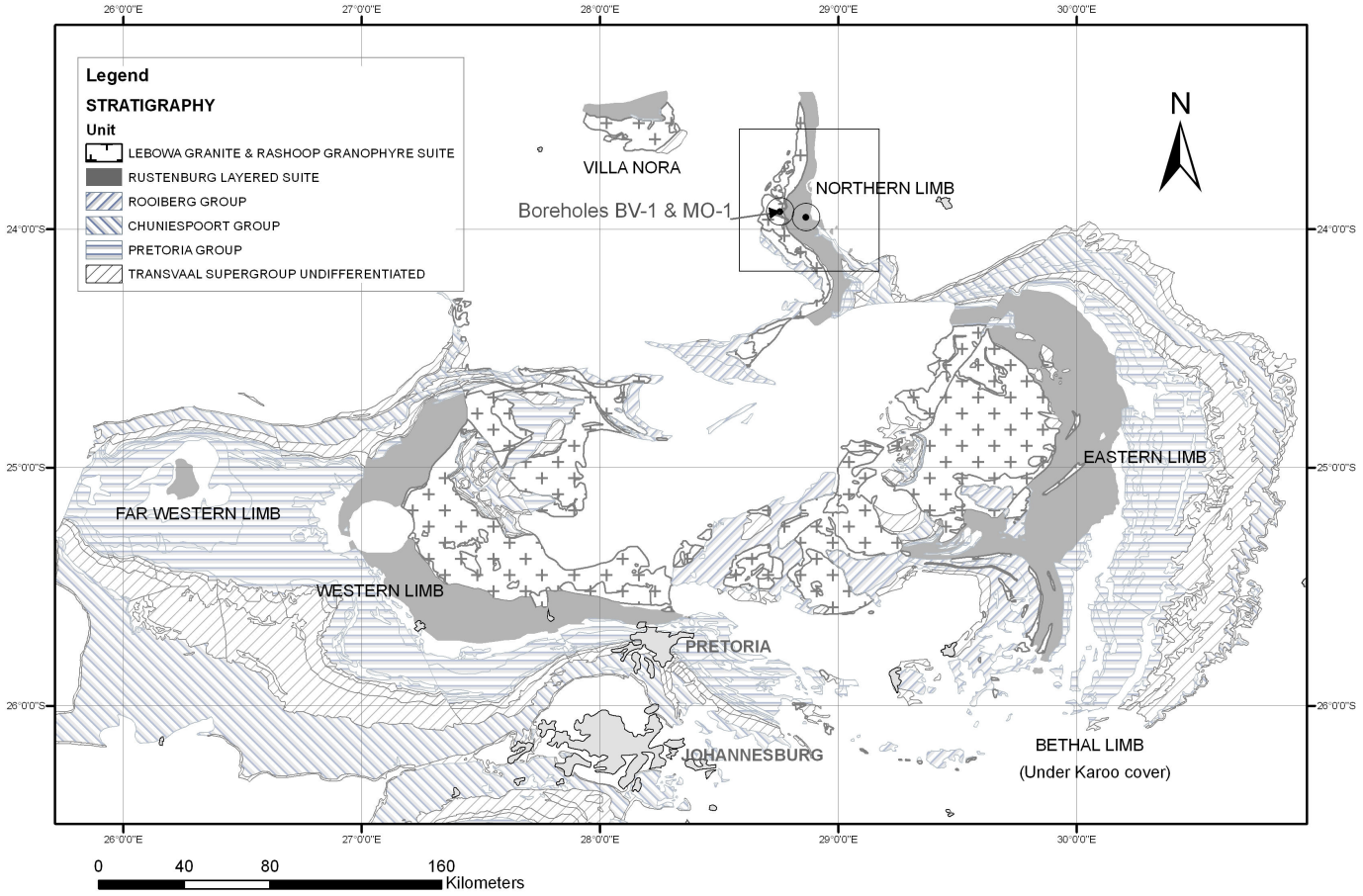

Figure 1: Geological map of the Bushveld Complex showing the locations of the various limbs and the positions of the MO-1 and BV-1 boreholes. Map compiled using geospatial data as supplied by the Council for Geoscience (South Africa).

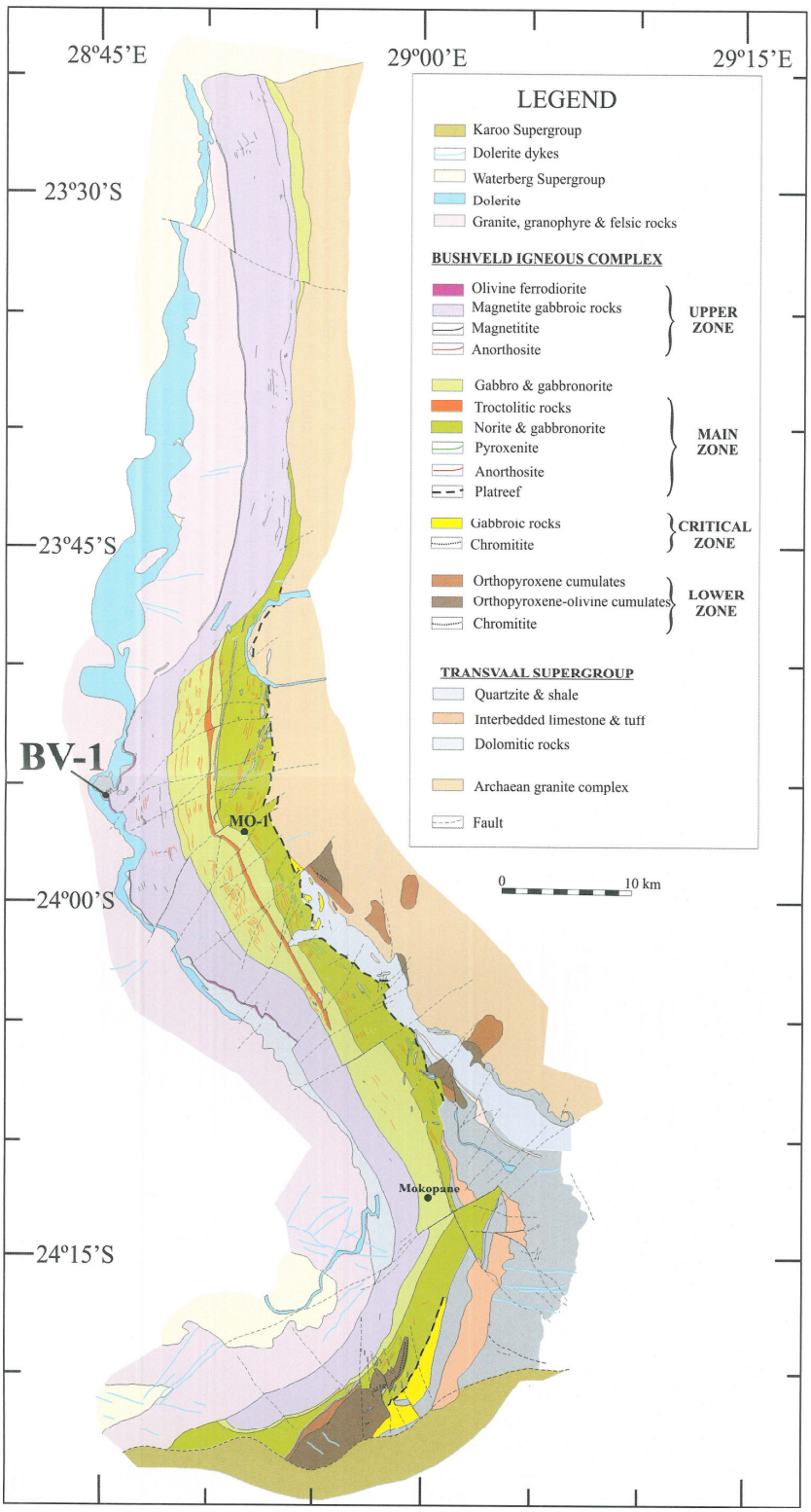

Figure 2: Geological map of the Northern Limb as mapped by Van der Merwe (1976) and as modified by Ashwal et al. (2005), showing the localities of the BV-1 and MO-1 boreholes.

in the south and east by the Waterberg Supergroup and in the west by the Karoo Supergroup (Van der Merwe, 1978).

The layered mafic to ultramafic sequence of the Bushveld Complex, formally known as the Rustenburg Layered Suite (SACS, 1980), has been informally divided into a number of zones, based mainly on the presence or absence of specific cumulus minerals and the positions of specific marker horizons (Hall, 1932; Wager & Brown, 1968; Willemse, 1969), with the exact placement of zone boundaries having been the subject of much debate (e.g. Kruger, 1990). The Lower Zone is composed of an ultramafic sequence dominated by bronzitites and olivine-bearing rocks (Willemse, 1964), with variable amounts of intercumulus plagioclase, clinopyroxene, biotite and chromite (Eales & Cawthorn, 1996). Chromitites are generally absent, except in the Northern Limb (Hulbert, 1983).

The Critical Zone, the host of the economically important Merensky and UG-2 reefs, consists of a lower sequence of pyroxenitic cumulates, followed by a sequence of eight cyclic units with ultramafic bases and anorthositic tops (Eales & Cawthorn, 1996), with the transition between the lower and upper Critical zones being characterized by the first appearance of cumulus plagioclase. In the Northern Limb, only rock types characteristic of the upper Critical Zone are developed (Von Gruenewaldt et al., 1989), termed the 'Grasvally norite-pyroxenite-anorthosite' by Hulbert (1983) and the 'GNPA member' by McDonald et al. (2005). Based on lithological, textural and geochemical evidence, McDonald et al. (2005) showed that the 'Critical Zone' of the Northern Limb cannot be correlated with the Critical Zone elsewhere in the complex and that the magma from which the GNPA member formed possessed Main Zone affinities rather than Critical Zone affinities.

The Main Zone is a succession of gabbroic cumulates, evidently lacking the fine-scale layering and extreme lithological diversity of the Critical Zone, as well as the minerals olivine and chromite (Eales & Cawthorn, 1996), with plagioclase, clinopyroxene and low-Ca pyroxene being cumulus phases (Wager & Brown, 1968). The Main Zone in the

Eastern Limb was divided by Molyneux (1970) into three subzones, A, B and C, from bottom to top, a scheme adopted without alteration by Von Gruenewaldt (1971). The base of the ~1200 m thick subzone A was taken as the Merensky Reef and its top as the Upper Mottled Anorthosite. Subzone B consists of ~1000 m of nearly uniform gabbroic rocks, whereas the 660 m thick subzone C, contains the 2 m thick Pyroxenite Marker at its base and the Mottled Magnetite Anorthosite at its top, the latter coinciding with the abrupt appearance of intercumulus and cumulus magnetite. Wager & Brown (1968) placed the base of the Main Zone approximately 100 m above the well-known platiniferous Merensky Reef, above the so-called 'Bastard Cyclic Unit', which is capped by the 'Giant Mottled Anorthosite', a subdivision also followed by Eales & Cawthorn (1996).

Mitchell (1990), working at Union Section in the northwestern Bushveld Complex on the lower parts of the Main Zone, equivalent to subzones A and B of Molyneux (1970) and Von Gruenewaldt (1971), divided the succession into six units based mainly on variations in the composition of low-calcium pyroxene. He termed the studied succession the lower Main Zone and the succession from the Pyroxenite Marker upwards, the upper Main Zone. Units were interpreted as the products of basal magma influxes, followed by mixing with liquid residua. To prevent confusion, it should be noted that subzone C was earlier assigned by Mitchell (1986) to the Upper Zone, following in the footsteps of Kruger et al. (1987) (Figure 3).

An important and interesting feature of the Main Zone is the phase change from orthopyroxene to pigeonite, which occurs approximately 1200 m above the Merensky Reef in the Roossenekal area. Orthopyroxene occurs as cumulus crystals in the majority of rocks of subzone A, only locally being present as an intercumulus phase. Von Gruenewaldt (1971) terms the intercumulus texture exhibited by the orthopyroxene "ophitic", as the orthopyroxene occurs as large, optically continuous grains enclosing laths of plagioclase. The appearance of pigeonite, now inverted to orthopyroxene, is concomitant with the textural change of orthopyroxene from cumulus crystals to ophitic crystals. The inverted pigeonite occurs enclosed or surrounded by augite as small, irregular grains. Primary orthopyroxene and inverted pigeonite co-exist for a further 1125

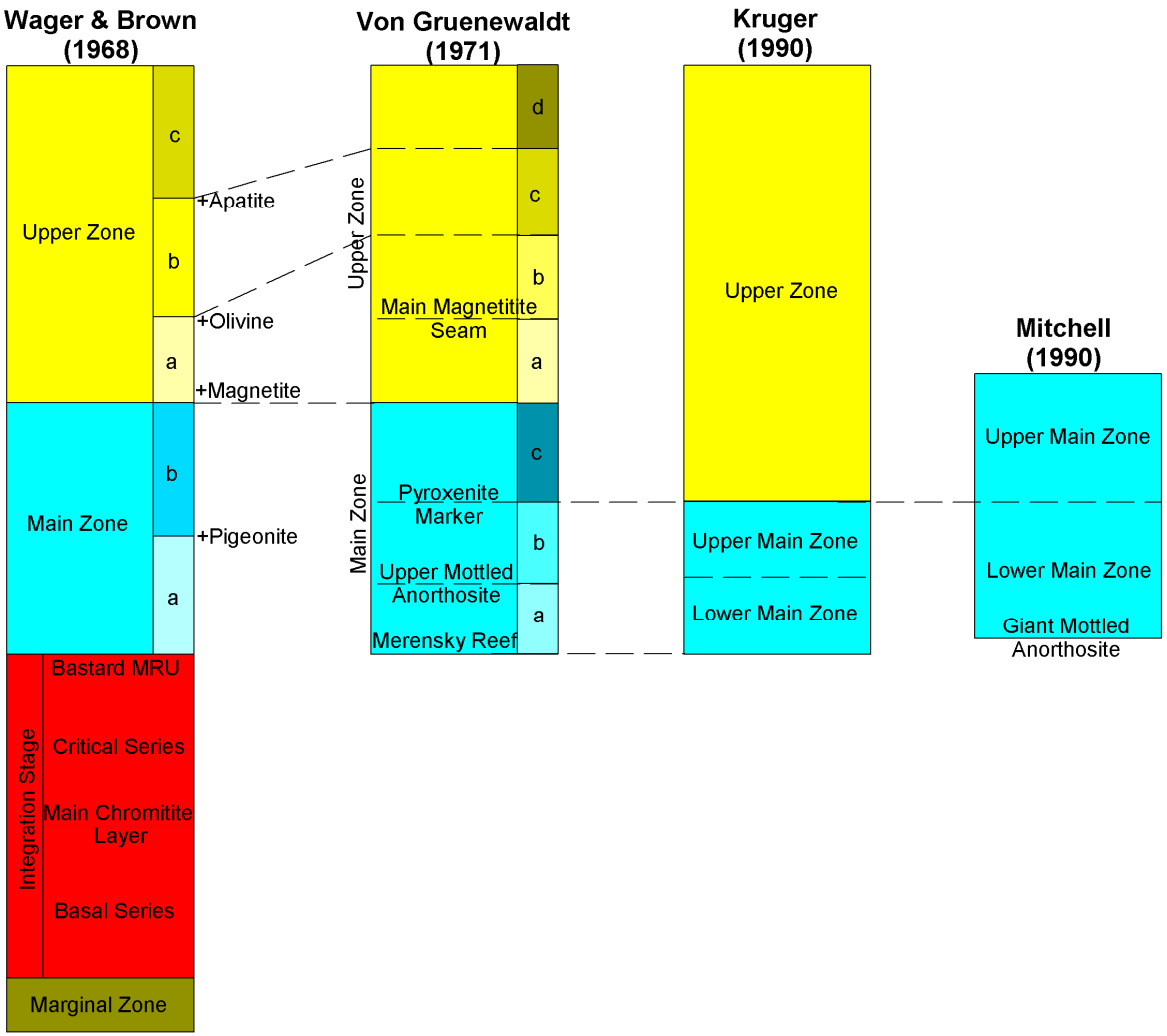

Figure 3: Stratigraphic subdivisions of the Bushveld Complex as suggested by different authors, with special emphasis on the Main Zone.

m after the first appearance of the latter, after which primary orthopyroxene exits the assemblage. At the level of the Pyroxenite Marker, inverted pigeonite makes way again for primary orthopyroxene. The sequence from primary orthopyroxene being the only low-Ca pyroxene, through to the co-existence of both types of low-Ca pyroxenes, to the existence of only inverted pigeonite is repeated in the succession of rocks above the Pyroxenite Marker. Markgraaf (1973) noted a broadly similar trend in the western Bushveld Complex. Of interest also is the presence of iron-rich inverted pigeonite towards the base of the Main Zone, which has been noted both in the Eastern (Von Gruenewaldt, 1971) and Western Limbs (Mitchell, 1990).

Ashwal *et al.* (2005) gives a brief overview of the petrology of the upper parts of the Main Zone pointing out two peculiarities of the Main Zone in the Northern Limb as opposed to the Eastern and Western Limbs. The first is the occurrence of a thick sequence (in excess of ~200 m thick) of troctolitic rocks with mineral compositions indicative of an upper Critical Zone affinity, occurring approximately halfway through the Main Zone, a feature that has also been mapped and described by Van der Merwe (1976, 1978, 1979). The second peculiarity is the apparent absence of the Pyroxenite Marker in the Northern Limb. A 4 m thick pyroxenite occurring ~390 m below the Upper Zone-Main Zone boundary is at approximately the stratigraphic level of the Pyroxenite Marker as present in the Eastern and Western Limbs but is accompanied by the virtual replacement of orthopyroxene with inverted pigeonite as opposed to the replacement of inverted pigeonite by primary orthopyroxene as in the Pyroxenite Marker *sensu stricto.*

The Upper Zone, which does not form part of this study, was divided by Molyneux (1974) into four subzones, three of which, except the basal cycle, consist of troctolite, followed by anorthosite, magnetites and finally relatively homogeneous magnetite gabbro from bottom to top. The basal cycle commences with magnetite anorthosite.

The Platreef is confined to the Northern Limb of the Complex, where it occurs as the basal unit at the eastern edge of the layered succession and comprises texturally heterogeneous and variably altered pyroxenites associated with gabbro, norite and

peridotite (Kinnaird et al, 2005). From south to north the footwall to the Platreef becomes progressively older, starting with the metasedimentary rocks of the Transvaal Supergroup in the south and ending on Archaean granite in the north. The Platreef is divided into three sectors based on footwall lithology: the Southern Sector with a footwall of Transvaal Supergroup shales, banded ironstones, calcsilicates, mudstones and siltstones, the Central Sector where the footwall is dolomite and the Northern Sector where the footwall is Archaean granite (Kinnaird et al, 2005). The question of where the Platreef fits into the zonal stratigraphy of the Bushveld Complex has been the matter of considerable debate and study. Wagner (1973) and White (1994) equated the Platreef to the Merensky Reef as present in the Eastern and Western limbs, whereas Van der Merwe (1976) assigned the Platreef to the base of the Main Zone. Recent work by McDonald et al. (2005) suggests that the Platreef cannot be correlated with the Critical Zone elsewhere, and Holwell et al. (2005) propose that a significant hiatus separated the intrusion of the Platreef and overlying Main Zone. Three-dimensional mapping of the Platreef as exposed in the Zwartfontein South mine by Holwell & Jordaan (2006) also attests to a hiatus between the Platreef and its hangingwall. Detailed Sr and Nd isotopic work by Pronost et al. (2008), however, suggests that the Platreef, its immediate hangingwall and the Merensky Reef share a common origin. For the moment it would appear as if there exist as many theories as to the origin of the Platreef as there are researchers studying it.

1.2 Motivation for the present study

The study by Ashwal et al. (2005) of the Bellevue borehole (BV-1) on the Northern Limb of the Bushveld Complex represents probably the highest density, continuous set of geophysical, petrological and mineralogical measurements made on the Bushveld Complex to date. The ~3 km Bellevue hole, which covers the entire Upper Zone and about half of the Main Zone yielded a number of interesting constraints on the magmatic evolution of the Bushveld Complex. The current study is in essence a continuation of the work by Ashwal et al. (2005) on the stratigraphy not covered by the Bellevue hole, i.e. the lower half of the Main Zone extending down into the Platreef and its footwall on the Northern Sector of the Northern Limb. The MO-1 borehole, a 1563.02 m deep hole drilled on the farm Moordkopje 813LR during late 1979 and early 1980 by Johannesburg

Consolidated Investments (JCI) presented itself as an obvious candidate for the study of the stratigraphic interval below that covered by BV-1.

The study was conceived in order to address a number of important and unresolved issues regarding the stratigraphy and petrogenesis of the Rustenburg Layered Suite. Firstly, the results of the study provides, in conjunction with the data by Ashwal et al. (2005), a near complete stratigraphic profile of the Rustenburg layered suite at a breadth and depth of study not previously attempted. Secondly, the study enables a comparison between the lower Main Zone of the Northern Limb and the Eastern and Western limbs and between the Platreef in the Northern Sector and the Platreef as present elsewhere in the Northern Limb. Thirdly, the study contributes to the current debate as to the origin and petrogenesis of the Platreef. Finally and perhaps most importantly, the study sheds light on the possibility that the bulk of the Main Zone was intruded not as a single influx of magma (Wager & Brown, 1968; Sharpe, 1985; Kruger, 1994) but rather injected in a series of smaller injections as suggested by some authors (Ashwal et al., 2005; Mitchell, 1986) and the mechanism by which said intrusions took place.

1.3 The MO-1 drill core: Geology and sampling

MO-1 is situated on the eastern border of the farm Moordkopje (Latitude 23.9490°S, Longitude 28.86426°E, Elevation 1075.2 m), approximately 11.3 km at a bearing of 103° from borehole BV-1 (Figure 4). Assuming a 17.5° westerly dip for the layered sequence in the vicinity of the borehole in keeping with Ashwal et al. (2005), it can be shown that ~490 m of stratigraphy is left unaccounted for between the bottom of the BV-1 drill core and the top of the MO-1 drill core. MO-1 intersected approximately 1350 m of lower Main Zone rocks, followed by ~200 m of Platreef rocks and ends in a pinkish granite forming the footwall to the Platreef (Figure 5).

The MO-1 drill core (Figure 6) is the property of Anglo Platinum and the core was viewed and sampled at the company's core storage facility in Germiston in December 2004 and January 2005. Initially, detailed re-logging of the core was planned, despite the availability of a relatively detailed core log. Unfortunately, this could not be done due to

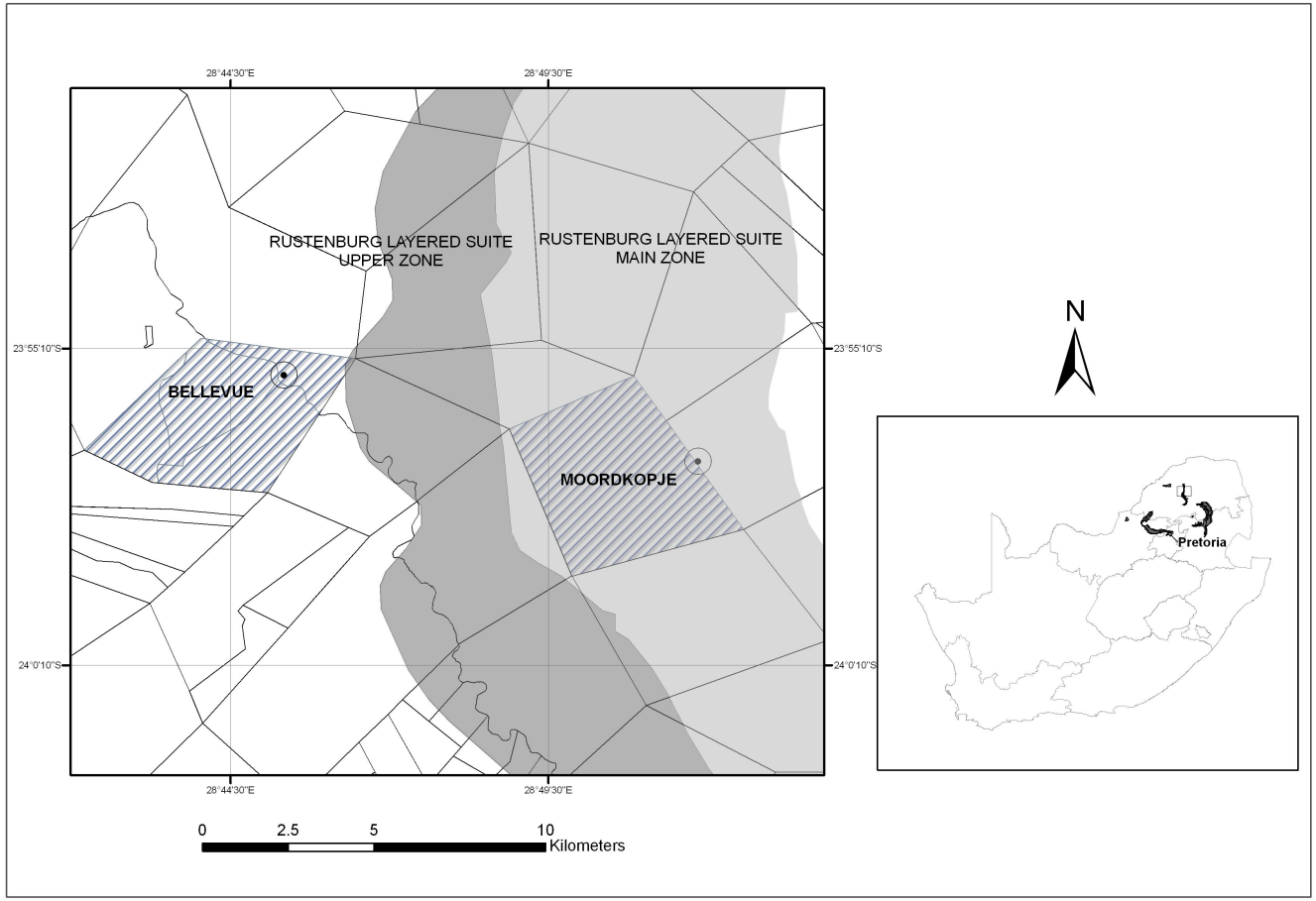

Figure 4: Map showing the localities of boreholes BV-1 and MO-1 relative to the Upper and Main Zones of the Bushveld Complex. Farm boundaries and the Mogalakwena River are also indicated. The inset map shows the distribution of the Rustenburg Layered Suite relative to the study area. Map compiled using geospatial data as supplied by the Council for Geoscience (South Africa).

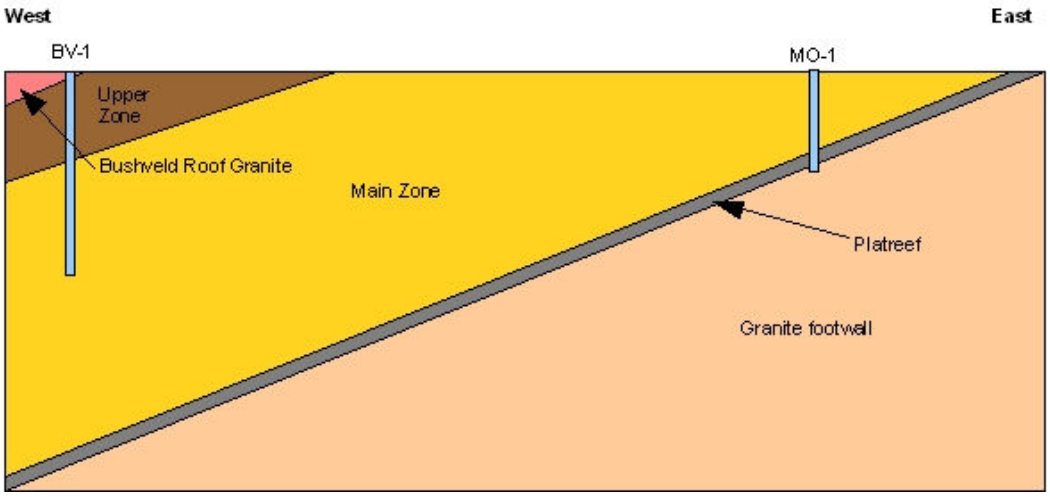

Figure 5: Diagrammatic cross section showing the penetration of the Bellevue (BV-1) and Moordkopje (MO-1) drill holes into the layered rocks of the Bushveld Complex.

Figure 6: The MO-1 drill core laid out at Anglo Platinum's core storage facility in Germiston.

a number of unforeseen circumstances. Somewhere between the date at which the core was drilled and the commencement of this study, the core was transferred from wooden trays into metal trays with the result that some core trays were lost or not properly marked. The use of wooden depth markers, some of which were deteriorated to such an extent that their numbers became illegible also made the task of re-logging nearly impossible. Because of this and the limited amount of time available for study of the core, it was decided to abandon re-logging of the core and to rely on the original core log as supplied by Anglo Platinum (Appendix A). One factor that greatly contributed towards the sorting of the core trays was the presence of portions of core that appeared to have been sampled on a previous occasion and that were successively numbered from the top to the bottom of the core.

I aimed to collect at least one sample from every tray of core, i.e. approximately every 9 m. Because of the limited amount of useable depth markers, taking more than one sample per core tray may have resulted in deeper samples being swapped with shallower samples and *vice versa.* More than one sample per core tray was only taken from trays where it was clear from depth markers how the core was orientated. The sample depths used in this study should therefore not be seen as absolute depths, but successively numbered samples do follow sequentially after one another. Sampling was conducted from the top of the core towards the bottom, using the supplied core log as an aid in determining depths based on prominent features. The last sample taken at the end of hole (EOH) was assigned a depth of 1572.5 m, in comparison to the true EOH of 1563.02 m. This difference constitutes a less than 1% error in depth over the entire core, although locally, sample depths used in this study may differ more from the actual depths in the hole. A total of 179 samples were collected, with 156 representing Main Zone rocks, 21 Platreef rocks and 2 granitic footwall rocks, for an average sampling interval of ~9 m.

All depths reported in this thesis are relative to the Upper Zone – Main Zone boundary calculated from a study of the surface geology and the work of Ashwal et al. (2005), with the depth relative to the Upper Zone – Main Zone boundary being the measured depth in the hole plus 1863.7 m.

2. METHODOLOGY

2.1 Petrography

Polished thin sections were prepared of all 179 samples collected and studied using transmitted light microscopy. The modal mineralogy of the samples was determined by point counting 200 points per sample using a mechanical stage. This method was preferred above the use of visual estimations because of the inherent subjectivity involved with the latter technique. The mineral modes are reported here without estimates as to their precision and accuracy, but conform quite closely to the mineral norms of the samples, suggesting that acceptable accuracy was obtained by counting 200 points. Minerals not encountered during point counting but observed microscopically were assigned concentrations of less than 0.5% by volume. The nomenclature used for the classification of the rocks was as far as possible that proposed by Le Maitre (1989).

The terminology used to describe the textures of the samples may need some clarification. The term 'intergranular' was used to describe the occurrence of discrete crystals of mafic silicates occurring between plagioclase laths. 'Sub-ophitic' was used to describe the texture in which plagioclase laths are partially enclosed by mafic silicates and 'ophitic' to describe the texture where plagioclase laths are entirely enclosed by mafic silicate crystals. 'Poikilitic' was used to describe the enclosure of one mafic silicate by another and 'poikilophitic' to describe the texture where both plagioclase laths and mafic silicate grains are enclosed within another mafic silicate. Von Gruenewaldt (1971) preferred the use of the term 'cumulus' to describe what is called here 'intergranular' but agrees on the usage of the term 'ophitic'. It should be noted that Ashwal et al. (2005) uses the term 'poikilitic' to describe what is here called 'ophitic' texture. Ophitic and sub-ophitic texture usually manifests on a macroscopic scale as mottling.

Severely altered and mineralogically complex samples were analysed by X-Ray Diffraction analysis using a Siemens D500 X-Ray Diffractometer. Powdered portions of the samples were scanned from 2° to 65° 2θ using $Cu_{K\alpha}$ radiation at a speed of 0.02° 2θ per second and generator settings of 35kV and 25mA. Semi-quantitative phase quantification was performed automatically by the evaluation software EVA Diffrac^{Plus}

(Version 10.0.1.0 with PDF-2 Database Sets 1-50) using the I/I_{cor} values for the identified phases.

2.2 Whole-rock major and trace element geochemistry

A portion of every sample collected during the study (n = 179) was crushed and milled using a jaw-crusher and swing mill, respectively. For major element analysis the milled sample was roasted at 1000°C for at least three hours to oxidize ferrous iron and sulfur and to determine the loss on ignition (L.O.I.). Fusion disks were prepared by fusing 2 g of the roasted sample and 8 g '12-22' flux consisting of 35% $LiBO_2$ and 64.71% $Li_2B_4O_7$ at 1050°C in platinum crucibles.

For trace element analysis 12 g of milled sample and 3 g Hoechst wax was mixed and the mixture poured into aluminum cups and pressed into a powder briquette with a hydraulic press at an applied pressure of ~25 ton. The prepared fusion disks and pressed powder briquettes were analysed by wavelength dispersive X-Ray Fluorescence spectrometry using the Council for Geoscience's PANalytical Axios XRF spectrometer equipped with a 4kW Rh-tube.

The accuracy and precision of the XRF analyses were determined by analysis of the NIM-N (SARM 4) norite certified reference material (CRM). Instrumental precision was determined by analysis of the same fusion disk and pressed powder pellet of NIM-N during subsequent analytical batches and repeatability by the analysis of a number of separately prepared NIM-N fusion disks and pressed powders (Table 1). Repeatabilities for the major elements expressed as percentage relative standard deviations (%RSDs) were all less than 10%, except for TiO_2 (%RSD=10.09%). The same is true of the trace elements, except for Cr (%RSD = 48.61%) and Ge (%RSD = 20.42%). Absolute relative errors for the major elements compared to the NIM-N CRM were <5% for all elements analysed, except for TiO_2 (5.91%) and Na_2O (10.25%). Zr had the highest absolute relative error for the trace element suite analysed (29.7%) and Sc the lowest (1.1%).

Table 1: Accuracy, precision and repeatability of the X-Ray Fluorescence analyses.

	1	2	3	4
SiO_2	**52.64**	51.98	0.98	0.06
TiO_2	**0.20**	0.19	10.09	0.44
Al_2O_3	**16.50**	16.08	6.77	0.16
Fe_2O_3	**8.97**	9.23	6.93	0.13
MnO	**0.18**	0.18	9.90	0.73
MgO	**7.50**	7.72	6.08	0.56
CaO	**11.50**	11.76	2.05	0.07
Na_2O	**2.46**	2.21	8.77	1.43
K_2O	**0.25**	0.25	8.47	0.49
P_2O_5	**0.03**	0.02	6.63	3.64
Cr_2O_3	**-**	0.01	9.66	8.96
LOI	**-0.40**	-0.14	-36.14	-
H_2O^-	**0**	-0.21	-359.19	-
As	**0.40**	**<4**	-	-
Ba	**102**	94	6.11	4.00
Bi	**0.011**	**<3**	-	-
Br	**-**	**<2**	-	-
Ce	**6**	**<10**	-	-
Co	**58**	57	1.82	3.46
Cr	**30**	38	48.61	6.41
Cs	**0.22**	**<5**	-	-
Cu	**14**	10	6.02	3.88
Ga	**16**	17	3.63	1.69
Ge	**1.54**	1	20.42	15.75
Hf	**0.38**	**<3**	-	-
La	**3**	**<10**	-	-
Mo	**0.89**	**<2**	-	-
Nb	**-**	**<1**	-	-
Nd	**0.3**	**<10**	-	-
Ni	**120**	106	2.25	0.72
Pb	**2.48**	**<2**	-	-
Rb	**5**	4	4.82	5.80
Sc	**37.4**	37	5.45	1.37
Se	**-**	**<1**	-	-
Sm	**0.8**	**<10**	-	-
Sr	**260**	249	2.42	0.26
Ta	**0.07**	**<2**	-	-
Th	**0.42**	**<3**	-	-
Tl	**0.019**	**<3**	-	-
U	**0.28**	**<2**	-	-
V	**220**	193	2.35	1.08
W	**0.19**	**<3**	-	-
Y	**7**	6	5.75	4.59
Yb	**0.7**	**<2**	-	-
Zn	**68**	53	2.09	1.23
Zr	**14**	10	4.31	3.54

1. Published values for NIM-N CRM (Pots et al., 1992); 2. Average values obtained for the analysis of 7 separately prepared NIM-N fusion disks and pressed powder pellets – where any of the analyses returned values below the detection limits of the respective elements, the detection limits have been given in bold; 3. Percentage relative standard deviations (%RSD) for the analysis of the 7 separately prepared fusion disks and pressed powder pellets of the NIM-N CRM; 4. %RSD for instrumental precision as determined from 9 replicate analyses performed on the same NIM-N fusion disk and pressed powder pellet.

2.3 Whole-rock rare-earth element geochemistry

Seventy-six whole-rock samples were analysed for the REEs by weighing off approximately 0.5 g of milled rock powder and 1.5 g dried lithium meta-tetraborate into Pt-Au crucibles and fusing the contents at 1000°C for approximately 30 minutes. The crucible contents were leached in 10% nitric acid solutions after cooling, whilst being continuously stirred, with total dissolution being achieved after approximately 2 hours. The solutions were then diluted with ultra pure water containing Ir in a 2% nitric acid matrix as internal standard and immediately analysed on a PerkinElmer SCIEX ELAN® 6000 Inductively Coupled Plasma Mass Spectrometer (ICP-MS) instrument equipped with a standard cross-flow nebulizer and a Scott-type Ryton® double-pass spray chamber. As a measure of the accuracy of the technique, the reader is referred to Webb et al. (2006), which reports the results of an international proficiency test in which the REE were analysed using the above technique (participant number T50). Using a k-value of 0.01 (the standard for pure geochemistry laboratories) for the Horwitz function, Z-scores ranged between -0.4 (for Gd) and +3.5 (for La), values between -2.0 and +2.0 being considered an acceptable standard. The Z-scores for all the REE except for La fell within the range of acceptable numbers and apart from La and Ce, all Z-scores were between -1.0 and +1.0.

2.4 Mineral chemistry

The major element compositions of minerals in carbon-coated polished thin sections were determined using JEOL 733 (orthopyroxene, clinopyroxene, olivine and plagioclase down to depth 2115.7 m) and JEOL JXA-8800RL (for the remainder of the plagioclase samples) electron microprobes. The operating parameters and calibration standards used are presented in Table 2 and the crystals and detectors used for the analysis of the various elements in Table 3. On-peak counting time was 10 seconds and 5 seconds at two symmetrical background positions for the analysis of plagioclase and orthopyroxene. For the analysis of olivine and clinopyroxene, on-peak counting times were optimized for the different elements present, whereas off-peak counting times remained at 5 seconds. Unknown element concentrations were determined using correction algorithms as supplied with the instruments. Depending on the abundance of the various minerals in the

Table 2: Operating parameters and calibration standards for electron microprobe analyses. Standards with USNM numbers are described in Jarosewich et al. (1980). AST standards as from AST MINM 25-53 mineral mount (serial #98-050).

	Orthopyroxene	**Plagioclase**	**Plagioclase**	**Clinopyroxene**	**Olivine**
Instrument	JEOL 733	JEOL 733	JEOL 8800	JEOL 733	JEOL 733
Accelerating voltage	15kV	15kV	15kV	15kV	15kV
Beam current	40nA	20-30nA	20nA	40nA	40nA
Beam diameter	2-3µm	3-5µm	5µm	2-3µm	2-3µm
Element	**Calibration standards**				
Si	Hypersthene, Johnstown Meteorite, USNM 746	Anorthoclase, Kakanui, New Zealand, USNM 133868	Plagioclase, AST	Augite, Kakanui, New Zealand USNM 122142	Olivine Fo_{90}, San Carlos, USNM 111312/444
Ti	Rutile, synthetic, Boyd, Carnegie Institution	-	Rutile, AST	Rutile, synthetic, Boyd, Carnegie Institution	Rutile, synthetic, Boyd, Carnegie Institution
Al	Pyrope, Kakanui, New Zealand, USNM 143968	Plagioclase (Labradotite), Lake County, OR, USNM 115900	Plagioclase, AST	Pyrope, Kakanui, New Zealand, USNM 143968	Pyrope, Kakanui, New Zealand, USNM 143968
Cr	Chromite, Tiebaghi Mine, New Caledonia, USNM 117075	-	-	Chromite, Tiebaghi Mine, New Caledonia, USNM 117075	Chromite, Tiebaghi Mine, New Caledonia, USNM 117075
Fe	Hypersthene, Johnstown Meteorite, USNM 746	Hornblende, Kakanui, New Zealand USNM 143965	Magnetite, AST	Pyrope, Kakanui, New Zealand, USNM 143968	Olivine Fo_{90}, San Carlos, USNM 111312/444
Mn	Rhodonite, Boyd, Carnegie Institution	-	-	Rhodonite, Boyd, Carnegie Institution	Rhodonite, Boyd, Carnegie Institution
Mg	Hypersthene, Johnstown Meteorite, USNM 746	Hornblende, Kakanui, New Zealand USNM 143965	-	Augite, Kakanui, New Zealand USNM 122142	Olivine Fo_{90}, San Carlos, USNM 111312/444
Ca	Augite, Kakanui, New Zealand USNM 122142	Plagioclase (Labradotite), Lake County, OR, USNM 115900	Plagioclase, AST	Augite, Kakanui, New Zealand USNM 122142	Pyrope, Kakanui, New Zealand, USNM 143968
Na	Hornblende, Kakanui, New Zealand USNM 143965	Anorthoclase, Kakanui, New Zealand, USNM 133868	Jadeite, AST	Hornblende, Kakanui, New Zealand USNM 143965	-
K	-	Microcline, USNM 143966	Sanidine, AST	-	-
Ni	-	-	-	-	Olivine Fo_{90}, San Carlos, USNM 111312/444

Table 3: Crystals and detectors used for microprobe analysis.

Element	Crystal	Detector
Si	TAP	Gas flow detector
Ti	PET	Xenon counter
Al	TAP	Gas flow detector
Cr	PET	Xenon counter
Fe	LiF	Xenon counter
Mn	LiF	Xenon counter
Mg	TAP	Gas flow detector
Ca	PET	Gas flow detector
Na	TAP	Gas flow detector
K	PET	Gas flow detector

samples, it was aimed to analyse at least 10 spots per mineral per sample, usually on 2 to 3 grains.

Samples from the study by Ashwal et al. (2005) were analysed in addition to the Moordkopje samples in order to assess whether the two datasets were fit for integration (Figures 7 to 9). The plagioclase of seven samples were also analysed on both the JEOL 733 and JEOL 8800 to assess whether the plagioclase data collected on both these instruments were compatible (Figure 10).

Over the range of magnesium numbers (Mg# = molar Mg/(Mg+Fe)) shown in Figure 7 for orthopyroxene, the results of Ashwal et al. (2005) are consistently on the order of ~0.01 higher than that obtained here, the discrepancy increasing with increasing magnesium number. There is, however, strong linear agreement between the results obtained here and those published by Ashwal et al. (2005). Clinopyroxene similarly shows good linear agreement (Figure 8), but the results of Ashwal et al. (2005) are consistently somewhat lower in Mg# (~0.01 to 0.03) than that obtained here, with the discrepancy decreasing with increasing magnesium number. Good linear agreement was also found for plagioclase (Figure 9), with the An%s for Ashwal et al. (2005) consistently on the order of ~3% lower than that obtained here. Plagioclase compositions as determined on the JEOL 733 and JEOL 8800 microprobes, respectively, also showed good agreement in general (Figure 10).

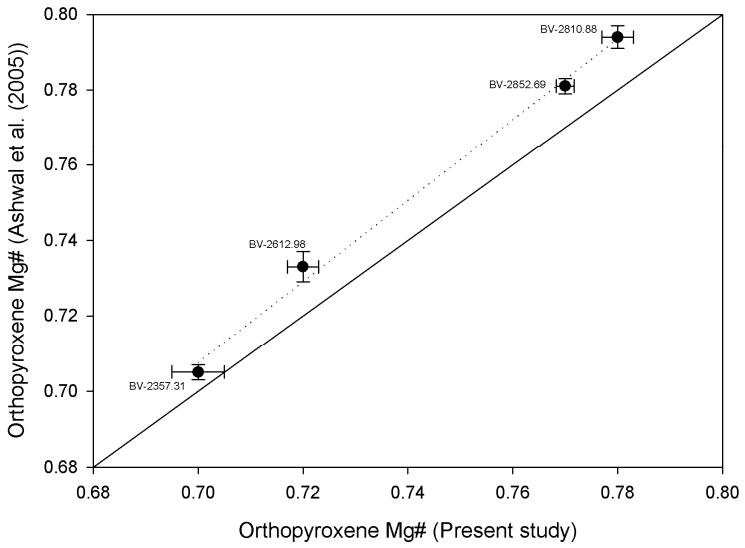

Figure 7: Comparison between orthopyroxene magnesium numbers as obtained by Ashwal et al. (2005) and as obtained during the present study. Numbers adjacent to data points are sample numbers of Ashwal et al. (2005). Error bars show 1-σ standard deviations. Dotted line is a best-fit line and solid line shows 1:1 correspondence.

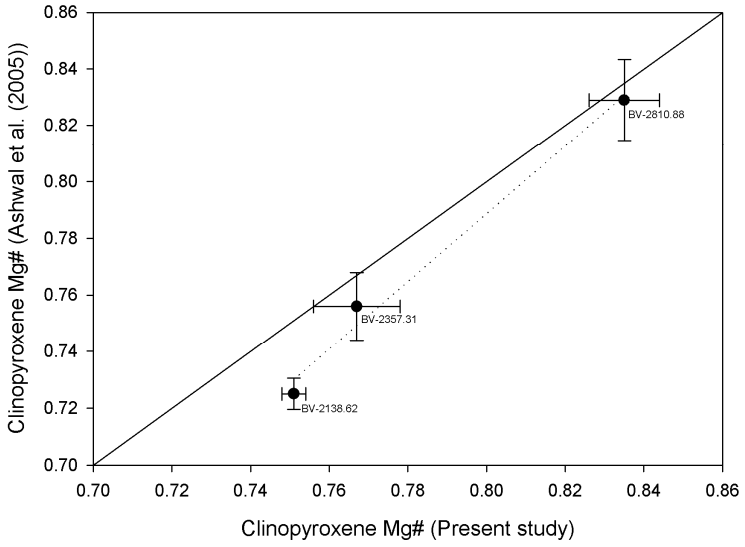

Figure 8: Comparison between clinopyroxene magnesium numbers as obtained by Ashwal et al. (2005) and as obtained during the present study. Numbers adjacent to data points are sample numbers of Ashwal et al. (2005). Error bars show 1-σ standard deviations. Dotted line is a best-fit line and solid line shows 1:1 correspondence.

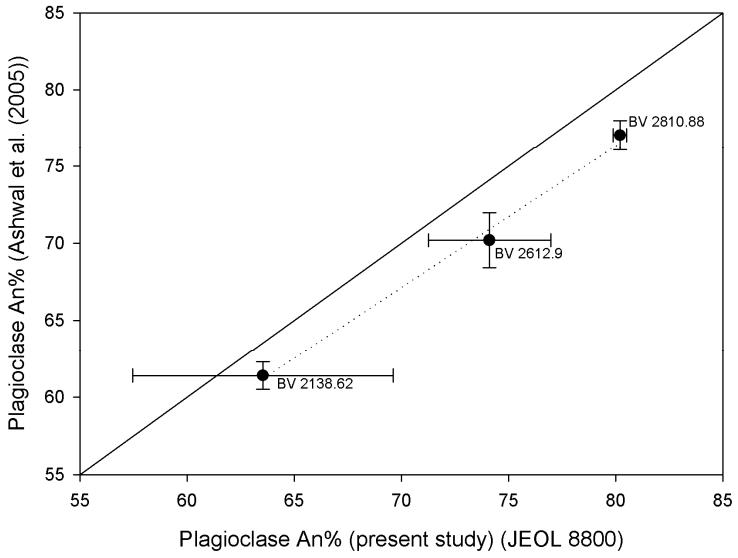

Figure 9: Comparison between plagioclase An% as obtained by Ashwal et al. (2005) and as obtained during the present study. Numbers adjacent to data points are sample numbers of Ashwal et al. (2005). Error bars show 1-σ standard deviations. Dotted line is a best-fit line and solid line shows 1:1 correspondence.

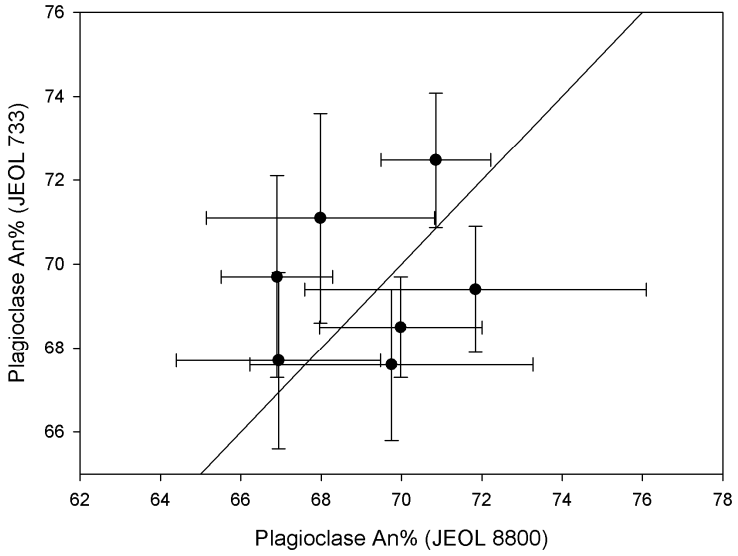

Figure 10: Comparison between plagioclase An% for seven samples as determined on both the JEOL 733 and JEOL 8800 electron microprobes. Error bars show 1-σ standard deviations. Solid line shows 1:1 correspondence.

2.5 Radiogenic isotope geochemistry

Reversals in the Mg# of pyroxene and the An content of plagioclase in the Bushveld Complex are frequently taken as *prima facie* evidence for magma replenishment (Ashwal et al., 2005; Mitchell, 1986). Numerous reversals in the compositions of pyroxene and plagioclase also characterize the Main Zone rocks of the MO-1 drill core, as will be discussed later in this thesis. To elucidate the mechanism(s) responsible for these reversals, the Rb-Sr and Sm-Nd isotopic systems were studied in samples spanning stratigraphic intervals exhibiting reversals in mineral compositions. A total of twelve Main Zone samples from two stratigraphic intervals (2063.66 m to 2212.63 m and 2547.91 m to 2696.44 m) were chosen for this purpose. Three samples from the Platreef were also chosen for isotopic study in an attempt to address the questions highlighted above as to the provenance of the magma or magmas parental to the Platreef.

Prevec et al. (2005) have recently shown the existence of isotopic disequilibrium amongst co-existing minerals from the Merensky Reef, which suggests that caution should be exercised in the interpretation of whole-rock isotopic compositions. For this reason mineral separates were prepared and analysed in addition to whole-rock samples. Whole-rock samples for isotopic study were portions of the same crushed and milled powders used for whole-rock major, trace and rare-earth element analysis by means of XRF and ICP-MS. The preparation of mineral separates involved crushing lengths of drill core using a jaw crusher, followed by screening of the crushed material in order to prepare size fractions suitable for subsequent separation of minerals by hand picking using a stereo microscope. Orthopyroxene, clinopyroxene and plagioclase were picked from the +250-500 μm and +500-1000 μm size fractions, depending on the amount of liberated material present in each of these fractions, with initial preference being given to the coarser grained fraction. Separates were subsequently milled to powders in an agate mortar.

Approximately 100 mg to 200 mg of milled sample was digested in a 4:1 mixture of concentrated HF:HNO_3 in clean Teflon beakers and placed onto a hotplate for ~48 hours. Following complete digestion, the samples were dried down on a hotplate and taken up in

2 ml of concentrated HNO_3, after which the samples were dried down and the process repeated for a second time. Approximately 2 g of 2M HNO_3 was added to the samples, with the mass of the added acid recorded to 5 decimal places. The beakers containing the samples were then transferred into an ultrasonic bath for approximately 20 minutes to allow for the complete dissolution of the sample into the added acid. Approximately 200 μl of the resulting solution was removed from each beaker with the mass of the removed solution accurately recorded, and transferred to clean Teflon beakers. This latter fraction was dried down, taken up in 2 ml of concentrated HNO_3, and dried down again for the subsequent determination of Rb, Sr, Sm and Nd concentrations on a PE SCIEX Elan 6000 ICP-MS (University of Cape Town) following dissolution and dilution with 5% HNO_3 containing an internal standard, with concentrations determined in duplicate for each sample. Total procedural blanks were determined in triplicate with values for Rb, Sr, Nd and Sm less than 5 ng, 123 ng, 7 ng and 2 ng, respectively. The international standard BHVO-2 was analysed with every batch of samples as a measure of the achieved accuracy and precision, the results of which are reported in Table 4.

Table 4: Accuracy and precision of Rb, Sr, Sm and Nd concentration determinations. All values are in ppm.

	BHVO-2 (reference values)	**Batch 1**	**Batch 2**	**Batch 3**
Rb	9.5	9.70±0.03	8.65±0.08	9.5±0.01
Sr	401	405±10.3	364±0.29	403±0.20
Nd	24.4	24.5±0.16	23.3±0.48	24.7±0.06
Sm	5.88	5.94±0.08	5.99±0.13	5.98±0.05

Sr was separated from the solutions remaining after extraction of the aliquots intended for the determination of concentrations using an Eichrome Sr resin bed. Sr fractions were dried down on a hotplate and taken up in 1.5 ml of 0.2% HNO_3, ready for the determination of Sr isotope ratios by MC ICP-MS. The waste fractions were dried down and converted to chloride salts by treatment with 2 ml of 6M HCl, followed by drying

down of the samples. This process was repeated for a second time before dissolving the residues in 1 ml of 0.5M HCl. The extraction of the REEs were achieved using AG50W cation resin (200-400#) columns. REE fractions were then dried down and converted to nitrate by the addition of 2 ml of concentrated HNO_3 followed by drying down of the samples on a hotplate. After repeating this process for a second time, the resultant residues were taken up in 1.75 ml of 0.05M HNO_3 and loaded onto Eichrome Ln resin columns for the collection of Nd. Nd fractions were dried down and taken up in 1.5 ml of 2% HNO_3, ready for the determination of Nd isotope ratios by MC ICP-MS.

Based on the known Sr concentrations of the original samples, 3 ml of 200 ppb Sr solutions were prepared from the Sr fractions using 0.2% HNO_3 and analysed using the NuPlasma HR MC ICP-MS at the University of Cape Town. On-peak background compositions were measured for 120 seconds while aspirating 0.2% HNO_3, with the background measurements, including any Kr present in the argon gas being subtracted from the measured signals. Instrumental mass fractionation was corrected using the exponential law and a fractionation factor based on the measured $^{86}Sr/^{88}Sr$ ratio and the accepted value of 0.1194. A 200 ppb Sr solution of the NIST SRM987 Sr isotope standard was analysed twice prior to any samples and after every fifth sample to assess instrument tuning and stability. The total Sr voltage measured during the analyses of the SRM987 standard and sample solutions varied between 4.3 – 11 V. The external, measured 2σ reproducibility of the SRM987 standard was 0.000025 (n=20) on an average $^{87}Sr/^{86}Sr$ ratio of 0.710265. All $^{87}Sr/^{86}Sr$ data are reported normalized to 0.710255. The average for the stable $^{84}Sr/^{86}Sr$ ratio was 0.05649±0.000016 (n=20), which is in agreement with published values of 0.056482±0.000032 (Waight et al., 2002).

Based on the known Nd concentrations of the original samples, 1.5 ml of 50 ppb Nd solutions were prepared from the Nd fractions using 2% HNO_3 and analysed on the same instrument used for the determination of Sr isotope ratios. Each analysis was preceded by a 30 second background measurement, which was subtracted from the signals measured during subsequent analysis. The measured ^{147}Sm signal intensity, an initial estimated fractionation factor of -2 and the exponential law were used to calculate and subtract the

^{144}Sm contribution on the measured 144 amu signal. Subsequently, instrumental mass fractionation was corrected using the exponential law and a fractionation factor based on the corrected observed ^{146}Nd/^{144}Nd ratio and the accepted value of 0.7219. All Sm interferences on ^{144}Nd, ^{148}Nd and ^{150}Nd, as well as Ce interference on ^{142}Nd, were then corrected using this second-stage fractionation factor and the measured ^{147}Sm and ^{140}Ce signals. A 50 ppb Nd solution of the JNdi-1 Nd isotope standard was analysed twice prior to any samples and after every fifth sample to assess instrument tuning and stability. The total Nd voltage measured during the analysis of the JNdi-1 standard and sample solutions varied between 1.5 – 13 V. The external, measured 2σ reproducibility of the JNdi-1 standard was 0.00029 on an average ^{143}Nd/^{144}Nd ratio of 0.512079. All ^{143}Nd/^{144}Nd data are reported normalized to 0.512115 (Tanaka et al., 2000).

Initial ^{87}Sr/^{86}Sr and ^{143}Nd/^{144}Nd ratios were calculated using decay constants of 1.42 x 10^{-11} y^{-1} (Steiger & Jager, 1977) and 6.54 x 10^{-12} y^{-1} (Begemann et al., 2001), respectively, for an age of 2.06 Ga (Buick et al., 2001).

2.6 Geophysics

The usefulness of geophysical properties such as density and magnetic susceptibility in complementing mineralogical and geochemical data with the aim of reconstructing the magmatic stratigraphy of the Bushveld Complex (and by extension other layered intrusions as well - see for example Maes et al. (2008)) has been strikingly illustrated by Ashwal et al. (2005). For this reason and also because the present study is in essence a continuation of the work by Ashwal et al. (2005) with the view of providing a complete stratigraphic profile of the Rustenburg Layered Suite, QuikLog Geophysics was contracted to conduct down-the-hole geophysical logging of the MO-1 drill hole at a 1 cm sampling interval. Logging tools included amongst others, an Auslog dual density tool with a 150 mCi source and an Auslog magnetic susceptibility tool. The former, also known as a gamma-gamma tool measures the proportion of gamma rays emitted by the source and back-scattered to the detector, which is a measure of the density of the rock mass in the vicinity of the source / detector combination. As such, two different density values were logged: a short spaced density in which the source / detector separation was

short and a long spaced density in which the source / detector separation was larger. For the purposes of this study, the average between the short spaced and long spaced density values were used. Tools were calibrated before and after logging in order to correct for any drift that may have occurred during logging. The density logging tools underwent a base calibration using a series of test jigs of known densities, whereas a two point calibration at 0.5 SI and 4.0 SI was performed for the magnetic susceptibility tool.

Laboratory measurements of magnetic susceptibility values and densities of selected samples were also undertaken for comparison with the values obtained in-situ. Magnetic susceptibilities were measured using a Digico Susceptibility Bridge, in which the change in inductance produced by the system when a sample is inserted into a balanced coil system was measured.

Densities were measured by first recording the mass of a sample on an electronic balance with a sensitivity of 1 mg. A thin copper wire was then tied around the sample and the sample weighed again to determine the mass of the attached wire. The sample was then hooked onto an extension underneath the balance, submerged in water and weighed again. The density was calculated by using the equation $\rho = M / (T - W)$, where M is the mass of the sample, T the mass of the sample and the attached wire and W the mass of the sample and attached wire suspended in water.

3. RESULTS

3.1 Petrography and mineral chemistry

A summary of the petrographic observations including mineral modes, grain sizes and textural information is provided in Appendix B, with the X-Ray Diffraction results for selected samples reported in Appendix C. Compositional data for orthopyroxene, clinopyroxene, plagioclase and olivine are reported in Appendices D-G.

3.1.1 Petrography

3.1.1.1 Main Zone

Of the 156 Main Zone samples studied, nearly half were leucogabbronorites, nearly 30% gabbronorites and approximately 5% anorthosites. Leucocratic varieties of norite and gabbro *sensu strictro* made up ~6% and ~8% of the samples studied, respectively. The Main Zone samples studied exhibit intergranular texture (Figure 11) as the dominant texture, accounting for ~57% of the samples studied. Samples with an ophitic texture account for a further ~36% and those with poikilitic or poikilophitic texture for a further 7% of samples studied. Many of the Main Zone samples studied are texturally heterogeneous, exhibiting different textures in different domains. Ophitic texture is the dominant texture in the more leucocratic gabbroic rocks and anorthosites, with poikilitic and poikilophitic textures found only from ~2415 m downwards and becoming relatively common from ~2865 m downwards and in the vicinity of the Platreef. Down to a depth of ~2560 m, the bulk of the samples (~70%) exhibit intergranular texture, with the exception of plagioclase-rich rocks that typically exhibit ophitic texture. Ophitic texture is the dominant texture in Main Zone rocks from a depth of ~2560 m down to the Platreef.

Plagioclase is an omnipresent phase in the Main Zone, modally constituting between 27% and 97% of individual Main Zone samples. It occurs as abundantly twinned laths, in many of the samples showing preferred orientation, which can probably best be described as igneous lamination. Plagioclase laths orientated parallel to the layering is especially abundant towards the top of the core. Obviously zoned plagioclase was encountered only in the immediate hanging wall to the Platreef (Figure 12). A ubiquitous feature of plagioclase in both the Main Zone and the Platreef is its alteration to a fine-grained,

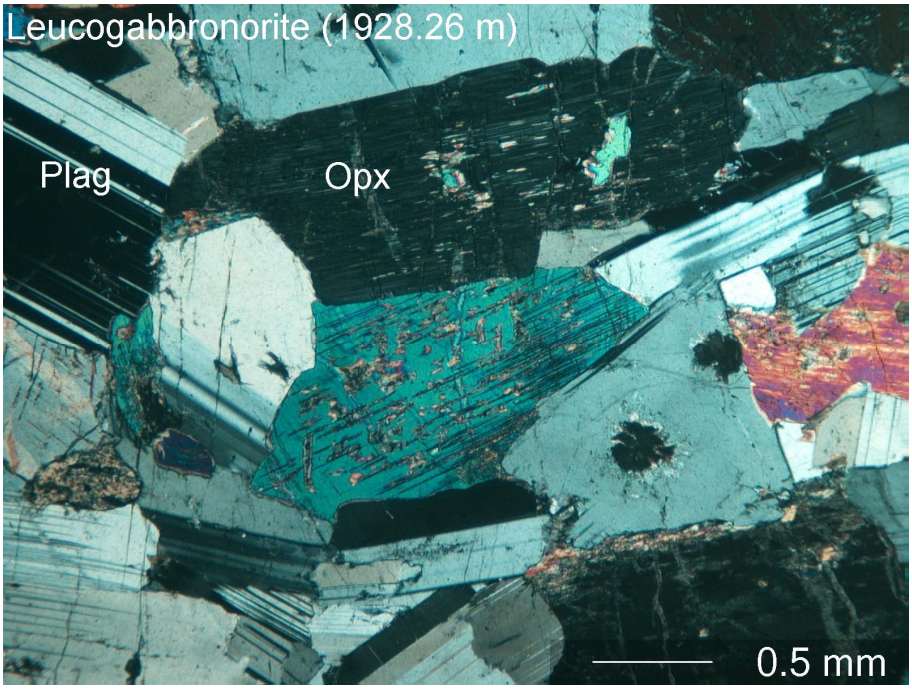

Figure 11: Photomicrograph of leucogabbronorite from a depth of 1928.26 m under cross polarized light, exhibiting intergranular texture.

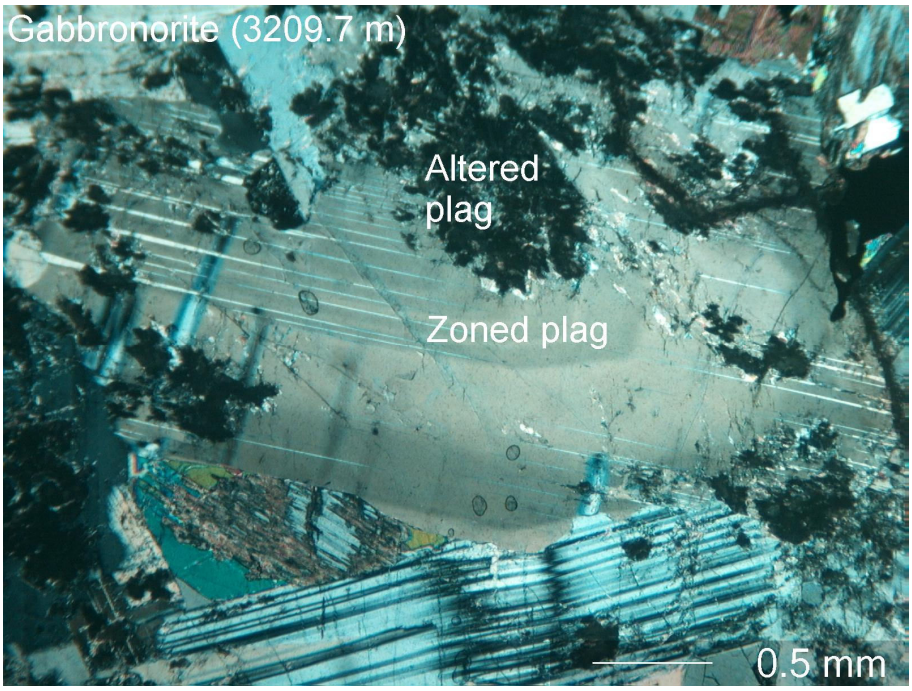

Figure 12: Zoned plagioclase in the hanging wall to the Platreef. Photomicrograph under cross polarized light of gabbronorite from depth 3209.7 m. Note also the fairly abundant patches of altered plagioclase.

murky substance appearing brown in plane polarized light and nearly isotropic in cross polarized light, which is probably a mixture of secondary minerals including epidote, smectite, chlorite and amphibole (Roelofse & Ashwal, 2008).

This alteration is confined mainly to patches in the plagioclase of the Main Zone, but in the Platreef, plagioclase has generally been altered to such an extent that very little to no features of the original plagioclase could be observed. The amount of altered plagioclase for the uppermost 1000 m of the Main Zone studied averages ~1.3% and then gradually increases to ~12% in the immediate hanging wall to the Platreef. Wedge-shaped and bent plagioclase twin lamellae are present in many of the samples studied (Figure 13), the latter feature interpreted by Von Gruenewaldt (1971) as indicative of deformation after deposition. In some samples, plagioclase growth appears to have been arrested by the simultaneous crystallization of pyroxene, with the result that plagioclase chadacrysts are finer grained than unenclosed plagioclase crystals (Figure 14). Plagioclase grain sizes in the samples studied vary from ~2 mm up to ~7 mm, as measured on the coarsest grain present in every sample, with no obvious trends being observed for the grain size data.

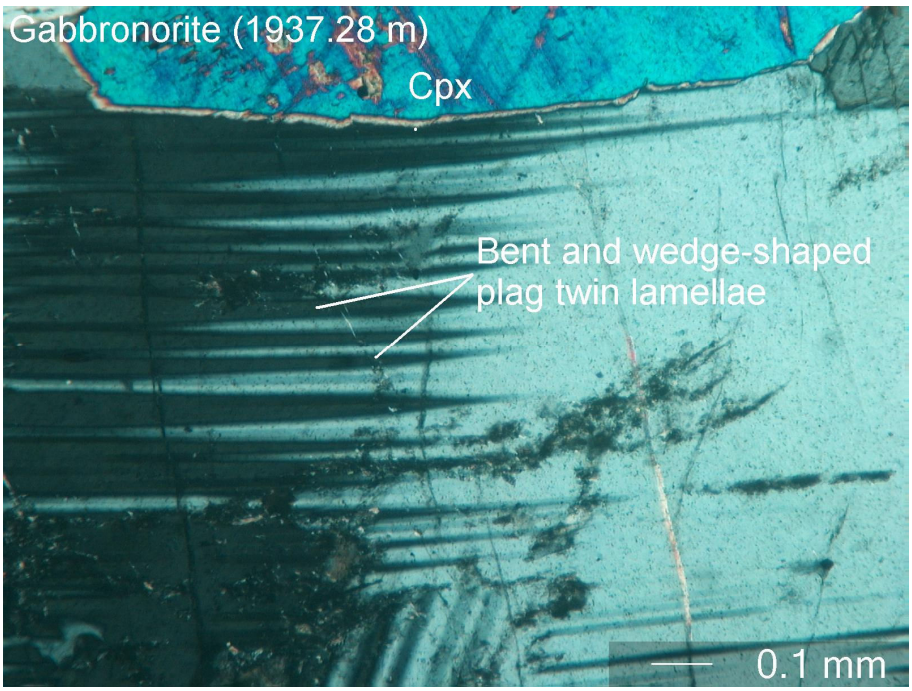

Figure 13: Bent and wedge-shaped twin lamellae in plagioclase in gabbronorite from depth 1937.28 m. Note also the altered wisps of plagioclase occurring especially towards the right of the image. Photomicrograph under cross polarized light.

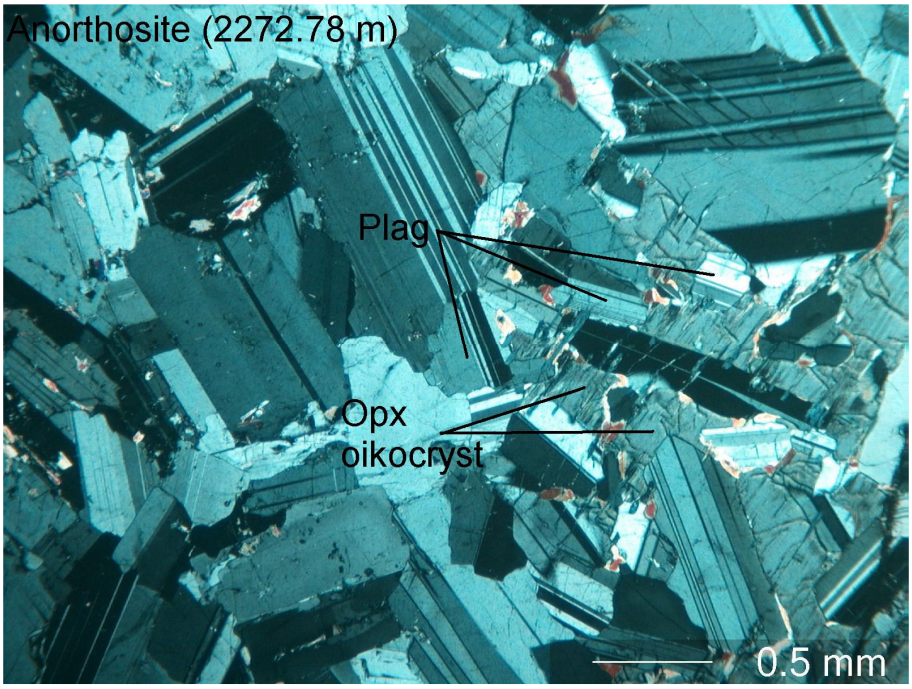

Figure 14: Photomicrograph under cross polarized light showing relatively coarse grained, unenclosed plagioclase laths on the left and finer grained plagioclase chadacrysts enclosed by an orthopyroxene oikocryst on the right. Anorthosite from depth 2272.78 m.

Orthopyroxene modally constitutes between 0% and 45% of the Main Zone samples studied and occurs as subhedral to anhedral grains throughout most of the Main Zone and normally contains an abundance of thin and closely spaced augite exsolution lamellae (Figure 15). Orthopyroxene also occurs as optically continuous oikocrysts enclosing plagioclase laths and very rarely also augite (Figure 16). In a number of samples, orthopyroxene also occurs as rims on plagioclase chadacrysts enclosed by augite oikocrysts (Figure 17). Orthopyroxene containing thick augite exsolution lamellae (Figure 18) was encountered in only three Main Zone samples, from depths 1973.29 m and 3128.7 m (both leucogabbros) and from depth 3215.7 m (leuconorite). The presence of thick augite exsolution lamellae in orthopyroxene was taken as indicative of inverted pigeonite (see Poldervaart & Hess, 1951).

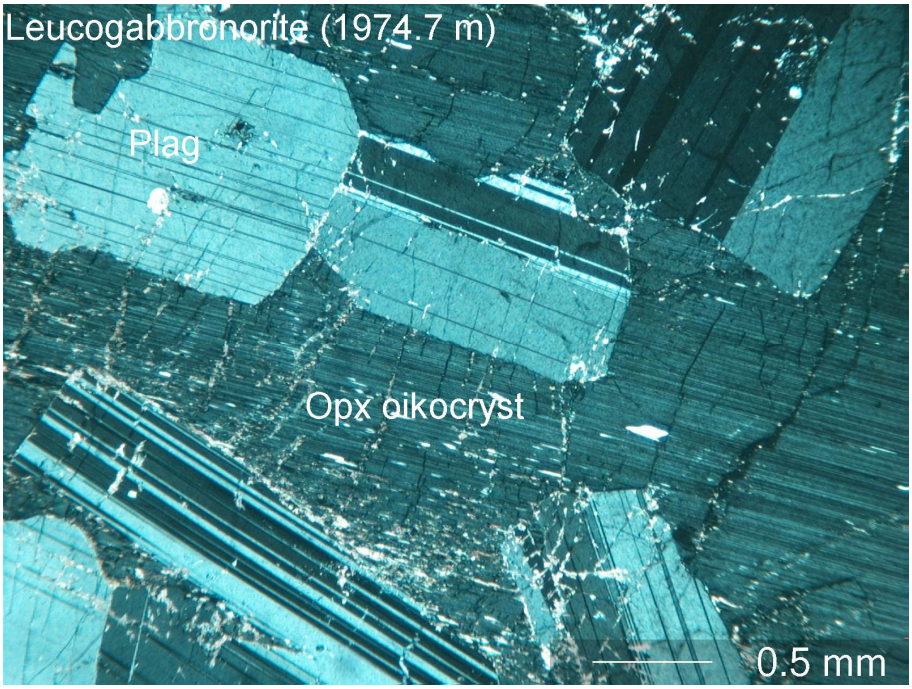

Figure 15: Orthopyroxene oikocryst with thin and closely spaced augite exsolution lamellae ophitically enclosing plagioclase crystals. Photomicrograph under cross polarized light of leucogabbronorite from depth 1974.7 m.

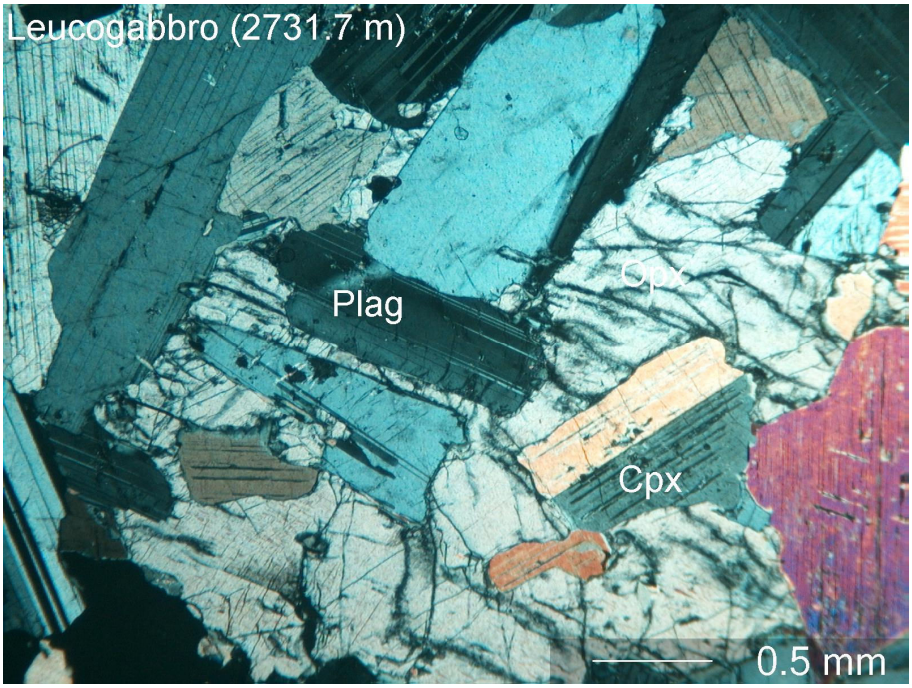

Figure 16: Plagioclase and twinned augite crystals enclosed by orthopyroxene oikocryst. Photomicrograph under cross polarized light of leucogabbro taken at depth of 2731.7 m.

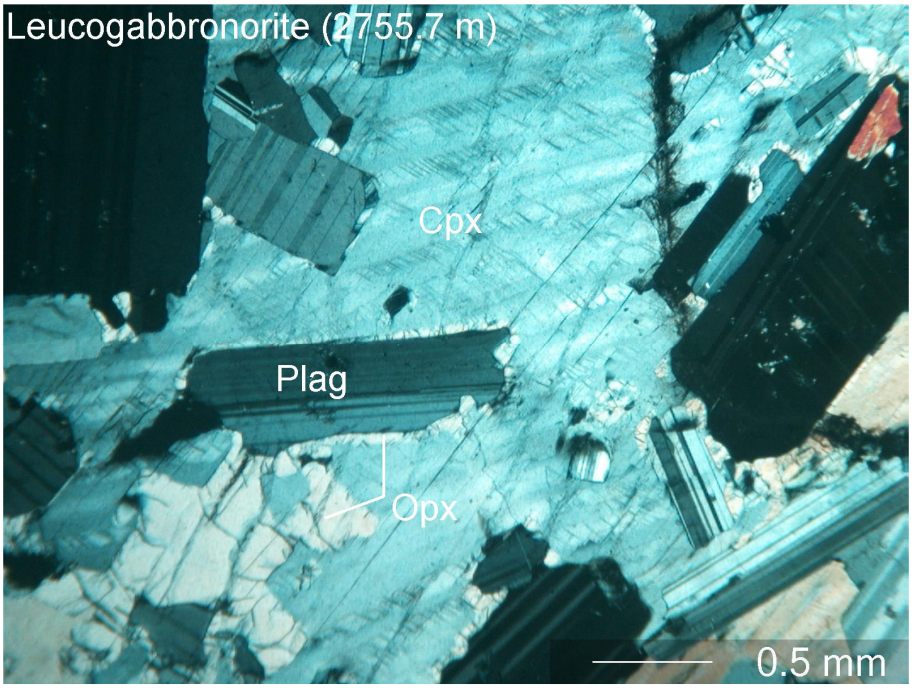

Figure 17: Orthopyroxene occurring as rims on plagioclase laths enclosed within an augite oikocryst. Photomicrograph under cross polarized light of leucogabbronorite taken at a depth of 2755.7 m.

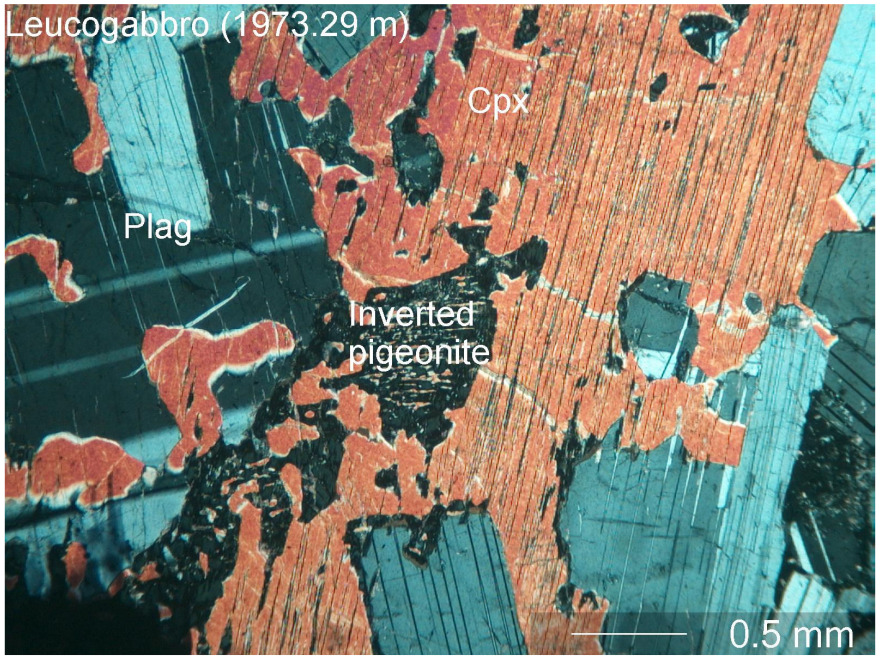

Figure 18: Orthopyroxene (inverted pigeonite) containing thick augite exsolution lamellae surrounded by an oikocryst of augite enclosing numerous plagioclase crystals with an embayed appearance. Photomicrograph under cross polarized light of leucogabbro taken from depth 1973.29 m.

Clinopyroxene modally constitutes between 0% and 39% of the samples studied and occurs either as anhedral to subhedral grains between plagioclase laths (see Figure 11) or as oikocrysts enclosing plagioclase and / or orthopyroxene (Figures 19 & 20). Clinopyroxene is usually characterized by relatively thick orthopyroxene exsolution lamellae and twinning is not uncommon (see Figure 16). In a single instance, augite was found to enclose an orthopyroxene grain, which in turn enclosed grains of plagioclase (Figure 21), suggesting the crystallization sequence plagioclase-orthopyroxene-clinopyroxene. Green pleochroic amphibole modally constitutes between 0% and 11% of the Main Zone samples studied and occurs mostly as patches in or as alteration rims on pyroxene crystals (Figure 22). The mineral also occurs interstitially, usually in association with other late magmatic minerals such as quartz and biotite and occassionaly also opaque minerals. The amphibole is generally featureless but in some samples it has a plumose morphology. Amphibole rims on pyroxenes occasionally grade into brown pleochroic biotite towards the edges.

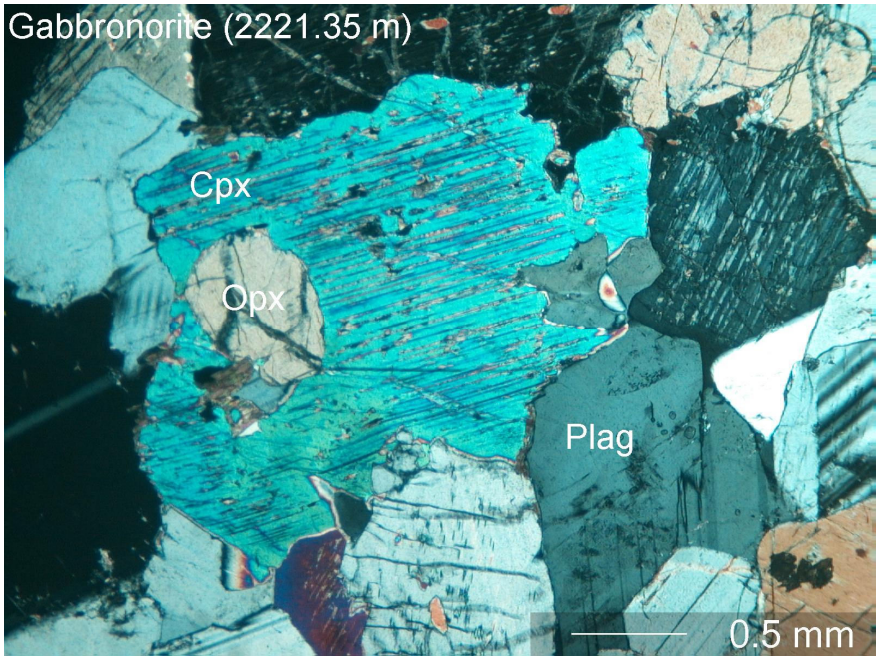

Figure 19: Augite with orthopyroxene exsolution lamellae enclosing a single grain of orthopyroxene. Photomicrograph under cross polarized light of gabbronorite taken at a depth of 2221.35 m.

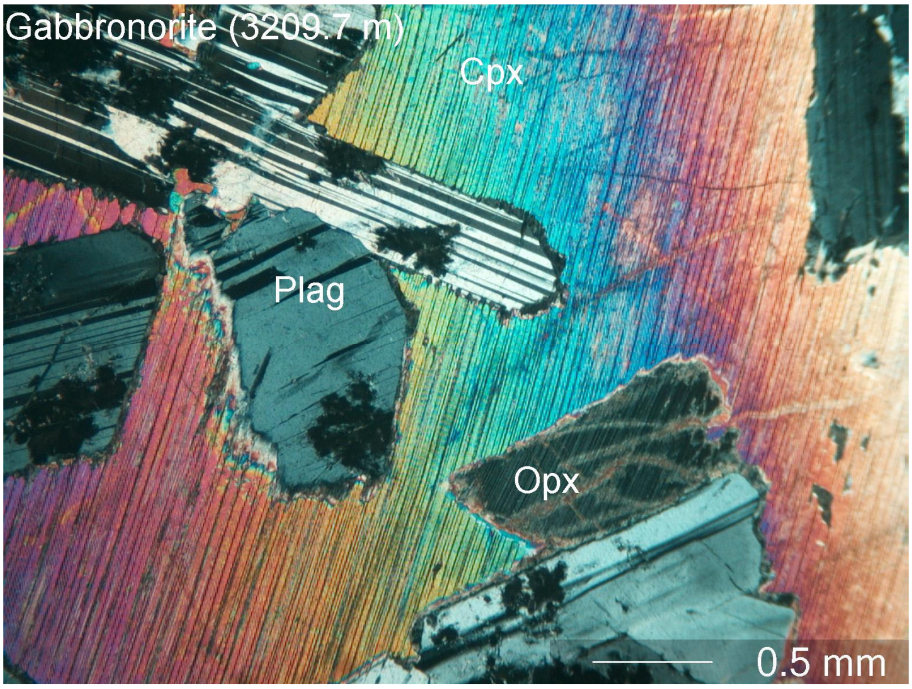

Figure 20: Optically continuous augite oikocryst enclosing plagioclase laths and a single orthopyroxene crystal. Photomicrograph under cross polarized light of gabbronorite taken at a depth of 3209.7 m.

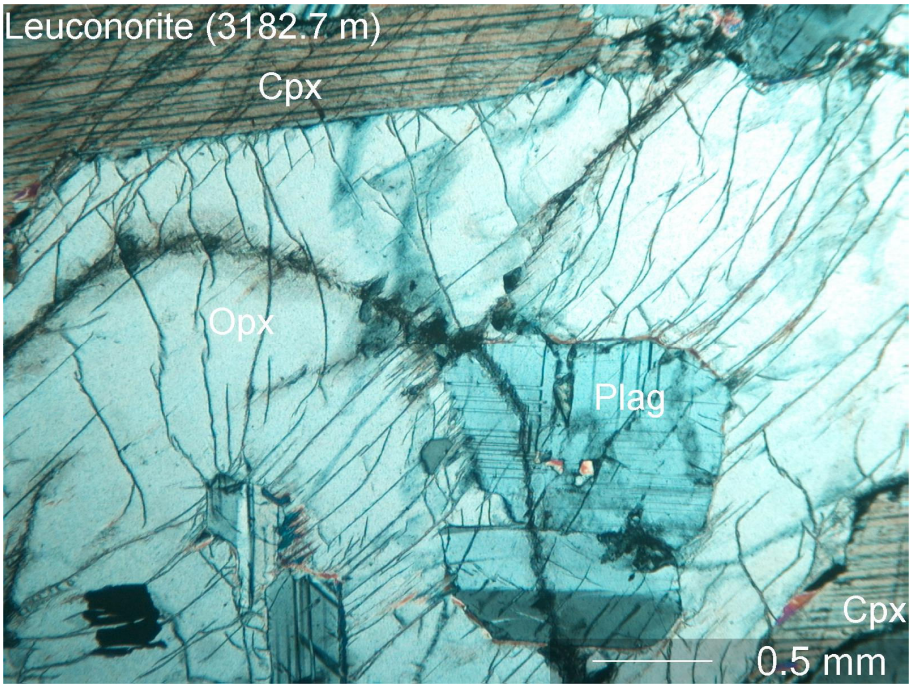

Figure 21: Plagioclase enclosed by orthopyroxene that is in turn enclosed by an optically continuous augite crystal. Photomicrograph under cross polarized light of leuconorite taken at a depth of 3182.7 m.

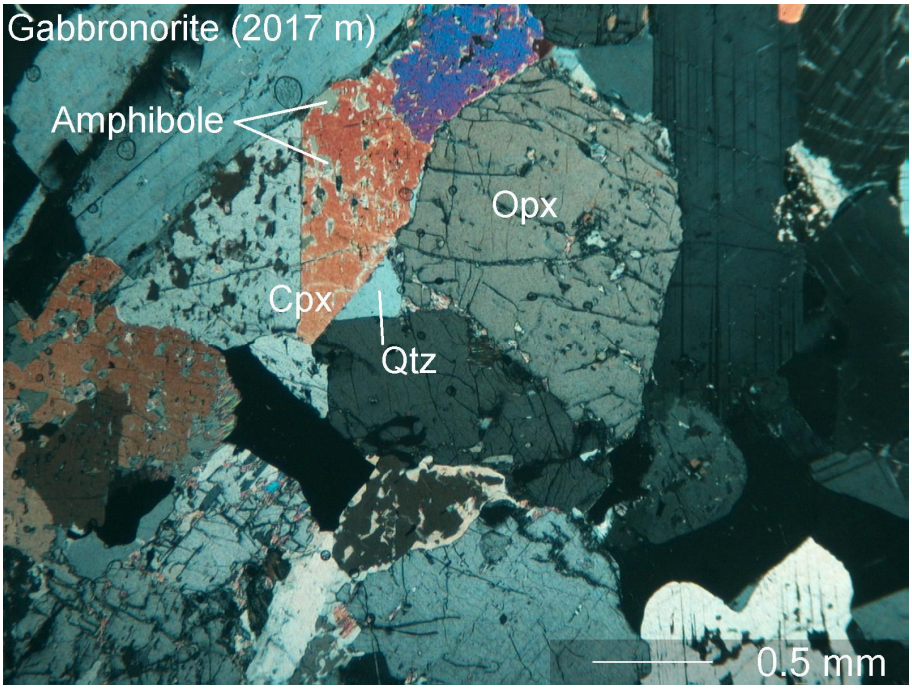

Figure 22: Patches of amphibole reminiscent of sieve texture, primarily confined to clinopyroxene. Photomicrograph under cross polarized light of gabbronorite taken from a depth of 2017 m. Also note the presence of quartz in the triangular interstice towards the centre of the image.

Quartz modally constitutes between 0% and 9% of the Main Zone samples studied and is mostly interstitial, but also occurs within the rare vein. It is only in a peculiar pegmatoidal sample from depth 3003.7 m, where quartz is seemingly not interstitial, but occurs as relatively coarse-grained, discrete, anhedral crystals. Biotite modally constitutes up to ~4% of the Main Zone samples studied and occurs either interstitially (Figure 23) or as rims on amphibole rims surrounding pyroxenes. Opaque minerals modally constitute up to 1.5% of the Main Zone samples studied and occurs either as fine-grained inclusions within silicate minerals or within interstitial patches, in some samples locally 'poikilophitically' enclosing silicate minerals (e.g. 2265.21 m). A detailed study of the opaque minerals was not performed due to their limited occurrence.

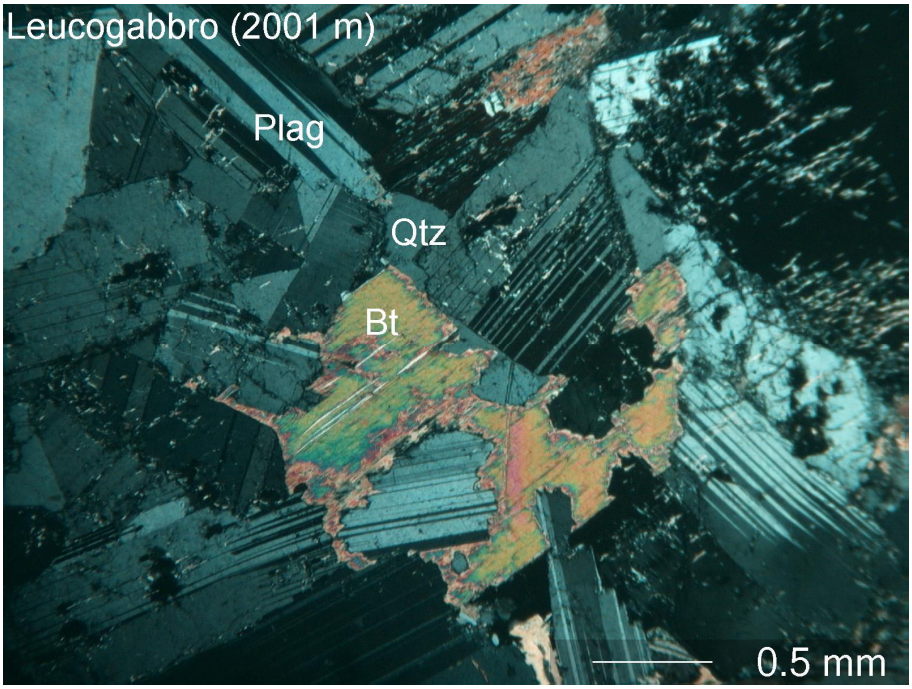

Figure 23: Interstitial biotite occurring in association with quartz in sample taken from a depth of 2001 m. Photomicrograph of leucogabbro under cross polarized light.

Other minerals encountered in the Main Zone samples include talc (as alteration product of pyroxenes), chlorite (as alteration product of both plagioclase and pyroxenes), calcite, colorless micas and apatite (confined to interstitial areas in association with quartz) and some minerals that could not be optically readily identified. Chlorite occurring as patches within plagioclase typically shows characteristic blue anomalous interference colours, whereas that associated with the pyroxenes are typically virtually isotropic.

X-Ray Diffraction analysis revealed the presence of a number of minerals that were not optically identified, including epidote, prehnite and serpentine in some of the Main Zone samples (see Appendix C).

Petrographic examination of the Main Zone samples showed the existence of an interesting texture occurring within the hanging wall to the Platreef, in which orthopyroxene exsolution lamellae within clinopyroxene protrude into adjacent plagioclase crystals (Figure 24, Appendix O). The texture that occurs in the gabbronorite from depth 3209.7 m was described by Roelofse et al. (2009) and was interpreted as

representing evidence for the late-stage infiltration of melt into a nearly solidified crystal mush. Similar textures have been described by Manyeruke (2007) from the Northern Sector of the Platreef at Nonnenworth, but were interpreted as being the result of clinopyroxene reacting with plagioclase to form orthopyroxene.

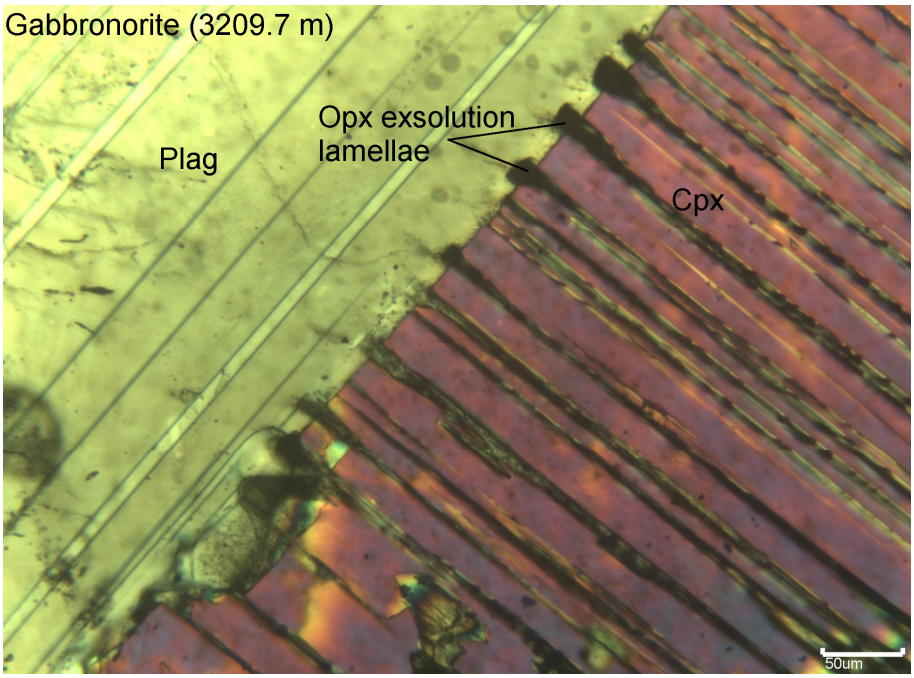

Figure 24: Photomicrograph under cross polarized light showing orthopyroxene exsolution lamellae within clinopyroxene protruding into adjacent plagioclase. Gabbronorite from depth 3209.7 m.

3.1.1.2 The Platreef

The Platreef is considerably more variable in terms of lithology in comparison to the overlying Main Zone and is apparent as an abrupt increase in colour index from typical Main Zone values of 2-71 (average = 29) to values typically higher than 70 and up to 100 (average = 77), occurring between depths 3215.7 m and 3220.7 m. Of the 21 Platreef and footwall samples studied, about 33% were melagabbronorites, ~9% websterites and gabbronorites, with lesser amounts of leuconorites, orthopyroxenites, leucogabbronorites, olivine melagabbronorites, harzburgites, melanorites, norites, altered ultramafics, gabbroids and granitoids.

The reef consists from top to bottom of about 140 m of orthopyroxene-rich cumulates, occasionally also being olivine-bearing, followed by a package of hybridized rocks below a depth of 3353.7 m in which interstitial quartz-feldspar graphic intergrowths abound, which is in turn followed by what was noted as 'pyroxene hornfels' in the original core log and then the granitic footwall.

Grain sizes as measured on the coarsest orthopyroxene grains present in every sample range between 4 mm and 14 mm for the orthopyroxene-rich cumulates and is on average much finer grained for the hybridized lithologies underlying the orthopyroxene-rich units. In some samples, none of the features of the original plagioclase could be identified, but on average, slightly more than 50% of the total plagioclase present in the samples has been altered. The heavy alteration underwent by the plagioclase made recognition of their textural relationships to the mafic silicates difficult (Figure 25), but it appears to be an intercumulate or at least a late crystallizing phase in most samples studied. A notable exception was found in the leucogabbronorite from depth 3258.2 m, which has an ophitic texture with oikocrysts of both ortho- and clinopyroxene enclosing plagioclase laths (Figure 26). Orthopyroxene in most of the orthopyroxene-rich samples is anhedral to subhedral and relatively unaltered. In both the olivine melagabbronorite (3284.7 m) and harzburgite (3305.7 m), anhedral to subhedral orthopyroxene oikocrysts locally enclose olivine crystals, suggesting that orthopyroxene crystallization was preceded by olivine (Figure 27). Clinopyroxene is everywhere subordinate to orthopyroxene within the Platreef, but is present in limited amounts in all of the samples studied. It generally occurs as anhedral to very rarely subhedral discrete crystals in most samples, but also as oikocrysts enclosing orthopyroxene in some (Figure 28). Olivine was encountered in three samples at depths of 3232.7 m, 3284.7 m and 3305.7 m. In the first sample, olivine occurred as completely serpentinised, subhedral grains with a maximum grain size on the order of 1.5 mm. The olivine pseudomorphs were set in a featureless matrix of chlorite and lesser calcite, the chlorite possibly having altered from pyroxene.

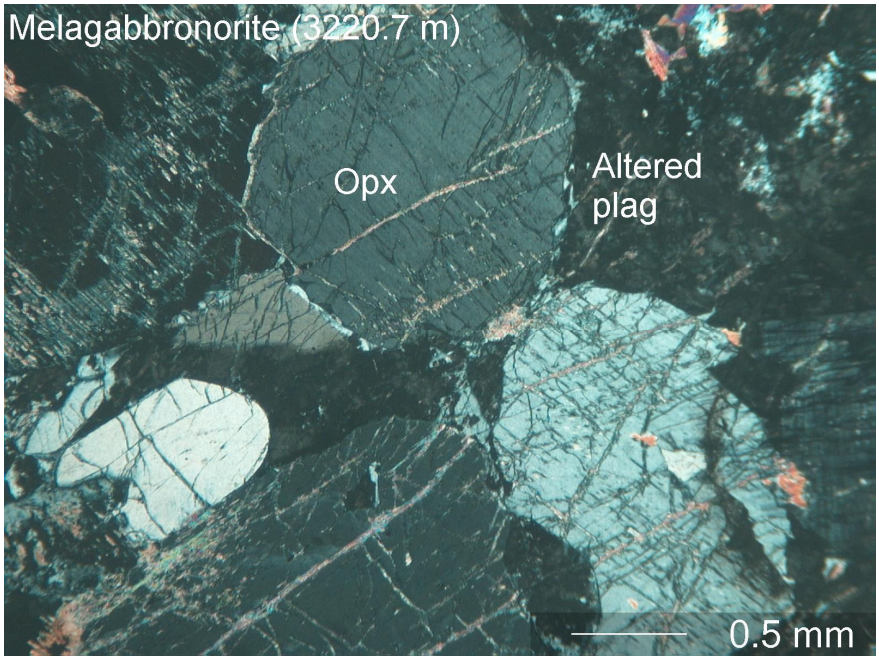

Figure 25: Heavily altered plagioclase in melagabbronorite from depth 3220.7 m – the textural relationship between plagioclase and pyroxene is impossible to tell. Photomicrograph under cross polarized light.

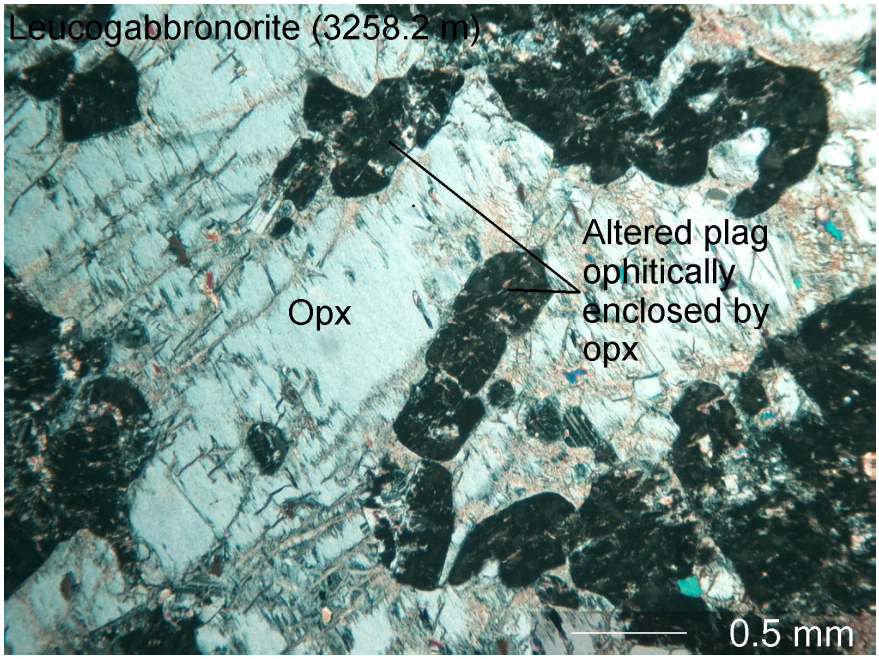

Figure 26: Ophitic texture in leucogabbronorite from depth 3258.2 m. Photomicrograph under cross polarized light. Original plagioclase has been virtually completely altered.

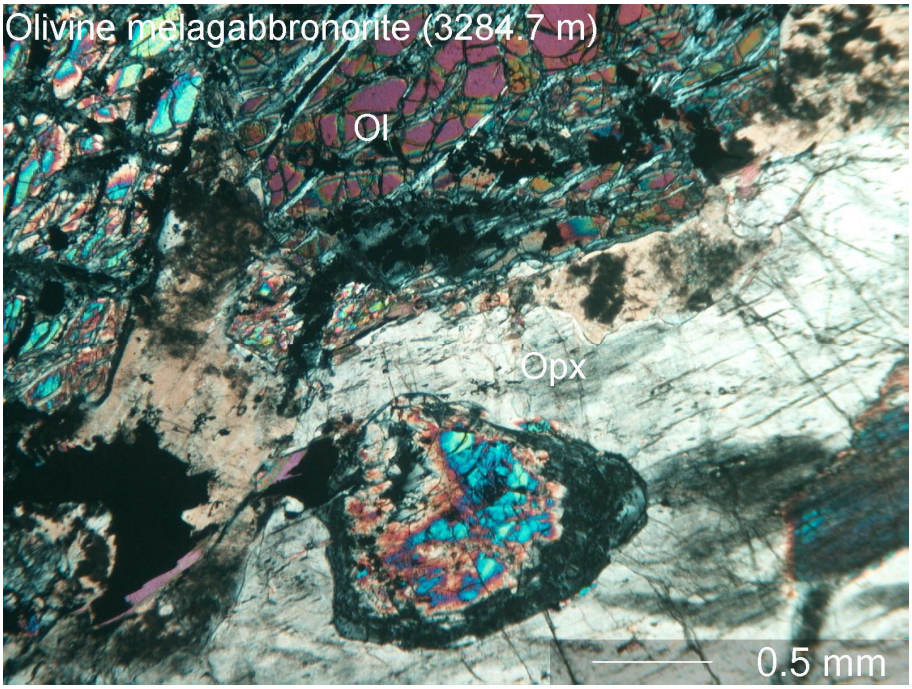

Figure 27: Partially serpentinised olivine enclosed by orthopyroxene oikocryst. Photomicrograph under cross polarized light of olivine melagabbronorite taken at depth 3284.7 m.

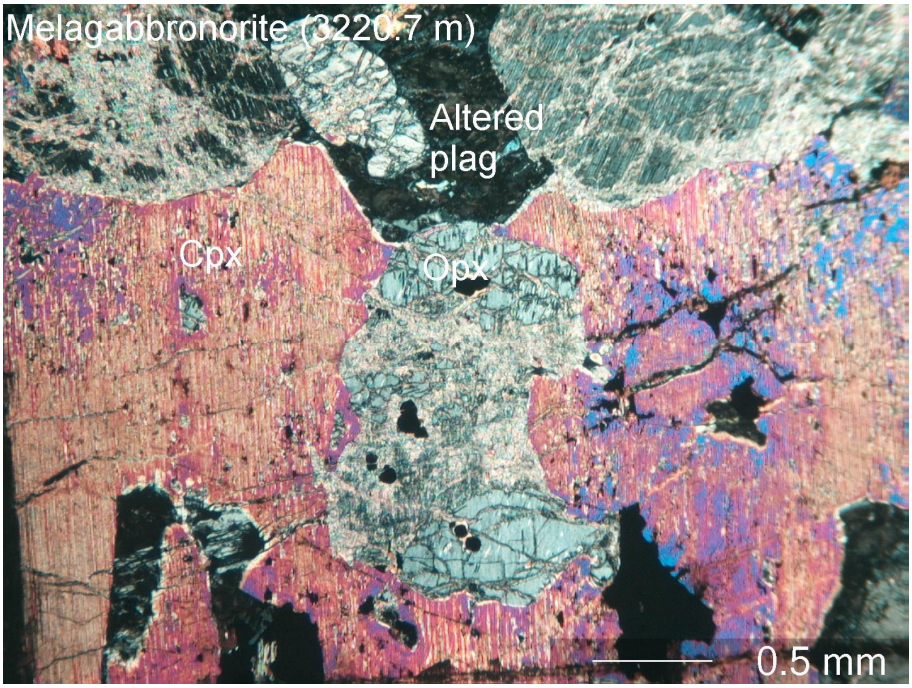

Figure 28: Clinopyroxene oikocryst enclosing partially altered orthopyroxene chadacryst. Photomicrograph under cross polarized light of melagabbronorite taken at a depth of 3220.7 m.

In the other two samples, olivine is present as anhedral to subhedral, partially serpentinised coarse-grained crystals, occurring mostly unenclosed but also as chadacrysts in orthopyroxene oikocrysts (cf. Figure 27).

Quartz was encountered in significant quantities only below 3353.7 m in the hybridized and underlying lithologies. A characteristic of the hybrid rock types is the presence of graphic intergrowths between quartz and feldspar, occupying the interstitial areas (Figure 29).

In the studied samples, interstitial and disseminated sulfides were confined to the orthopyroxene-rich samples higher up in the reef, with the hybridized rocks lower down in the reef seemingly barren of sulfides. Sulfides constitute up to 7% by volume of some of the thin sections studied (e.g. 3240.7 m). Opaque oxides were encountered in some samples, occurring either as regularly shaped polyhedra throughout the silicates, suggestive of a high temperature genesis (Figure 30), or within the fractures of partially serpentinised olivine crystals.

The so-called 'pyroxene hornfels' occurring towards the bottom of the reef and the pinkish granite (Figure 31) footwall was not studied in great detail, but the latter can probably be assigned to the Utrecht granite described by Holwell & McDonald (2006) in core drilled on the farm Overysel, which is immediately east of Moordkopje.

A rare form of exsolution texture known as symplectitic augite was encountered in the melagabbronorite from depth 3328.7 m and described by Roelofse & Ashwal (2008), who interpreted the texture as representing evidence for the presence of a water-rich fluid phase within the Platreef magma (Figure 32, Appendix P).

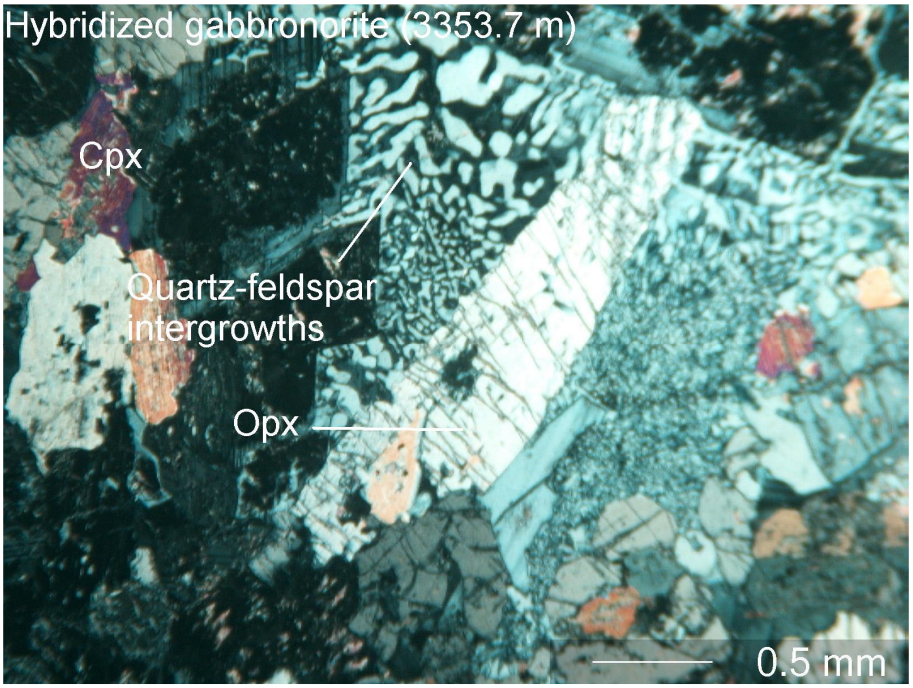

Figure 29: Interstitial graphic intergrowths between quartz and feldspar, a characteristic feature of the hybridized rocks below 3353.7 m. Photomicrograph under cross polarized light of hybridized gabbronorite taken at depth 3353.7 m.

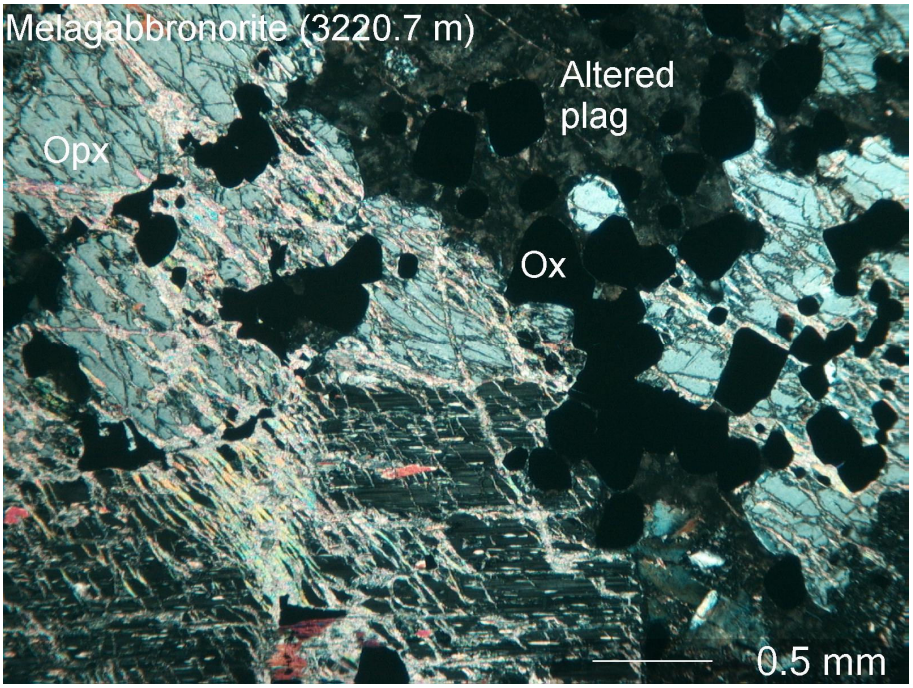

Figure 30: Equant opaque oxides occurring as inclusions in both orthopyroxene and plagioclase (now completely altered). Photomicrograph under plane polarized light of melagabbronorite taken at a depth of 3220.7 m.

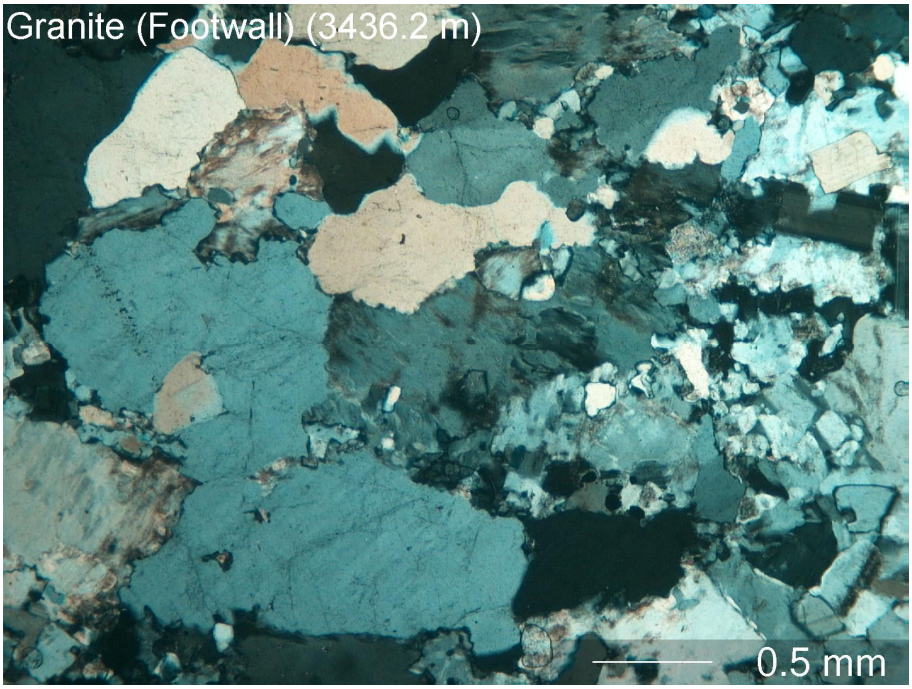

Figure 31: Photomicrograph under cross polarized light showing a part of the granite footwall at depth 3436.2 m.

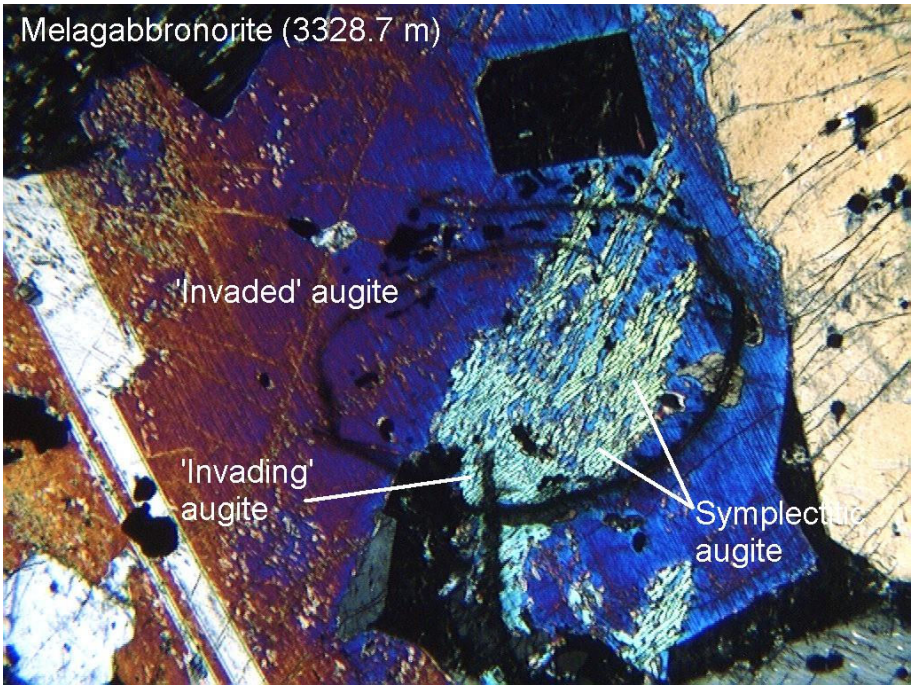

Figure 32: Photomicrograph under cross polarized light showing symplectitic augite as described by Roelofse & Ashwal (2008), developed in melagabbronorite from depth 3328.7 m. Width of field of view approximately 5.25 mm.

3.1.2 Mineral chemistry

3.1.2.1 Main Zone

The composition of plagioclase within the Main Zone is fairly constant with an average An% of 71.7 ± 2.2% (Figure 33)* for the whole succession. This average does not take into account two samples in which plagioclase appears to have undergone albitization, i.e. samples from depths 2653.7 m and 3003.7 m with average anorthite contents of 3.8% and 63.1%, respectively. Average anorthite contents for individual Main Zone samples as determined by electron microprobe range between 66.3% and 76.7%, with within sample variation expressed as 1σ-standard deviation on average ~2.5%. The maximum An% of plagioclase in individual rocks is on average 75.0 ± 2.2% and varies between 68.2% and 79.1%, whereas the minimum An% is on average 68.1 ± 2.6%, varying between 61.2% and 75.2%. There exists good agreement in general between the average plagioclase An% of individual samples and the maximum and minimum measured plagioclase An% of the same samples, suggesting that any of these measures may be used for comparative purposes and that the minima and maxima do not represent analyses that should be considered outliers (Figure 34). I therefore chose to make use of the maximum plagioclase An% in the discussion to follow.

In terms of the maximum An% of plagioclase, the basal part of the Main Zone up to a depth of ~2393.7 m shows very little variation or distinct trends, with the maximum An% of samples over this interval scattered about a value of ~ 76.0%. At a depth of 2393.7 m, a rapid decrease in the maximum An% of plagioclase is observed to values of ~72.0%, followed by a gradual reversal over a stratigraphic interval of approximately 130 m to values as high as 78.0%. At depth ~2264 m, another sudden decrease in maximum plagioclase An% is observed to values of ~71.0%, followed by a gradual and somewhat scattered reversal to values as high as ~76.0% at depth ~1964 m. The uppermost portion of the Main Zone exhibits a decrease in the maximum An% of plagioclase to values of ~70.0% again followed by what is perhaps a gradual reversal in An% to the top of the core.

* Plagioclase An% = 100 x molar Ca/(Ca+Na+K)

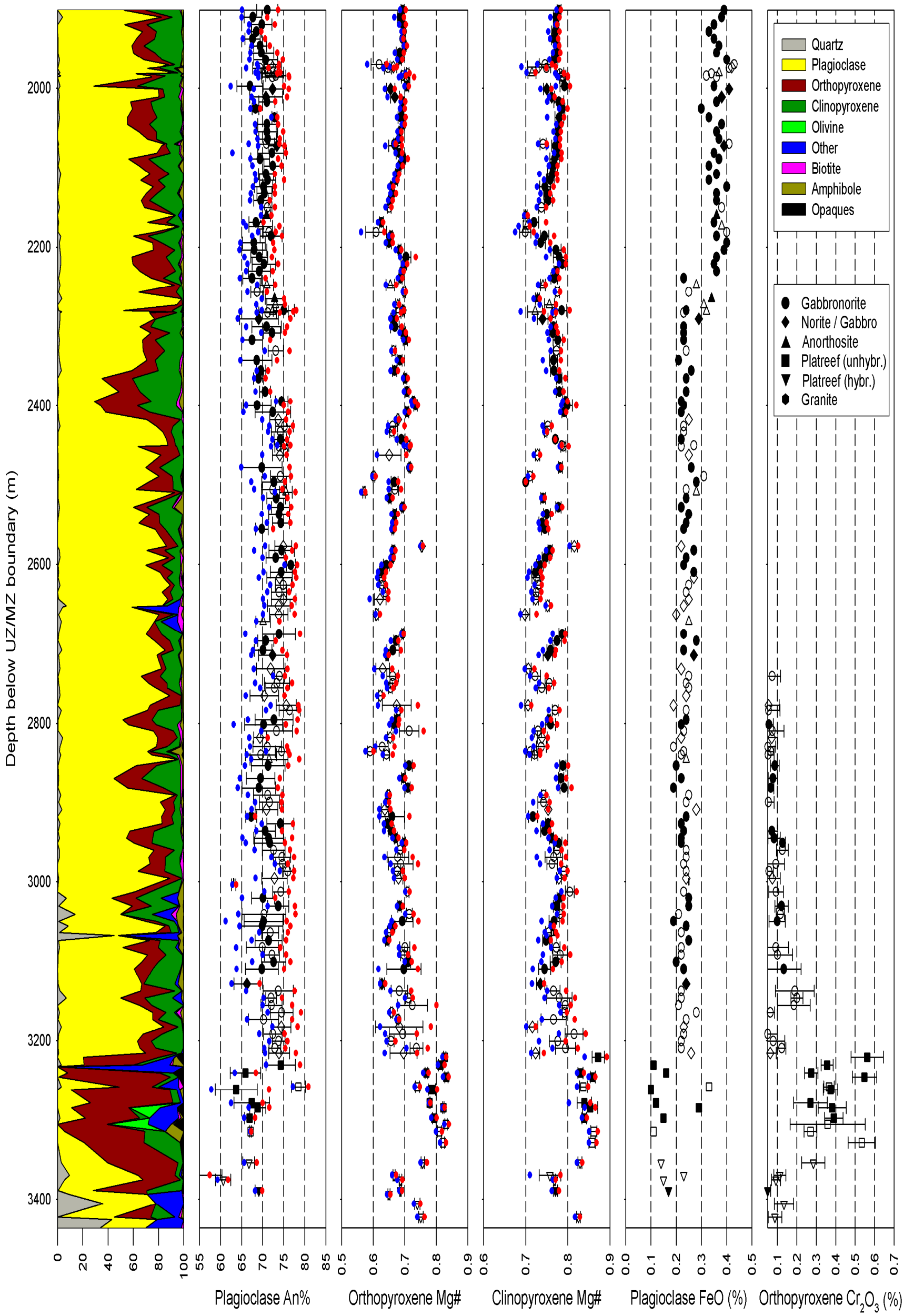

Figure 33: Variation in modal mineralogy and mineral compositions with depth. Solid symbols indicate samples with intergranular texture whereas open symbols represent samples with poikilitic, ophitic or mixed textures. Red and blue data points show maximum and minimum plagioclase An% and pyroxene Mg#, respectively. Error bars indicate 1σ-standard deviations.

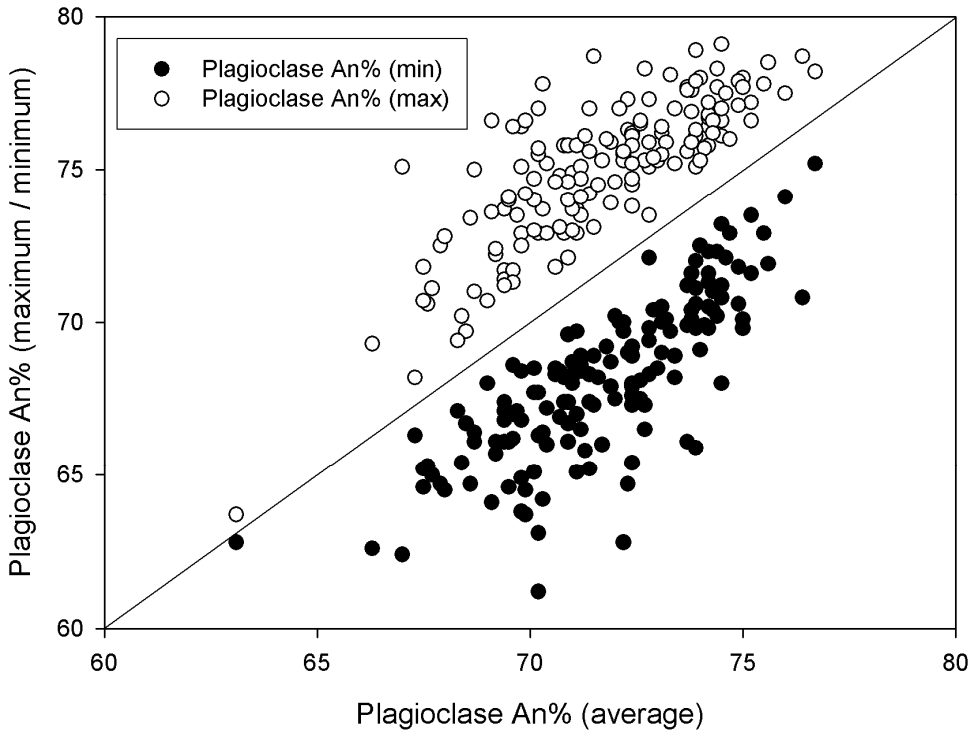

Figure 34: Comparison between the average, maximum and minimum plagioclase An% obtained on individual samples. Solid line indicates a 1:1 correspondence.

The FeO content of plagioclase in the Main Zone exhibits interesting behaviour, with values scattered around 0.23% from the base of the Main Zone up to a depth of 2290.5 m, followed by an interval exhibiting FeO contents intermediate between those seen below and above this interval and then relatively constant FeO contents of ~0.36% to the top of the core (Figure 33).

The average Mg# (molar Mg/(Mg+Fe)) of orthopyroxene from individual Main Zone samples ranges between 0.57 and 0.75, and is on average 0.67 ± 0.03 for the whole succession (Figure 33). Within sample variation of Mg# expressed as 1σ-standard deviation rarely exceeds 0.01. Notably larger within sample variations are typical of samples exhibiting ophitic or poikilitic textures and may reflect the intercumulus nature of orthopyroxene in those samples.

For rocks exhibiting intergranular texture, reversed differentiation trends as shown by pyroxene Mg# appear to be the norm rather than the exception for the Main Zone rocks sampled by the MO-1 drill core. Also, the lower part of the Main Zone exhibits numerous sudden shifts in pyroxene Mg# between consecutive samples, with only short stratigraphic intervals exhibiting trends of either normal or reversed differentiation. For the upper part of the drill core, from a depth of ~2364 m, sudden shifts in pyroxene Mg# do not occur. Instead, this part of the stratigraphy exhibits either virtually no differentiation of pyroxene with depth (e.g. the depth interval 2230.33 m to 2355.7 m), normal differentiation (e.g. 2169 m to 2212.63 m) or reversed differentiation (e.g. 2088.68 m to 2212.63 m). Localized minima in pyroxene Mg# are often also associated with localized minima in the colour index of samples (e.g. 2069.82 m).

The Mg# of clinopyroxene strongly mimics that of orthopyroxene and is on average ~0.06 higher than that of co-existing orthopyroxene. The average Mg# of clinopyroxene in the Main Zone averages 0.76 ± 0.03 and ranges between 0.70 and 0.82 in individual Main Zone samples. Within sample variation in the Mg# of clinopyroxene is on average ~0.01.

The behaviour of Cr in pyroxene is also noteworthy. Cr_2O_3 in orthopyroxene down to a depth of ~2764 m was typically below the detection limit of 0.05%, with samples down to the base of the Main Zone exhibiting Cr_2O_3 contents as high as 0.2%, but typically up to a maximum of about 0.15% (Figure 33). The Cr_2O_3 content of clinopyroxene down to depth 2764 m was typically also below detection limit (i.e. 0.05%) but from depth 2764 m to the base of the Main Zone, many samples had Cr_2O_3 contents above detection limit and up to ~0.25% Cr_2O_3. Although many samples below 2764 m still had Cr_2O_3 contents in pyroxene below detection limit, the general trend from the base of the Main Zone up to a depth of ~2764 m appears to be one of decreasing Cr in pyroxene.

Contrasting behaviour is apparent in the behaviour of plagioclase and the pyroxenes when these minerals are considered together (Figure 35). Intervals are present exhibiting:

- Normal differentiation of plagioclase associated with very limited differentiation of pyroxenes (e.g. 2045.34 m (An% = 73.7%, Mg# = 0.70) to 2025.7 m (An% = 69.4%, Mg# = 0.70); Figure 35a).
- Normal differentiation of plagioclase associated with normal differentiation of pyroxenes (e.g. 2394.7 m (An% = 76.6%, Mg# = 0.73) to 2365.39 m (An% = 70.7%, Mg# = 0.71); Figure 35b).
- Normal differentiation of plagioclase associated with reversed differentiation of pyroxenes (e.g. 1963.72 m (An% = 74.8%, Mg# = 0.69) to 1946.18 m (An% = 71.7%, Mg# = 0.71); Figure 35c).
- Limited differentiation of plagioclase associated with limited differentiation of pyroxenes (e.g. 2908.7 m (An% = 74.6%, Mg# = 0.65) to 2890.7 m (An% = 74.7%, Mg# = 0.65); Figure 35d).
- Limited (albeit scattered) differentiation of plagioclase associated with normal differentiation of pyroxenes (e.g. 2977.7 m (An% = 76.0%, Mg# = 0.74) to 2926.7 m (An% = 77.2%, Mg# = 0.66); Figure 35e).
- Limited differentiation of plagioclase associated with reversed differentiation of pyroxenes (e.g. 2417.7 m (An % = 75.6%, Mg# = 0.68) to 2399.5 m (An% = 75.0%, Mg# = 0.74); Figure 35f).
- Reversed differentiation of plagioclase associated with limited (albeit scattered) differentiation of pyroxenes (e.g. 2355.7 m (An% = 71.3%, Mg# = 0.68) to 2330.7 m (An% = 76.4%, Mg# = 0.67); Figure 35g).
- Reversed differentiation of plagioclase associated with normal differentiation of pyroxenes (e.g. 2017 m (An% = 73.0%, Mg# = 0.70) to 2001 m (An% = 76.2%, Mg# = 0.67); Figure 35h).
- Reversed differentiation of plagioclase associated with reversed differentiation of pyroxenes (e.g. 2169 m (An% = 70.2%, Mg# = 0.63) to 2088.68 m (An% = 73.7%, Mg# = 0.71); Figure 35i).

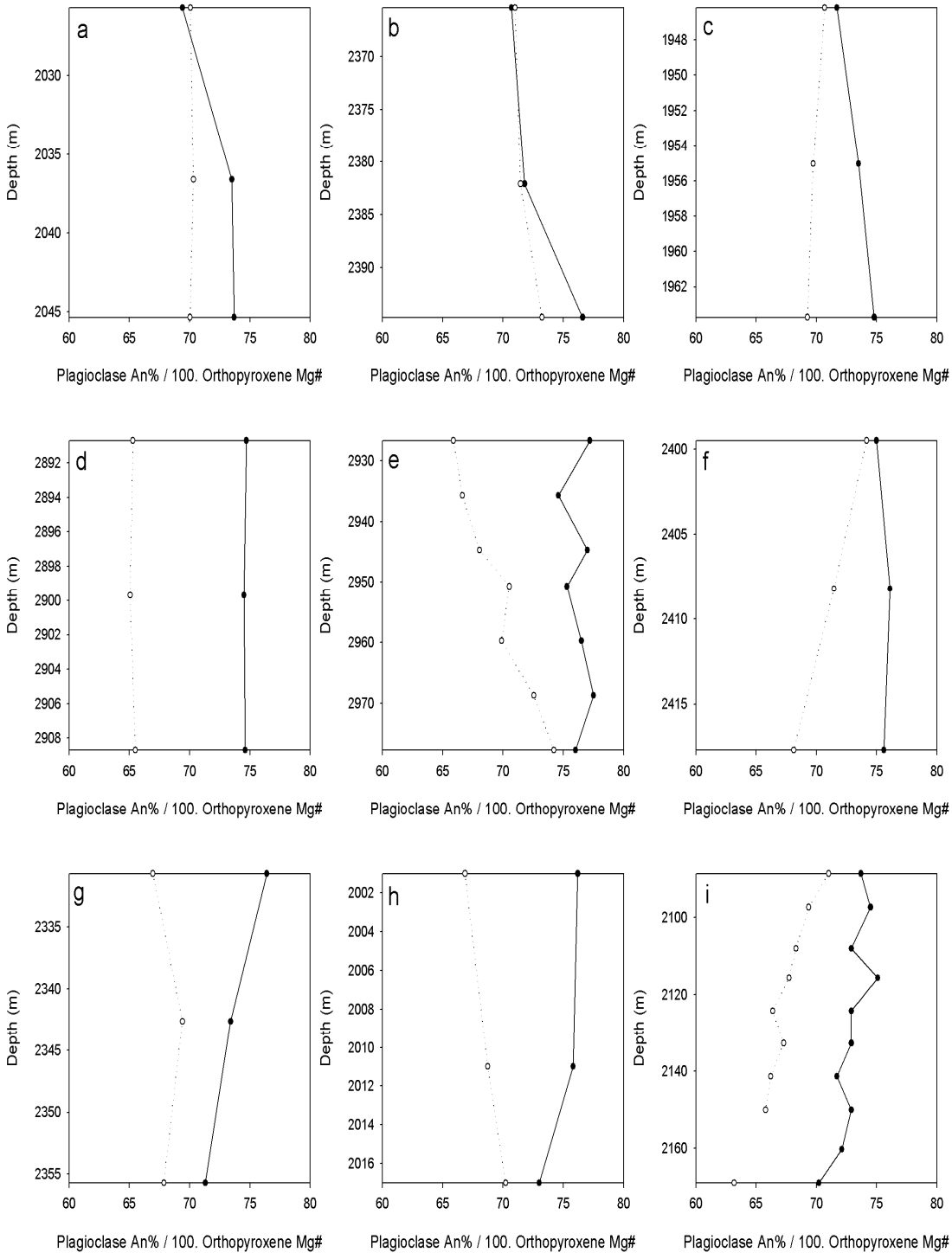

Figure 35: Contrasting behaviour in maximum plagioclase An% (solid circles) and maximum orthopyroxene Mg# (open circles) over selected depth intervals. See text for details.

3.1.2.2 The Platreef

The Platreef is characterized by plagioclase that is typically more sodic than that of the Main Zone. The unhybridized Platreef down to a depth of 3328.7 m contains plagioclase with maximum An% ranging between 67.3% and 80.9%, with a general but scattered increase in An% upward. On average, the An% of plagioclase in the hybridized Platreef is lower than that of the unhybridized Platreef with values ranging between 57.4% and 69.9%.

The Platreef is characterized by pyroxenes exhibiting higher Mg# and Cr contents in comparison to the Main Zone (Figure 36 & 37). The unhybridized Platreef down to a depth of 3328.7 m contain orthopyroxene and clinopyroxene exhibiting Mg# ranging from 0.74 to 0.83 and 0.83 to 0.87, respectively, with no trend being apparent. The hybridized Platreef lithologies show a lot of scatter in the Mg# of ortho- and clinopyroxene with values ranging between 0.65 and 0.76, and 0.76 to 0.83, respectively.

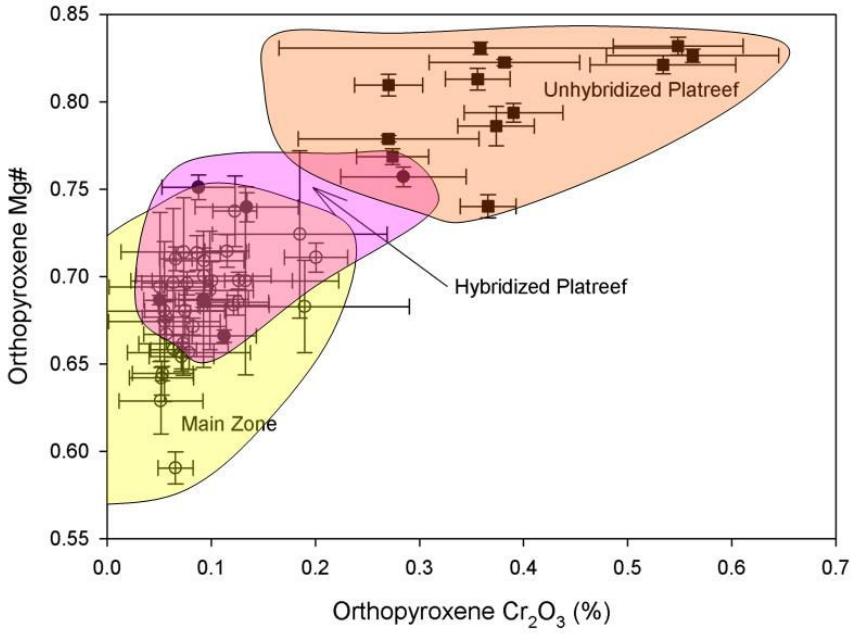

Figure 36: Relationship between Mg# of orthopyroxene and the Cr_2O_3 content thereof. Open circles, solid circles and solid squares represent Main Zone, hybridized Platreef and unhybridized Platreef samples, respectively.

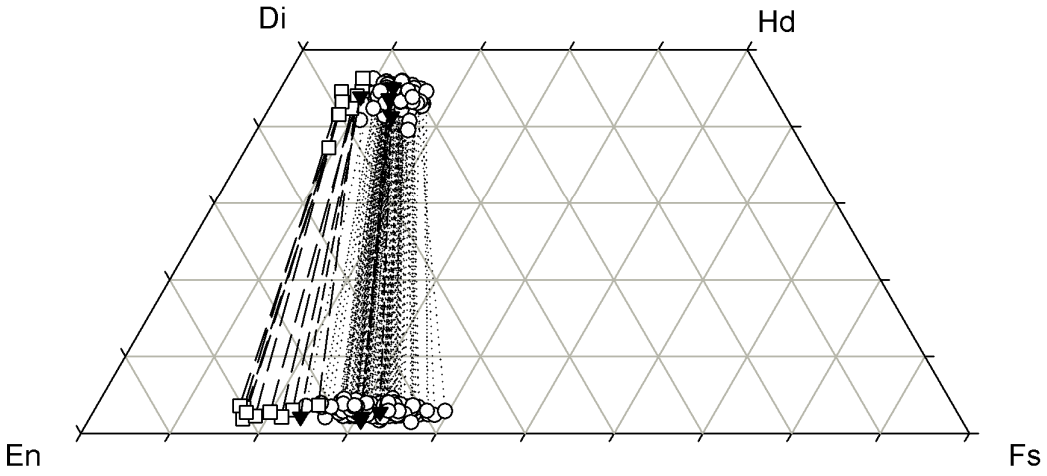

Figure 37: The pyroxene quadrilateral showing average compositions of pyroxene from the Main Zone and Platreef (Open circles = Main Zone, Open squares = Unhybridized Platreef, Solid triangles = Hybridized Platreef).

3.1.3 Summary of noteworthy findings

A number of findings that I deem to be important for the petrogenetic interpretation of the lower Main Zone of the Northern Limb will be shortly discussed and expanded upon in later sections of this thesis. The lower Main Zone in the MO-1 drill core is characterized by very limited differentiation as exhibited by plagioclase An% and pyroxene Mg# when compared to other localities within the Bushveld Complex (see Folder 1). This feature may be suggestive of the repeated influx of magma into the Bushveld Complex magma chamber in this part of the layered succession. The decoupling of the differentiation trends of plagioclase and pyroxenes discussed in section 3.1.2.1 and depicted graphically in Figure 35, and also seen in the vicinity of the Pyroxenite Marker in the Western Limb (Nex et al., 2002) attests to the complex mixing of minerals crystallized from geochemically distinct magmas. Repeated influx of magma into the main Bushveld Complex magma chamber is further attested to by the paucity of inverted pigeonite in the studied succession, with intruding magmas never becoming sufficiently evolved to allow for this mineral's crystallization. The behaviour of FeO in plagioclase towards the top of the MO-1 drill core may have bearing on the subsequent evolution of the Main Zone, as will be discussed in later sections.

3.2 Whole-rock major and trace element geochemistry

Whole-rock major and trace element analyses are reported in Appendix H and calculated CIPW norms in Appendix I.

3.2.1 Major elements

Binary variation diagrams of MgO versus the other major elements are presented in Figure 38. The variation in major elements is unremarkable and as expected, largely reflective of the modal mineralogy of individual samples. SiO_2 is fairly constant for the majority of samples analysed, showing a slight increase from ~50% for MgO-poor samples to ~54% for samples richer in MgO. The granite footwall and especially the lower part of the hybridized Platreef have SiO_2 in excess of 70%.

Whole-rock Al_2O_3 is apparently controlled nearly exclusively by modal plagioclase, showing a strong negative correlation with MgO, the same being true for CaO and Na_2O. The variation of Al_2O_3 with CaO is, however, more complex as a result of the incorporation of CaO into clinopyroxene in addition to plagioclase. K_2O is typically <0.5%, except in the hybridized Platreef rocks and granite footwall, the latter with values up to ~4%, and shows a weak negative correlation with MgO.

Fe_2O_3 and MnO both exhibit positive correlations with MgO, with values ranging between ~1% and ~14% and between ~0.02% and ~0.25%, respectively, with the latter values being consistent with the virtual lack of MnO in plagioclase and contents up to ~0.6% in pyroxene, specifically orthopyroxene. In the Platreef, both Fe_2O_3 and MnO show very little variation with MgO content, both remaining fairly constant despite large differences in MgO content.

Whole-rock Cr_2O_3 exhibits a positive correlation with MgO and in the Main Zone is typically present in concentrations <0.02%, with higher values encountered only in rocks from below ~2764 m, with the rocks below this depth forming an array extending to values as high as ~0.5% in the Platreef.

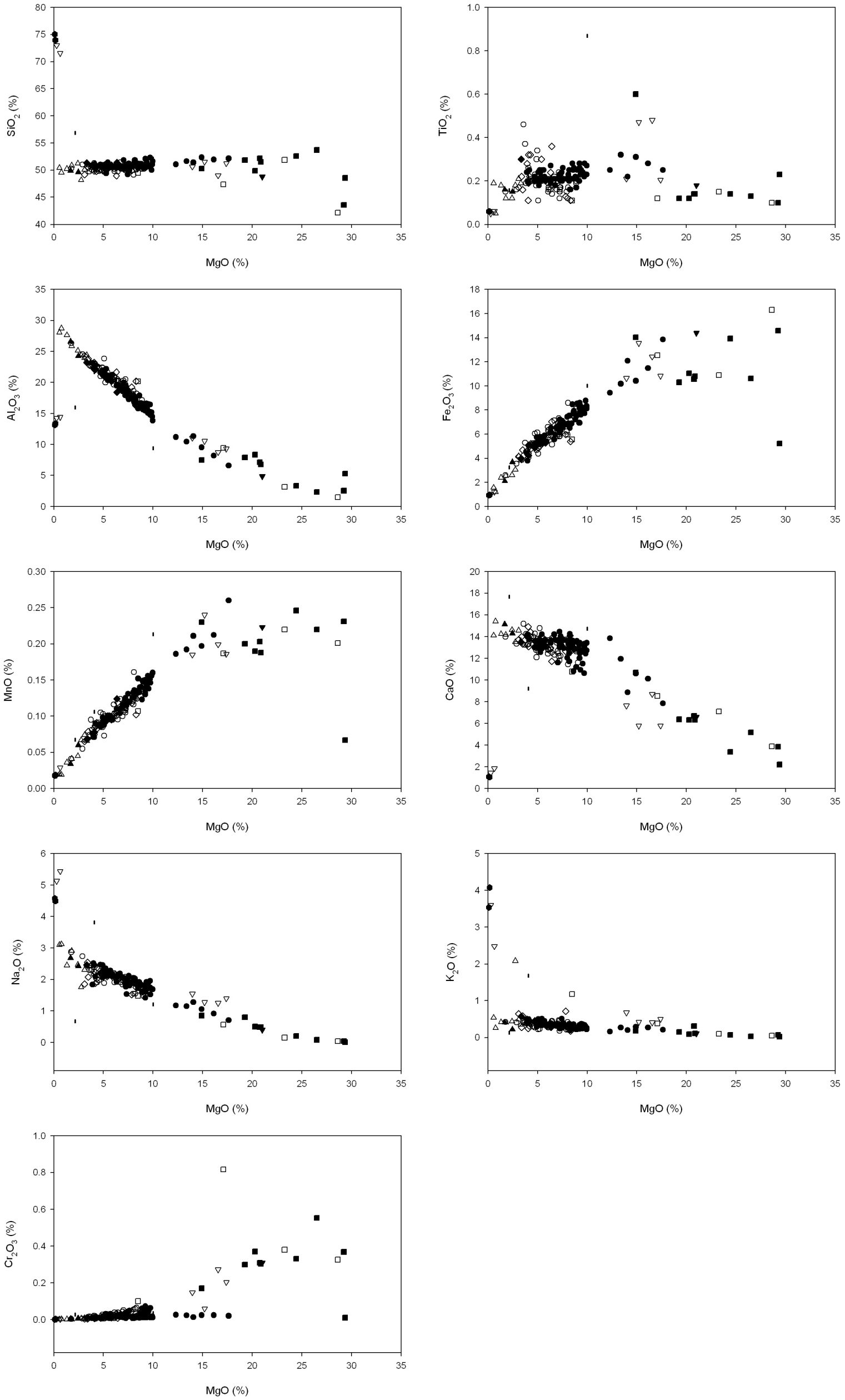

Figure 38: Binary variation diagrams of selected major elements versus MgO. See Figure 33 for explanation of symbols used.

This behaviour is consistent with that exhibited by the pyroxenes, in which higher Cr_2O_3 contents are also confined to Main Zone samples occurring deeper than ~2764 m.

Whole-rock TiO_2 and P_2O_5 contents are typically below 0.4% and 0.1%, respectively, and their contents do not correlate with modal mineralogy, suggesting incompatible behaviour with respect to the dominant rock-forming minerals.

There exists good agreement between the modal mineralogy as determined optically and the norm, at least in terms of positive correlations obtained for the different minerals as determined using both methods. However, normative plagioclase is generally somewhat lower than modal plagioclase, with the pyroxenes, especially clinopyroxene showing opposite behaviour. Most samples, including many from the Platreef, are quartz normative. Whole-rock Mg# (0.67 ± 0.04) and plagioclase An% (70.5±3.1%) as calculated from the norm exhibit very little overall variation for the Main Zone and are generally consistent with variations in the mineral chemistry as presented above. Plagioclase anorthite contents as calculated from the norm vary between 67.9% and 99.8% for the unhybridized Platreef, between 10.1% and 75.6% for the hybridized Platreef and averages ~10.1% in the granite footwall, with whole-rock Mg# varying between 0.68 and 0.92 in the unhybridized Platreef, between 0.36 and 0.76 in the hybridized Platreef and averaging ~0.22 in the granite footwall.

3.2.2 The modified differentiation index (MDI)

Von Gruenewaldt (1971) adapted two parameters, the differentiation index (Thornton & Tuttle, 1960) and the crystallization index (Poldervaart & Parker, 1964) for the study of igneous differentiation using whole-rock data for the Bushveld Complex to also take into account the effects of amongst others, iron enrichment. The modified differentiation index (MDI) is an indication of the degree of differentiation of a magma as reflected by the amounts of normative quartz, alkali feldspar, nepheline and leucite, and also taking into account the effect of iron enrichment typical of many basaltic magmas, whereas the modified crystallization index (MCI) is essentially a measure of the progression of magmas away from the primitive system An-Di-Fo. As such, these two parameters show contrasting behaviour with highly evolved rocks characterized by high MDI and low MCI values and primitive rocks by low MDI and

high MCI values. As a result of the predictable behaviour with which these two parameters will vary, we will only consider the MDI here.

MDI values (Figure 39) for the Main Zone show very little overall variation, with values on average 30.8 ± 2.4. The unhybridized Platreef samples have MDI values ranging between 6.6 and 30.2, with those of the hybridized Platreef having MDI values of between 24.3 and 93.7. The granite footwall has MDI values on the order of 95.

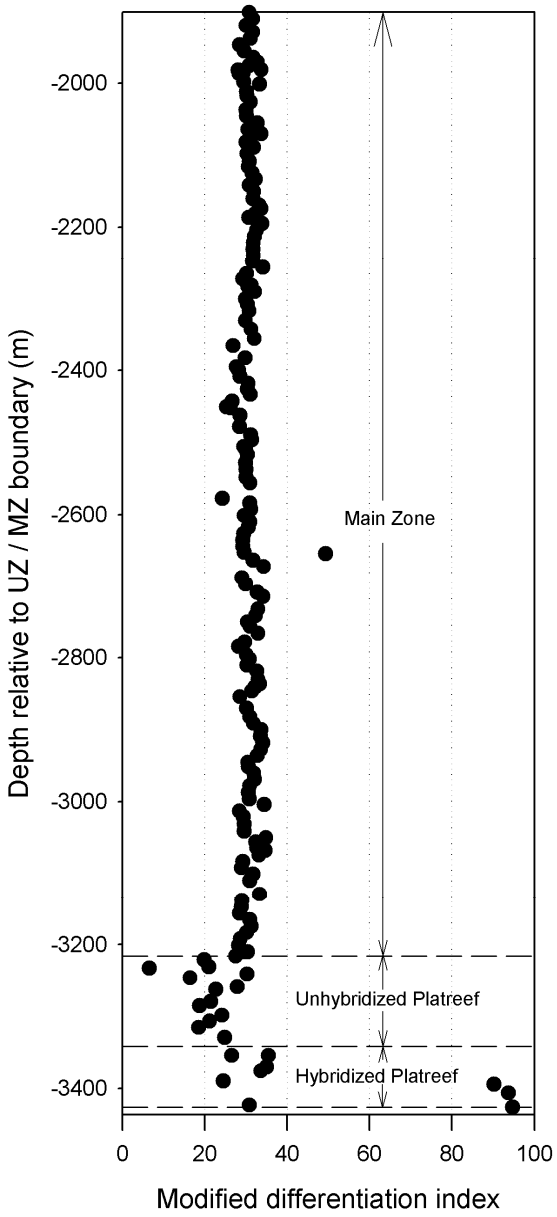

Figure 39: Modified differentiation index versus depth in the MO-1 drill core.

3.2.3 Trace elements

Binary variation diagrams for selected trace elements versus MgO are presented in Figure 40 and their variation with depth in Figure 41. For the most part, the behaviour of the trace elements within the Main Zone and Platreef can be explained satisfactorily by comparing individual element distribution coefficients for basaltic rocks for the three major rock forming silicates, viz. plagioclase, orthopyroxene and clinopyroxene (Table 5).

Ba shows a negative correlation with MgO content, reflecting its preference for plagioclase rather than the pyroxenes, and ranges between ~100 ppm for plagioclase-rich rocks of the Main Zone to ~20 ppm for the plagioclase-poor rocks of the Platreef. Notable exceptions occur over the depth interval 2653.7-2671.7 m, where Ba concentrations of up to ~280 ppm occur. This interval is characterized by rocks that have been rather pervasively altered and the higher than typical Ba concentrations are therefore probably of a secondary rather than primary magmatic origin. The hybridized Platreef has Ba concentrations up to ~570 ppm, whereas the granite footwall has Ba of ~ 730 ppm.

Whole-rock Co shows a positive correlation with MgO and ranges between ~2 ppm in plagioclase-rich rocks to ~65 ppm in the more mafic gabbroic rocks, which is consistent with the higher distribution coefficient for Co into pyroxene in comparison to plagioclase. For the unhybridized Platreef, whole-rock Co ranges between ~18 ppm and 218 ppm, with those rocks exhibiting low concentrations either being rich in plagioclase or being heavily altered, and with higher concentrations typically seen in olivine-bearing rocks, e.g. from the harzburgite at depth 3305.7 m. Whole-rock Co varies between ~1 ppm and ~160 ppm within the hybridized Platreef and has values below 1 ppm within the granitic footwall.

For the Main Zone, whole-rock Cu varies between ~7 ppm and ~80 ppm, the latter value recorded in the immediate hangingwall to the Platreef, with Cu values showing a weak positive correlation with MgO. Whole-rock Cu values range between ~30 ppm and ~3100 ppm within the unhybridized Platreef, and is generally below ~200 ppm in the hybridized Platreef and less than 10 ppm in the granitic footwall.

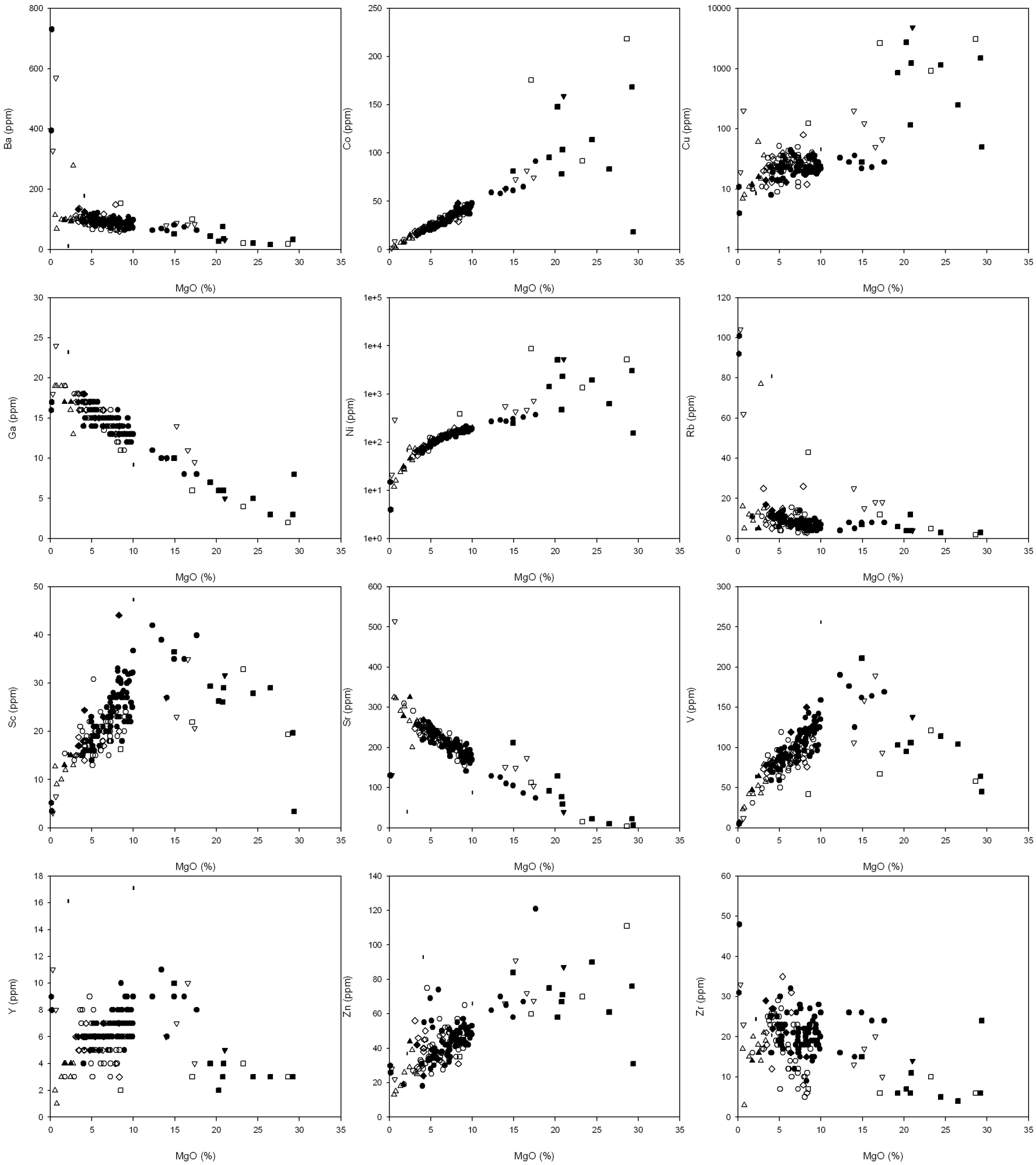

Figure 40: Binary variation diagrams of selected trace elements versus MgO. See Figure 33 for explanation of symbols used. Note logarithmic scale for Cu & Ni diagrams.

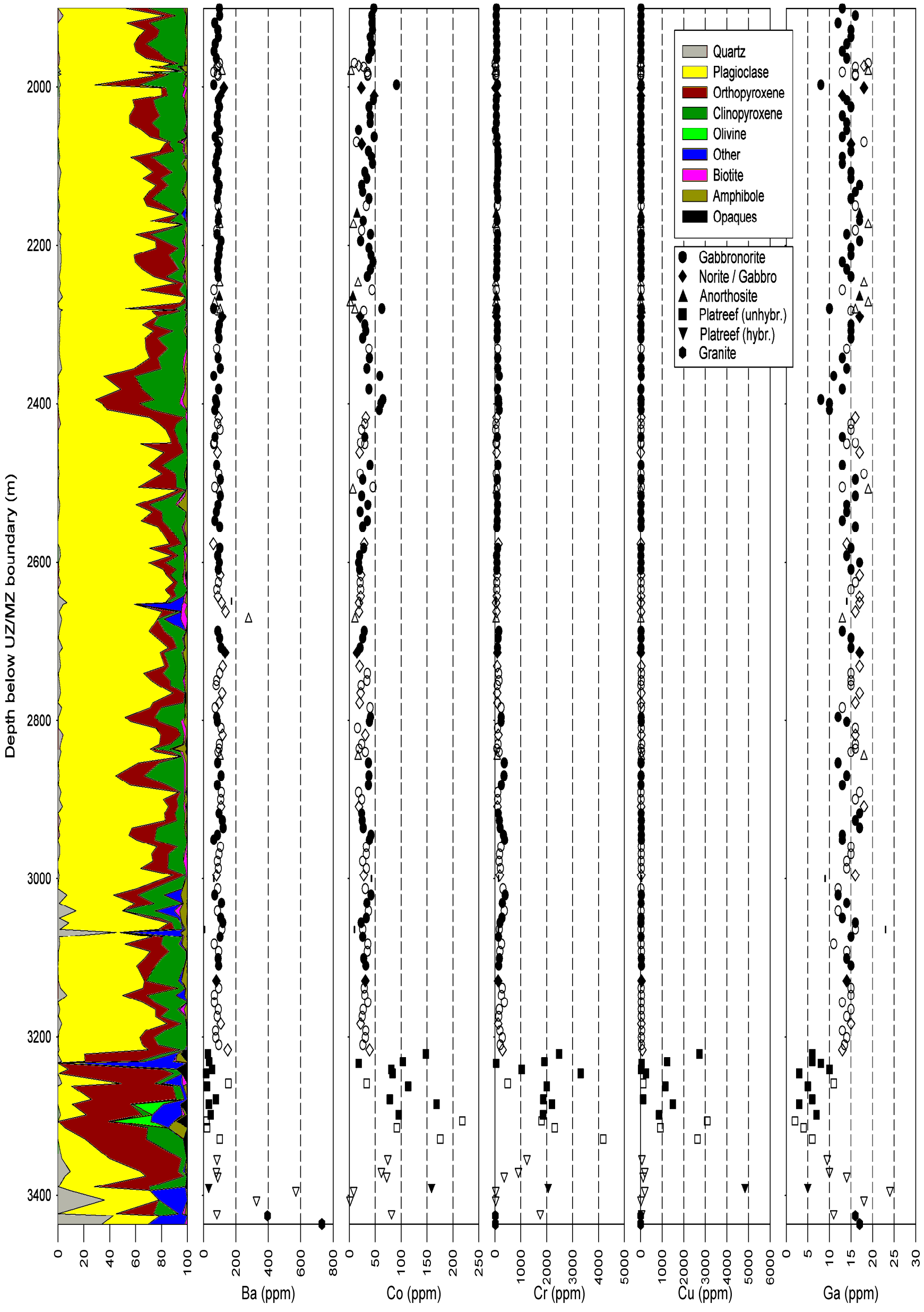

Figure 41: Variation in trace element concentrations with depth relative to the Upper Zone – Main Zone boundary in the MO-1 drill core. Modal mineralogy shown for comparison.

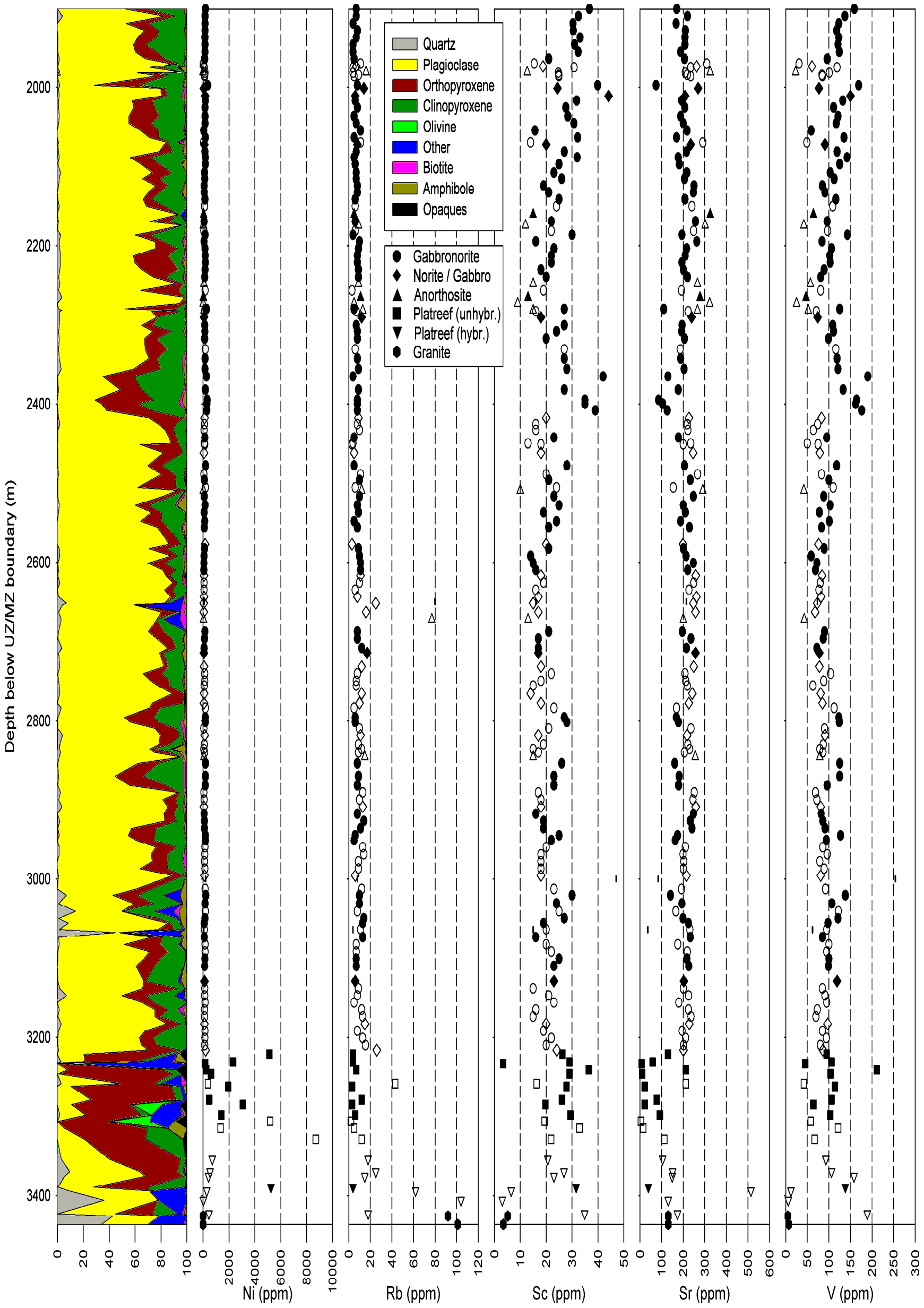

Figure 41: (continued)

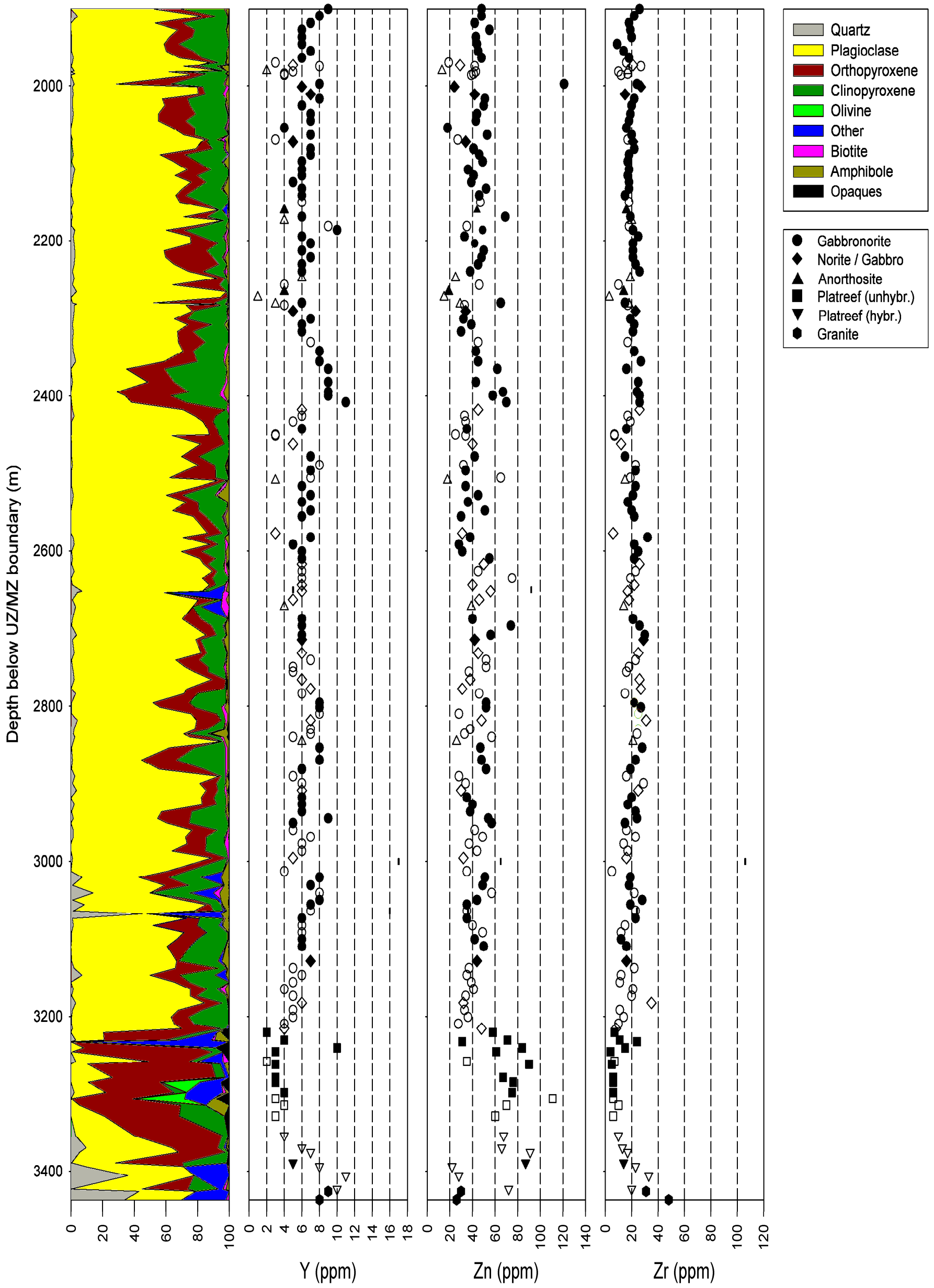

Figure 41: (continued)

Table 5: Distribution coefficients for selected trace elements into plagioclase, orthopyroxene, clinopyroxene and olivine for basaltic liquids.

	Plagioclase	Orthopyroxene	Clinopyroxene	Olivine
Ba	0.68[b]	$<1.11 \times 10^{-5}$[i]	0.00068[g]	
Co	0.03[b]	2[a]	1.2[a]	3.1[b]
Cu	<0.1[b]	<0.1[b]	<0.1[b]	
Cr	0.02[c]	3.7-17[j]	13[c]	1.1[c]
Ga	1.7[b]		<0.25[b]	
Ni	0.06[c]	1.1[d]	2.6[d]	
Rb	0.1[e]	0.0006[e]	0.011[e]	
Sc	0.008[b]		3.3[b]	
Sr	2[e]	0.007[e]	0.067[e]	
V	0.1[c]	0.3[a]	1.5[a]	
Y	<0.282[f]		0.467[g]	
Zn	0.13[b]		0.49[b]	1.8[b]
Zr	0.0127[f]	0.02[h]	0.123[g]	

References: a) Frey et al. (1978); b) Paster et al. (1974); c) Bougault & Hekinion (1974); d) Mysen (1978); e) McKenzie & O'Nions (1991); f) Bindeman et al. (1998); g) Hart & Dunn (1993); h) Keleman & Dunn (1992); i) Beattie (1993); j) Ewart et al. (1973)

The highest Cu content was recorded in the melagabbronorite from depth 3389.04 m, with a Cu content of 4836 ppm.

Whole-rock Ga varies between ~10-20 ppm in the Main Zone and shows a fairly well defined negative correlation with MgO, reflecting its preference for plagioclase over the pyroxenes. The concentration of Ga within the unhybridized Platreef is generally below ~10 ppm, and typically between ~10 ppm and 24 ppm within the hybridized Platreef. The granitic footwall has whole-rock Ga of ~16 ppm.

Whole-rock Ni shows a strong positve correlation with MgO, varying between ~10 ppm in plagioclase-rich rocks to ~350 ppm in the more mafic gabbroic rocks of the Main Zone, reflecting its preference for the pyroxenes over plagioclase. Whole-rock Ni in the Platreef shows a generally positive correlation with whole-rock Cu, suggesting the presence of sulfides, the only phase into which both metals are preferentially incorporated ($D_{Cu}^{Sulfide} = 380; D_{Ni}^{Sulfide} = 4300$ (Pedersen, 1979)). In the unhybridized Platreef, whole-rock Ni concentrations vary between ~150 ppm and 8700 ppm, in the hybridized Platreef between ~20 ppm and 5250 ppm and in the granitic footwall Ni is less than ~20 ppm.

Whole-rock Rb does not vary systematically with MgO, with whole-rock concentrations typically less than ~15 ppm for the Main Zone and unhybridized Platreef, a reflection of its incompatible behaviour towards the main rock-forming minerals of the Main Zone and Platreef. In the hybridized Platreef, Rb ranges between ~15 ppm and ~100 ppm, the latter value also being recorded for the granite footwall. Notably higher Rb concentrations characterize the depth interval 2653.7-2671.7 m, where concentrations as high as 80 ppm occurs (which is linked to anomalous Ba values probably related to alteration processes), and the sample constituting the immediate hangingwall to the Platreef (3215.7 m) with a Rb concentration of 26 ppm.

For the Main Zone, Sc shows a positive correlation with whole-rock MgO, exhibiting values of between ~12 ppm in plagioclase-rich rocks and ~40 ppm in the more mafic gabbroic rocks, which reflects its preference for pyroxene over plagioclase. For the Platreef, Sc shows a negative correlation with MgO, varying between ~3 ppm and ~35 ppm for both the unhybridized and hybridized Platreef. Sc in the granite footwall averages ~4 ppm.

There exists a strong negative correlation between whole-rock Sr and MgO content, with values ranging between ~300 ppm and ~70 ppm for the Main Zone, between ~5 ppm and 210 ppm for the unhybridized Platreef, between ~40 ppm and 510 ppm for the hybridized Platreef and averaging ~130 ppm in the granite footwall. This behaviour is commensurate

with the preference of Sr for plagioclase and the relative paucity of plagioclase in the Platreef.

Whole-rock V varies between ~30 ppm for plagioclase-rich rocks and ~170 ppm for the more mafic gabbroic rocks of the Main Zone and shows a positive correlation with MgO, reflecting its preference for the pyroxenes. Whole-rock V in the unhybridized Platreef ranges between ~40 ppm and 210 ppm and between ~5 ppm and 190 ppm in the hybridized Platreef, with whole-rock V in the granitic footwall on average ~5 ppm. There appears to exist a weak negative correlation between V and MgO within the Platreef, similar to that observed for Sc, which may suggest control by a phase other than pyroxene or olivine, perhaps spinel ($D_V^{Spinel} = 5.08$ to 31.22 (Canil, 1999)).

The concentrations of Y in the bulk of the Main Zone samples analysed were <10 ppm, with whole-rock Y showing a weak positive correlation with MgO content, reflecting the higher distribution coefficient for Y into pyroxene Whole-rock Y is typically below 4 ppm in the unhybridized Platreef, but ~10 ppm in the websterite from depth 3240.7 m. The hybridized Platreef has Y ranging between ~4 and 10 ppm and the granitic footwall between ~8 and 9 ppm.

In the Main Zone, whole-rock Zn shows a well defined positive correlation with MgO content, ranging between ~25 ppm in plagioclase-rich rocks and ~70 ppm in the more mafic gabbroic rocks, reflecting the preferential incorporation of Zn into pyroxenes rather than plagioclase. Zn in the unhybridized Platreef ranges between ~30 ppm and 110 ppm, with the highest value seen in the harzburgite from depth 3305.7 m, which is a reflection of the preference for Zn into olivine. For the hybridized Platreef Zn values range between ~20 ppm and 90 ppm, whereas for the granitic footwall, whole-rock Zn is on the order of ~28 ppm.

Whole-rock Zr shows virtually no correlation with MgO, reflecting its incompatible behaviour towards plagioclase and pyroxene and therefore its preference to remain in the residual liquid Whole-rock Zr varies between ~3-35 ppm in the Main Zone samples

analysed and is generally below ~10 ppm for the bulk of the unhybridized Platreef, with higher values up to ~20 ppm noted only in the altered ultramafic rock from depth 3232.7 m and in the websterite from depth 3240.7 m. In the hybridized Platreef there is a generalized tendency for whole-rock Zr to increase with depth from ~10 ppm to ~30 ppm, with the granitic footwall exhibiting Zr ranging between ~30 ppm and 50 ppm.

Whole-rock U in the Main Zone and Platreef is generally below the detection limit of 2 ppm, with higher values up to ~8 ppm only seen in the lower part of the hybridized Platreef and granitic footwall.

3.2.3 Interelement ratios

Mitchell (1986) used a number of interelement ratios to assess fractionation trends in the lower Main Zone, which will also be used here for comparison (Figure 42). The petrological significance of the different ratios has been adequately discussed by Mitchell (1986) and is summarized here as follows:

- The Cr/Sc ratio of a magma crystallizing clinopyroxene will tend to decrease as fractionation proceeds in the absence of a spinel phase, because $D_{Cr}^{Cpx} > D_{Sc}^{Cpx}$.
- The V/Cr ratio of a magma crystallizing clinopyroxene will tend to increase as fractionation proceeds, because $D_{V}^{Cpx} < D_{Cr}^{Cpx}$.
- The Ni/Co ratio of a magma crystallizing pyroxene will tend to decrease as fractionation proceeds, because $D_{Ni}^{Px} > D_{Co}^{Px}$.
- The Ba/Sr ratio of a magma crystallizing plagioclase will tend to increase as fractionation proceeds, because $D_{Sr}^{Plag} > D_{Ba}^{Plag}$.

The Cr/Sc ratio of the Main Zone rocks below a depth of ~2664 m shows a fair amount of scatter, ranging from a high of ~19 to ~3 and showing a generalized decrease upwards. From a depth of ~3128.7 m up to depth ~3012.7 m, samples exhibiting intergranular texture record an increase in the Cr/Sc ratio from 5.4 to 13.6, with samples exhibiting textures other than intergranular texture not conforming strictly to this trend.

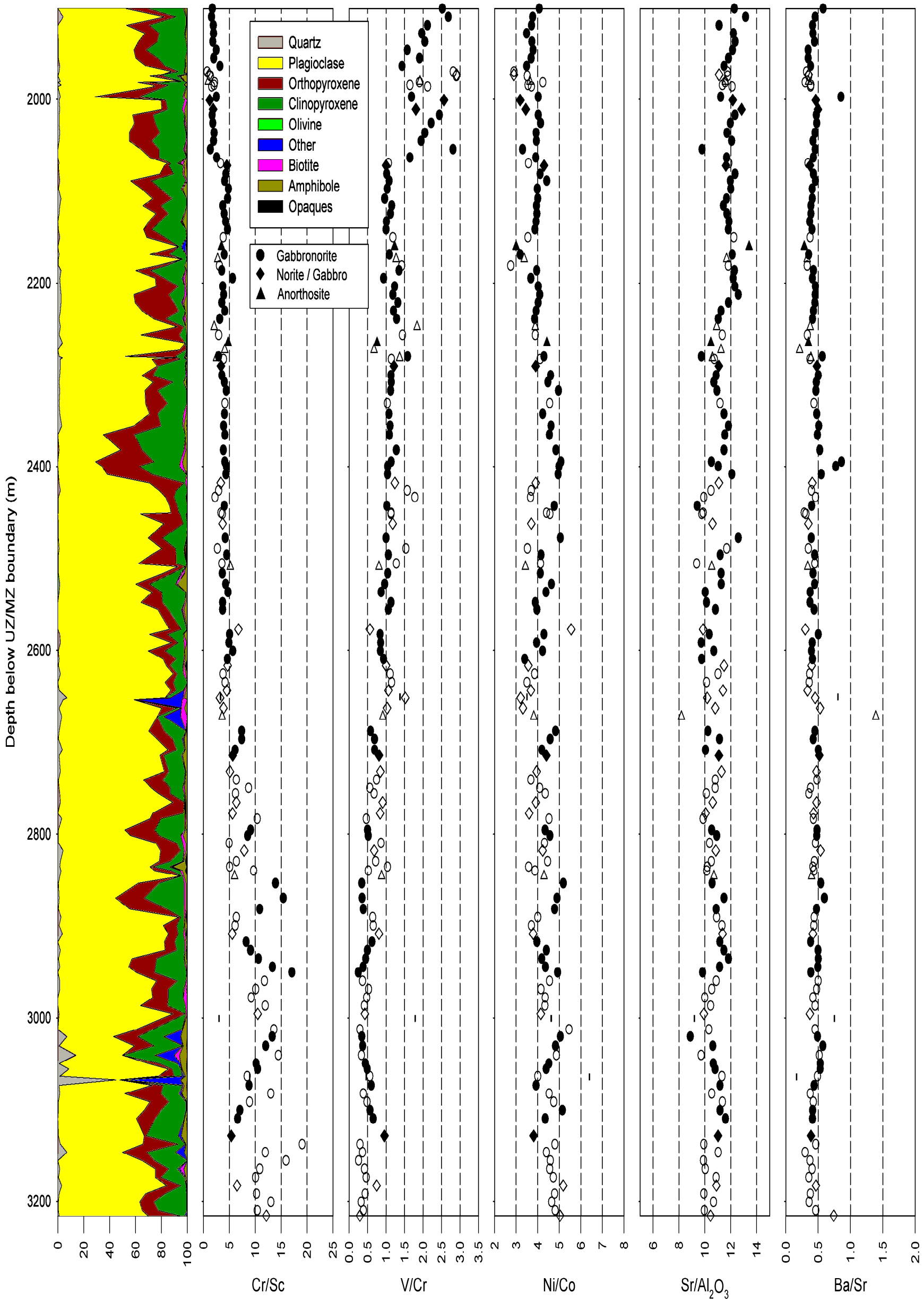

Figure 42:Plots of Cr/Sc, V/Cr, Ni/Co, Sr/Al_2O_3 and Ba/Sr in Main Zone whole-rocks versus depth. Modal mineralogy shown for comparison.

A similar albeit reversed trend is evident in samples between depths 2950.7 m and 2917.7 m, which exhibits an upward decline in Cr/Sc ratio from 17 to 8.3. Above ~2664 m, the Cr/Sc ratio remains fairly constant at ~4, shifting to ~2 at a depth of ~2064 m and remaining at around this level to the top of the core.

V/Cr in the Main Zone mirrors the behaviour of Cr/Sc, albeit in an opposite sense. As an example, the depth interval 3128.7 m to 3012.7 m shows an upward decrease in V/Cr from ~1 to ~0.3, which is coupled to upward increasing Cr/Sc as highlighted above. The overall trend in V/Cr for the Main Zone is an upward increasing one, from values as low as ~0.25 to as high as ~2.9. The behaviour of Cr/Sc at depth ~2064 m is mirrored by V/Cr, which shows an upward shift from values of ~1 to values of ~2 over this interval.

For the most part, the behaviour of Ni/Co is analogous to that of Cr/Sc, with values for the Main Zone typically ranging between ~2.8 and 6.4. Sr/Al_2O_3 shows a fair amount of scatter and little variation for the Main Zone up to depth ~2264 m, with values typically ranging between ~10 and ~12, whereas above ~2264 m, the amount of scatter decreases, with Sr/Al_2O_3 between ~11 and ~12. Ba/Sr too shows little variation over the Main Zone, with values ranging between ~0.2 and ~1.4 (average 0.4).

The interelement ratios considered thus far were for trace elements exhibiting compatible or at least partly compatible behaviour towards plagioclase and/or pyroxene. The variation with depth in ratios of some trace elements usually considered to be incompatible is presented in Figure 43, with the data for Ce, Sm and Th drawn from Appendix J. Ce/Sm in the Main Zone ranges between 7.5 and 13.7 and is on average ~10.9, whereas values range between 4.3 and 15.8 for the unhybridized Platreef with an average of ~8.6. The hybridized Platreef records an upward decrease in Ce/Sm with values ranging between that of the granite footwall (average Ce/Sm of 13.9) and the unhybridized Platreef.

Th/Sm in the Main Zone varies between 0.5 and 2.0 (average 1.1) and in the unhybridized Platreef between 0.1 and 1.1 (average 0.7). As for Ce/Sm, Th/Sm records an upward decrease in the hybridized Platreef with values between that of the

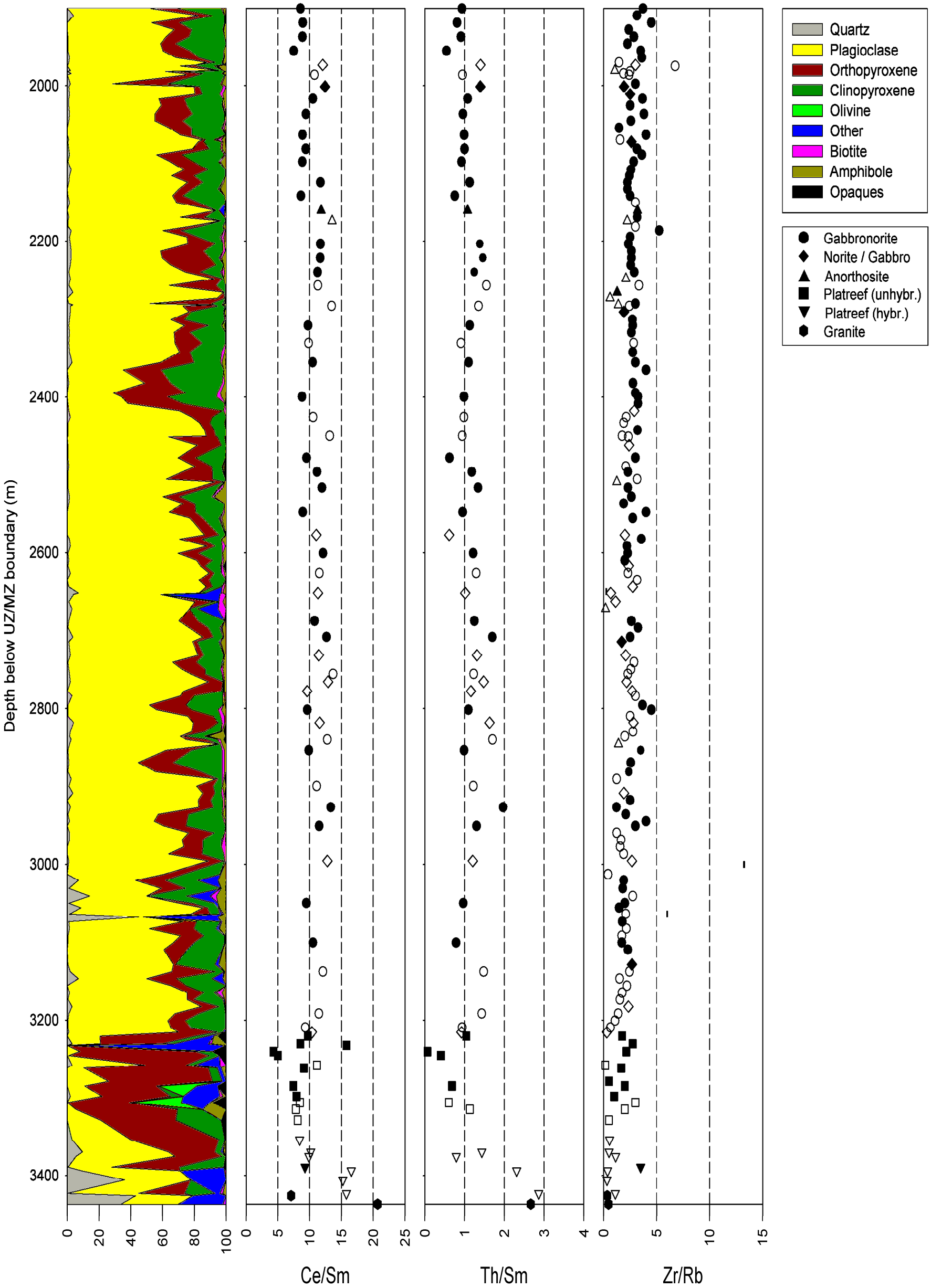

Figure 43: Plots of Ce/Sm, Th/Sm and Zr/Rb in whole-rocks versus depth. Modal mineralogy shown for comparison.

granite footwall (Th/Sm ~2.7) and the unhybridized Platreef. Zr/Rb in the Main Zone varies between 0.2 and 13.2 with an average of 2.5 and in the unhybridized Platreef between 0.2 and 3.0 with an average of 1.6. Zr/Rb in the granite footwall is ~0.4 and the hybridized Platreef exhibits values ranging between 0.3 and 3.5.

3.2.4 Summary of noteworthy findings

Whole-rock major and trace element compositions of the Main Zone and Platreef for the most part reflect changes in modal mineralogy, as expected. Whole-rock geochemical parameters such as whole-rock Mg#, plagioclase An% calculated from the norm and the modified differentiation index (MDI) all support the assertion that the lower Main Zone as exposed by the MO-1 drill hole shows very little overall differentiation, which may be interpreted as being the result of multiple influxes of magma. Multiple injection cycles within the Main Zone are also borne out by variations in the ratios of certain compatible trace elements such as Cr/Sc and V/Cr, both of which are indicators of pyroxene fractionation, but their behaviour is decoupled from the behaviour of ratios reflecting plagioclase fractionation such as Ba/Sr and Sr/Al_2O_3, which shows very little variation over the studied succession of Main Zone rocks. From a comparative viewpoint, even the variation in Cr/Sc and V/Cr is less pronounced than that observed at other localities within the Bushveld Complex, such as at Union Section, where Mitchell (1986) reports Cr/Sc values of 0.3-107 and V/Cr values of <0.35-19.4 in Main Zone rocks below the Pyroxenite Marker, compared to values typically covering the range 0.7-19 and 0.3-2.9, respectively, within the Main Zone rocks of MO-1.

Incompatible trace element ratios such as Ce/Sm, Th/Sm and Zr/Rb do not show extreme variation over the studied succession, but clearly indicate interaction between the Platreef and its granitic footwall as shown by distinct trends within the hybridized Platreef ranging from values similar to that of the unhybridized Platreef at its top and values typical of the granitic footwall at its bottom.

3.3 Whole-rock rare-earth element geochemistry

Lanthanide, uranium and thorium concentrations for the analysed rocks are presented in Appendix J, with the variation of the REEs with whole-rock MgO shown in Figure 44.

3.3.1 The Main Zone

The Main Zone has La concentrations covering the range 8-39 times chondrites and Lu concentrations covering the range 2-7 times chondrites* (Figure 45), with all rocks being slightly enriched with respect to the LREEs (Ce/Sm_N on average 2.65). The rocks show virtually no fractionation of the HREEs with Tb/Yb_N being on average 1.25. Most samples have positive europium anomalies, which is consistent with the abundance of plagioclase in the rocks (Eu/Eu^* on average 1.48).

3.3.2 The Platreef and its footwall

The unhybridized Platreef rocks have La concentrations covering the range 3-13 times chondrites and Lu concentrations covering the range 1-5 times chondrites (Figure 46). Their Ce/Sm_N ratios range from ~1.2 to ~2.7 and their Tb/Yb_N ratios between ~0.8 and 1.7. Eu/Eu^* values range between ~0.7 and ~2.1. Two samples from the unhybridized Platreef package have anomalous REE concentrations, the first being the websterite from depth 3240.7 m, with REE concentrations between ~7 and ~16 times chondrites and a largely unfractionated REE pattern (Ce/Sm_N = 1.05 and Tb/Yb_N = 1.49). The other sample showing REE concentrations and patterns not following the mainstream behaviour of rocks for the unhybridized Platreef is the altered ultramafic from depth 3232.7 m, with REE concentrations covering the range ~0.1 to ~2.0 times chondrites and a trough shaped REE pattern with a prominent Tb spike (Ce/Sm_N = 3.86 and Tb/Yb_N = 2.17).

* The normalization factors of Anders & Grevesse (1989) are used throughout where chondrite-normalized patterns are shown and discussed.

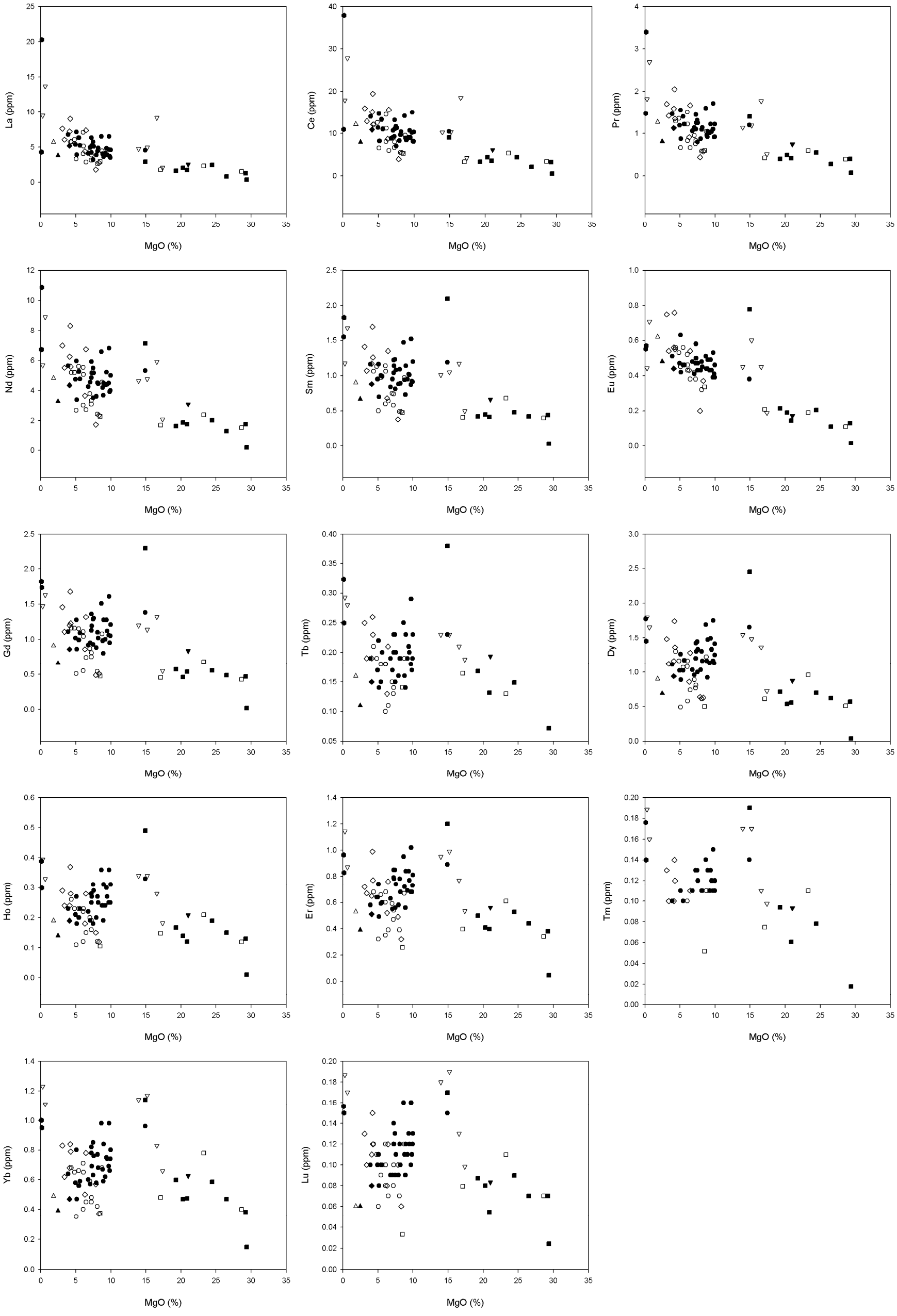

Figure 44: Binary variation diagrams of the REE versus MgO. See Figure 33 for explanation of symbols used.

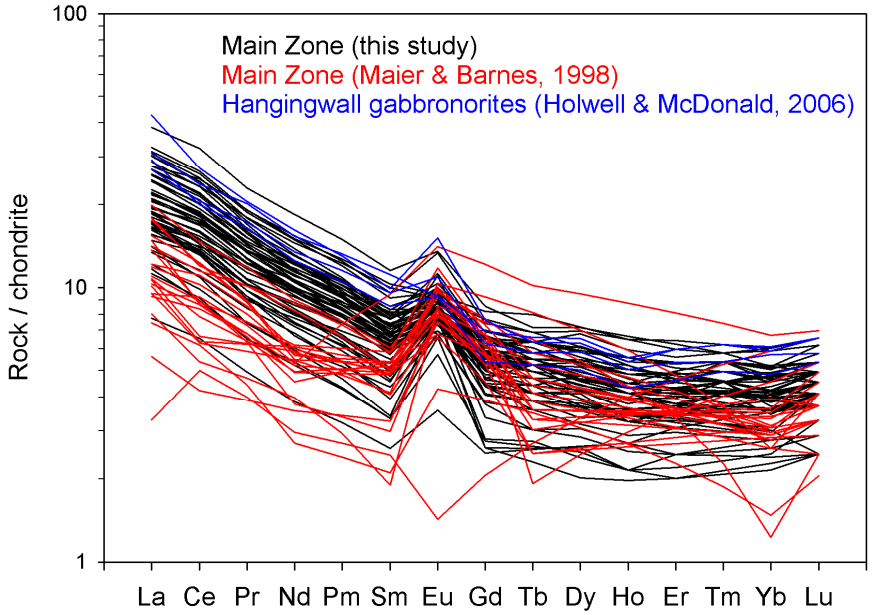

Figure 45: Chondrite normalized REE abundances of Main Zone rocks of the Moordkopje drill core, at Union Section (Maier & Barnes, 1998) and of hangingwall gabbronorites at Overysel (Holwell & McDonald, 2006).

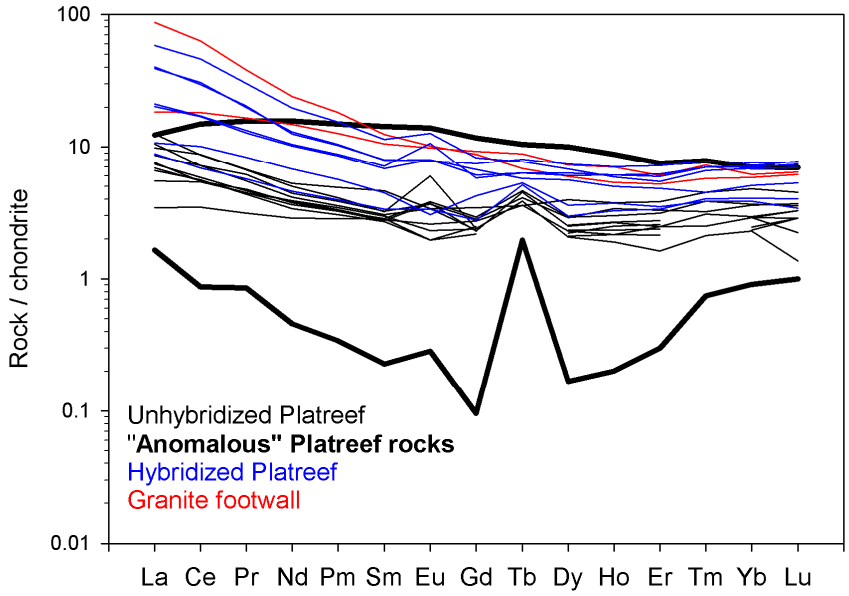

Figure 46: Chondrite normalized REE abundances in the unhybridized and hybridized Platreef and granite footwall as intersected by the Moordkopje drill core.

The hybridized Platreef rocks have La concentrations covering the range 8-58 times chondrites and Lu concentrations covering the range 4-8 times chondrites, with Ce/Sm_N ratios ranging between ~2.0 and ~4.0, Tb/Yb_N ratios between ~0.9 and ~1.4 and Eu/Eu^* values ranging between ~0.7 and ~1.7.

There is considerable overlap between the REE patterns of the hybridized Platreef and unhybridized Platreef rocks at lower REE concentrations and the hybridized Platreef and the granitic footwall at higher REE concentrations. La concentrations for the latter cover the range 18-87 times chondrites and with Lu concentrations of 6-8 times chondrites, with Ce/Sm_N ratios of between ~1.7 and 5.0 and Tb/Yb_N ratios of ~1.3. The footwall is further characterized by the absence of an europium anomaly.

3.3.3 Summary of noteworthy findings

The Main Zone rocks analysed for REE have concentrations overlapping those of Main Zone rocks from other localities within the Bushveld Complex (e.g. Maier & Barnes, 1998; Holwell & McDonald, 2006). For the Platreef, the REE concentrations of the hybridized Platreef are intermediate between those of the unhybridized Platreef and the granitic footwall, suggesting assimilation of granitic footwall material by the intruding Platreef magmas, as was also proposed by Barton et al. (1986).

3.4 Geophysical properties

Due to the size of the geophysical dataset collected, the data are not reported as an Appendix but is summarized graphically in Figure 47.

3.4.1 The Main Zone

In-situ density values for the Main Zone as determined by down-the-hole logging range between 2.15 $g.cm^{-3}$ and 4.12 $g.cm^{-3}$, with the densities as determined in the laboratory on selected Main Zone samples exhibiting a narrower range of between 2.73 $g.cm^{-3}$ and 3.16 $g.cm^{-3}$. A comparison of these rock density values with the densities of the main constituents of the rocks, viz. plagioclase (2.62 - 2.76 $g.cm^{-3}$), clinopyroxene (2.96 – 3.52

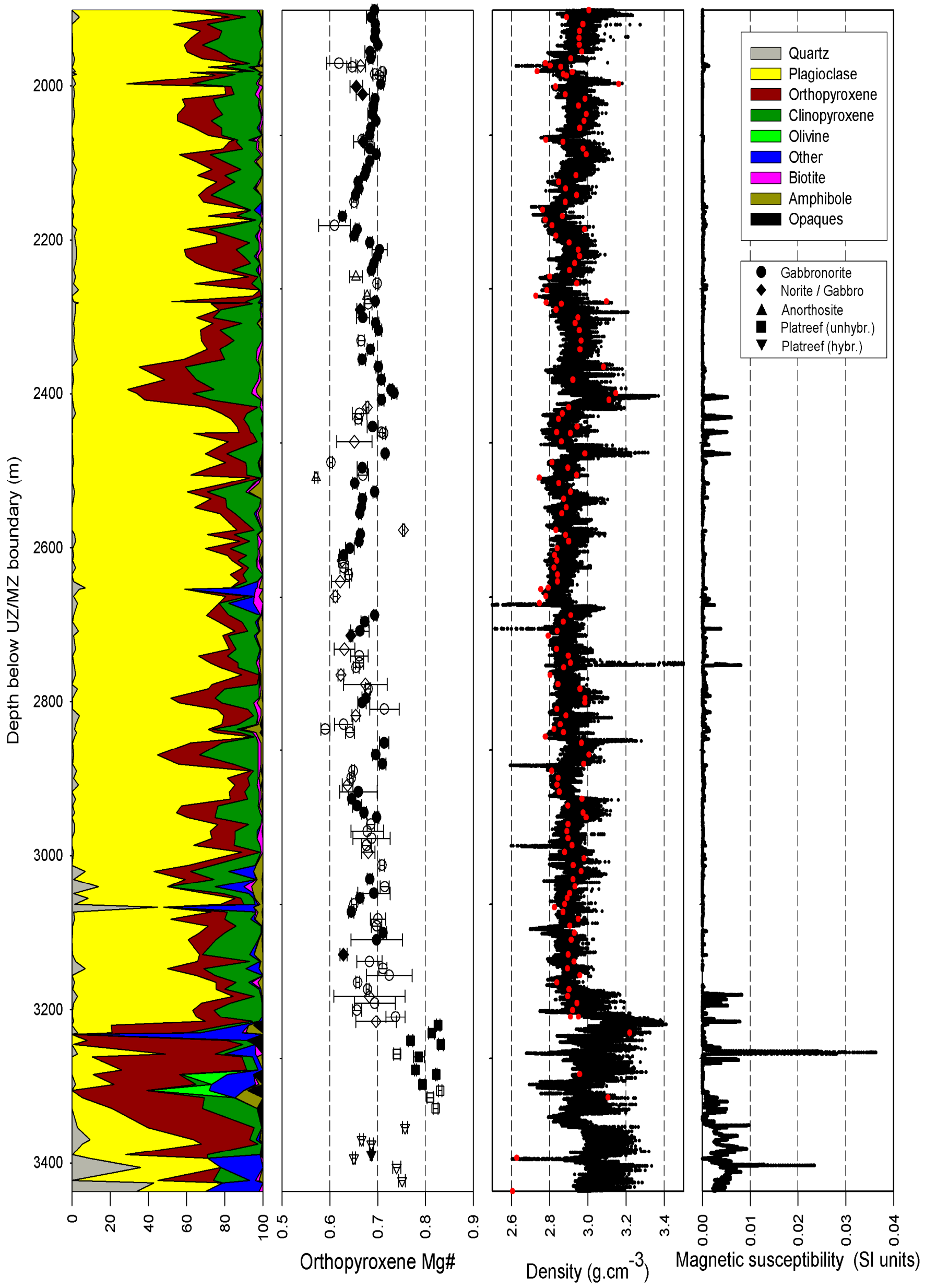

Figure 47: Variation in modal mineralogy, orthopyroxene Mg#, density and magnetic susceptibility with depth. Red symbols on density plot are density values as obtained in the laboratory.

g.cm^{-3}) and orthopyroxene (3.21 – 3.96 g.cm^{-3}) as listed by Deer et al. (1980), suggests that the in-situ measurements at least locally need some clarification.

Density values lower than ~2.6 g.cm^{-3} were recorded in only two narrow intervals at depths of ~2674 m and ~2706 m. No samples were collected of either of these intervals, however, the original core log (Appendix A) makes mention of "highly altered, serpentinised mottled norite, with a pinkish tinge to the feldspars, with numerous thin, irregular, subvertical veining" over the depth interval 803.20 – 807.80 m (as per original core log) and of "a zone of serpentinite and pinkish quartzofeldspathic material" over the depth interval 838.48 – 838.75 m (as per original core log). The presence of quartzofeldspathic veining and associated alteration zones however still cannot adequately explain density values as low as 2.15 g.cm^{-3}, and similar veining elsewhere in the core also did not show up as very low density intervals, which opens the possibility that intervals exhibiting density values lower than ~2.6 g.cm^{-3}, although volumetrically unimportant, may be due to localized instrumental shortcomings or difficulties.

Density values higher than ~3.4 g.cm^{-3} were similarly confined to a narrow interval at depth ~2752 m and could possibly also be ascribed to instrumental shortcomings. However, the same interval is also characterized by elevated magnetic susceptibility values up to ~0.01 SI units, which could be indicative of the presence of magnetite (5.2 g.cm^{-3}), but a density of ~4.15 g.cm^{-3} as seen at a depth of 2752 m would require the presence of ~50% magnetite in an otherwise gabbronoritic matrix, making these density values also suspect.

In general, the density data vary systematically with observed mineral modes (Figure 47), with the more mafic samples exhibiting higher densities than the more leucocratic, plagioclase-rich varieties. There is remarkable cyclicity in the density data similar to that described by Ashwal et al. (2005), which is especially apparent above a depth of ~2464 m. Intervals exhibiting reversed differentiation trends (for example increasing Mg# of orthopyroxene up sequence) are typically characterized by increasing density up sequence, which is reflected in up sequence increases in the ratio of pyroxene to plagioclase.

Magnetic susceptibility values for the Main Zone as determined in-situ are invariably below 0.01 SI units, reflecting the paucity of minerals such as magnetite within the Main Zone. The integrity of the in-situ measured magnetic susceptibility values are supported by the laboratory measurements conducted on selected samples, the highest of which had a magnetic susceptibility of 0.008 SI units and by the data of Ashwal et al. (2005) for Main Zone rocks from the Bellevue drill core which invariably had magnetic susceptibilities below 0.05 SI units and generally below 0.02 SI units.

3.4.2 The Platreef and its footwall

In-situ density values for the Platreef as determined by down-the-hole logging range between 2.61 $g.cm^{-3}$ and 3.41 $g.cm^{-3}$, with the densities as determined in the laboratory on selected samples exhibiting a narrower range of between 2.61 $g.cm^{-3}$ and 3.22 $g.cm^{-3}$, the former representing the density of the granitic footwall. On average, the density of Platreef rocks is slightly higher than the rocks of the Main Zone, reflecting the lower plagioclase content of the former in general. Magnetic susceptibility values for the Platreef are as high as ~0.04 SI units, but typically less than ~0.01 SI units. On average however, the magnetic susceptibility of Platreef rocks exceeds that of Main Zone rocks and this is probably largely attributable to the presence of minor secondary magnetite formed during serpentinisation of olivine, which is a local constituent of the Platreef and / or the presence of sulfides.

3.5 Radiogenic isotope geochemistry

The concentrations of Rb and Sr and the $^{87}Sr/^{86}Sr$ ratios of whole-rocks and mineral separates selected for analysis are presented in Appendix M, with Sm and Nd concentrations and $^{143}Nd/^{144}Nd$ ratios for the selected samples presented in Appendix N. Rb-Sr and Sm-Nd isochron diagrams are presented in Figures 48 - 53 and the variation in initial $^{87}Sr/^{86}Sr$ and $^{143}Nd/^{144}Nd$ (calculated for an age of 2.06 Ga) with depth are presented in Figure 54. Two intervals from the Main Zone (viz. 2063.66 m to 2212.63 m and 2547.91 m to 2696.44 m) showing reversed differentiation trends in terms of orthopyroxene Mg# were chosen for detailed isotopic characterization in an attempt to elucidate possible mechanisms for reversals of this sort. The implications of the results were, however, more profound than initially expected, as will be discussed in subsequent sections.

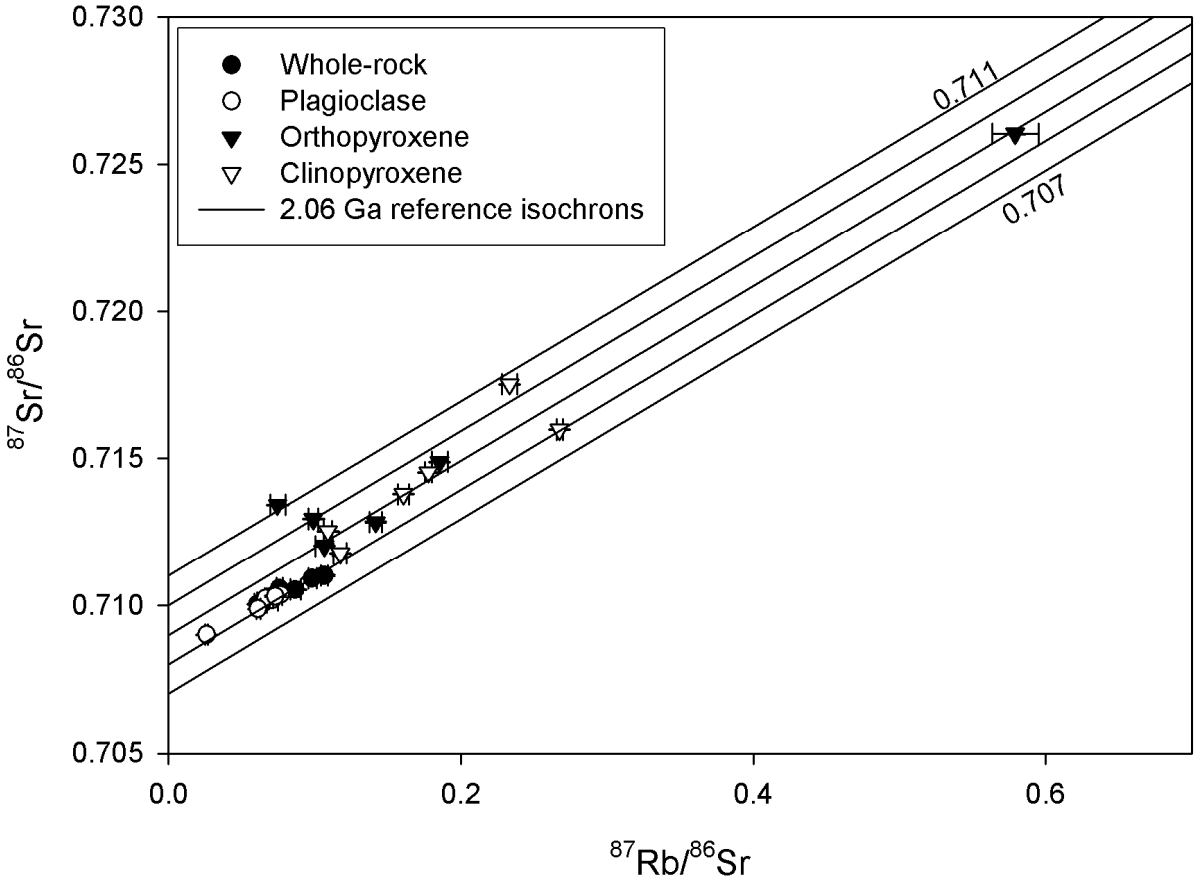

Figure 48: Rb-Sr isochron diagram for whole-rocks and mineral separates covering the depth interval 2063.66 m to 2212.63 m.

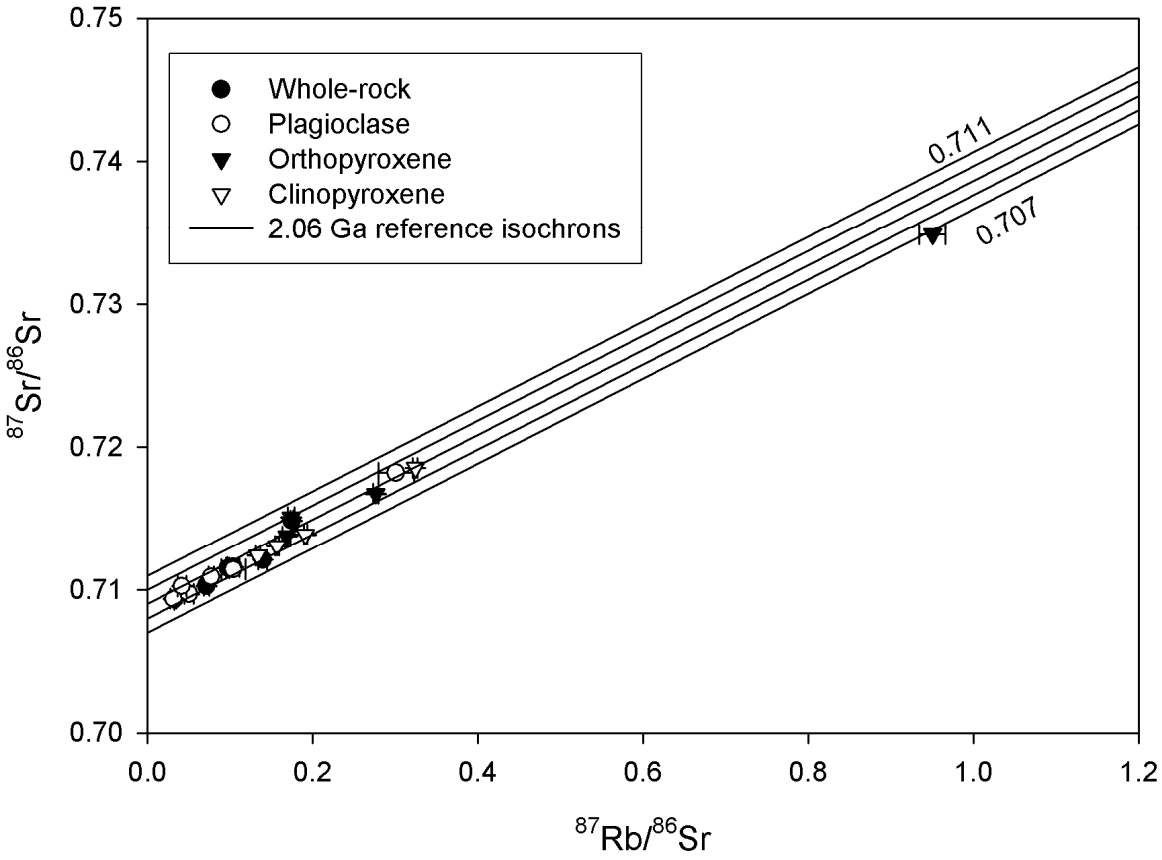

Figure 49: Rb-Sr isochron diagram for whole-rocks and mineral separates covering the depth interval 2547.91 m to 2696.44 m.

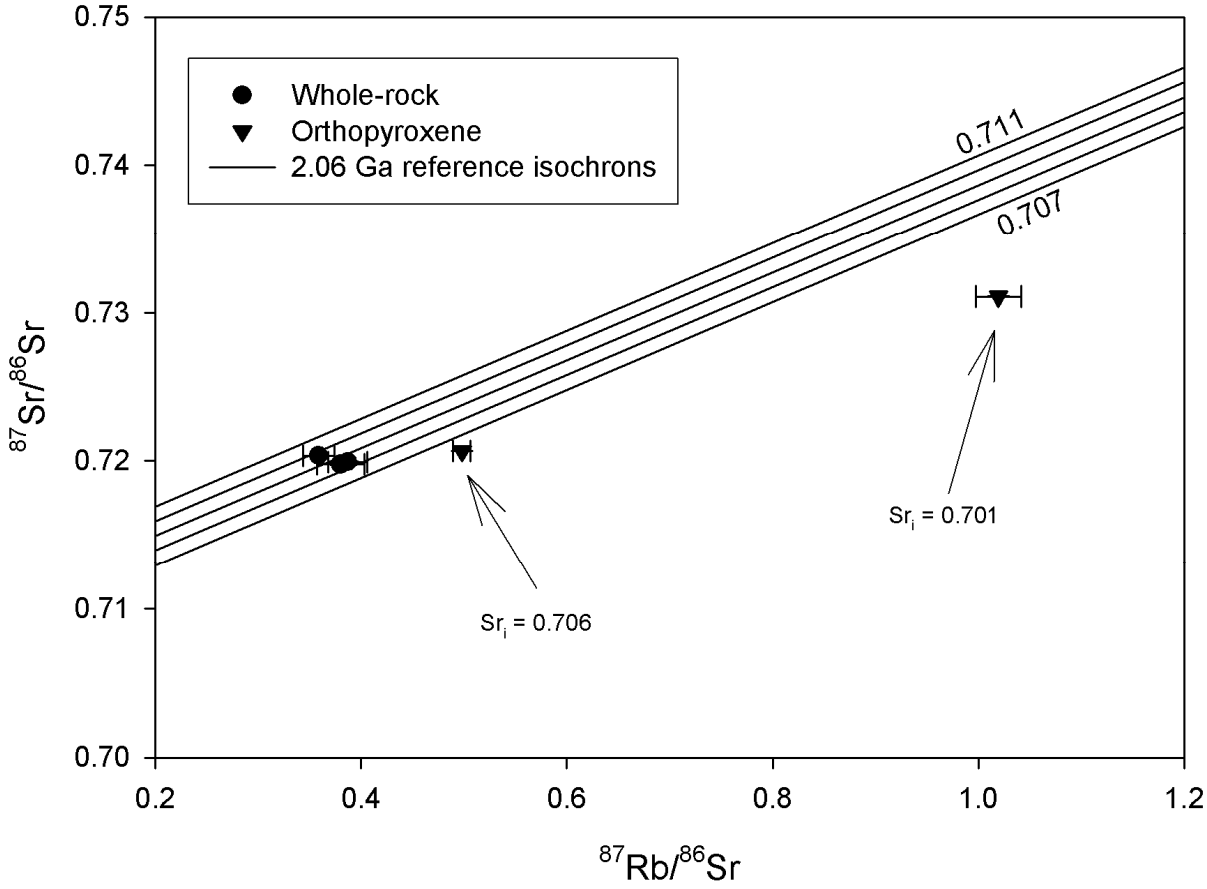

Figure 50: Rb-Sr isochron diagram for whole-rocks and orthopyroxene mineral separates for selected unhybridized Platreef samples.

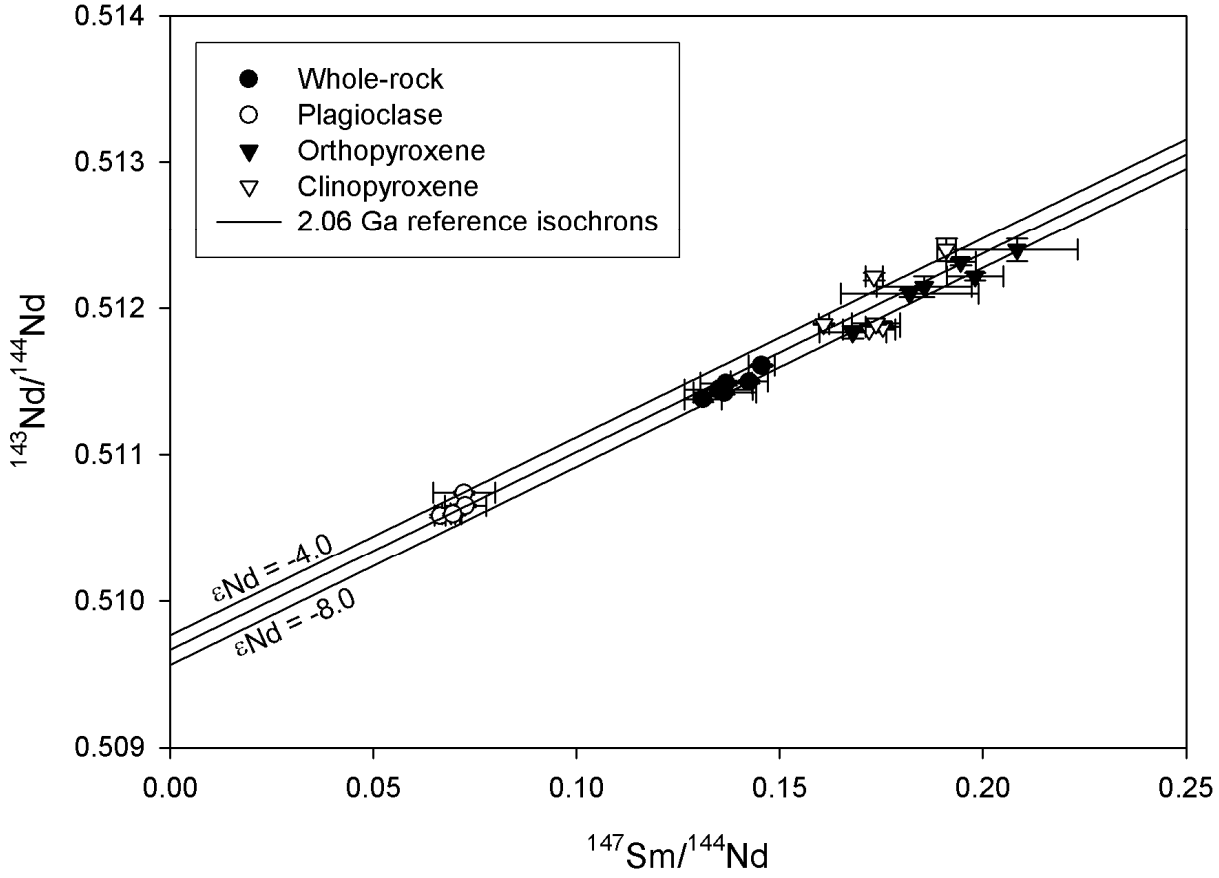

Figure 51: Sm-Nd isochron diagram for whole-rocks and mineral separates covering the depth interval 2063.66 m to 2212.63 m.

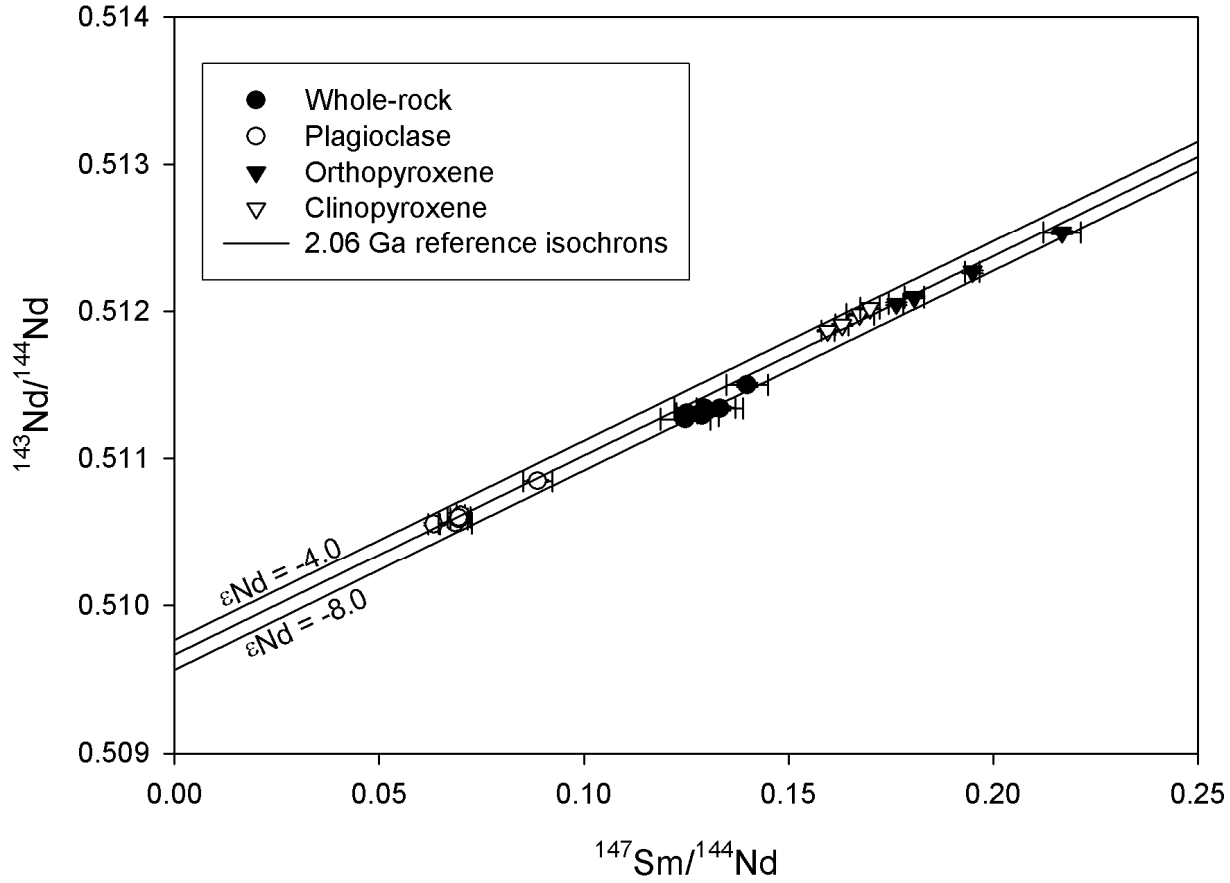

Figure 52: Sm-Nd isochron diagram for whole-rocks and mineral separates covering the depth interval 2547.91 m to 2696.44 m.

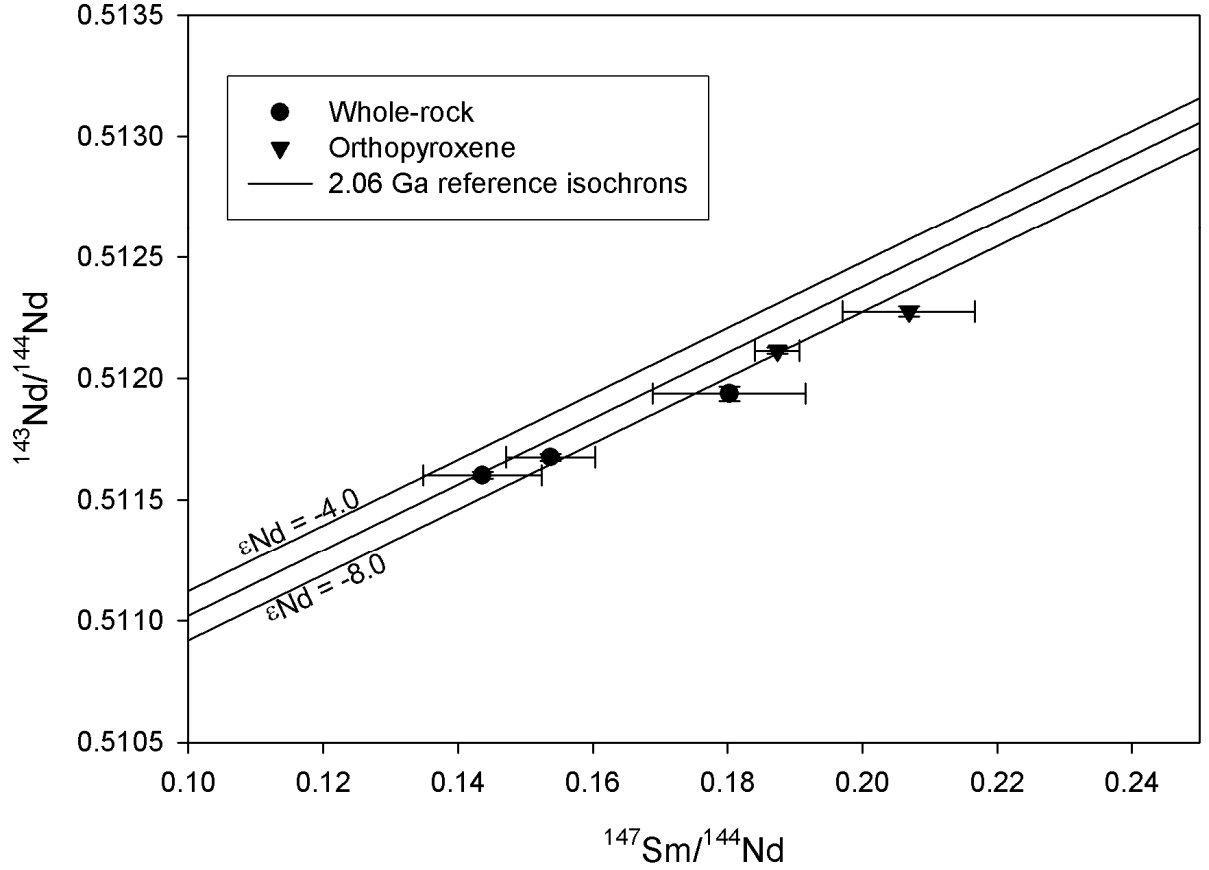

Figure 53: Sm-Nd isochron diagram for whole-rocks and orthopyroxene mineral separates for selected unhybridized Platreef samples.

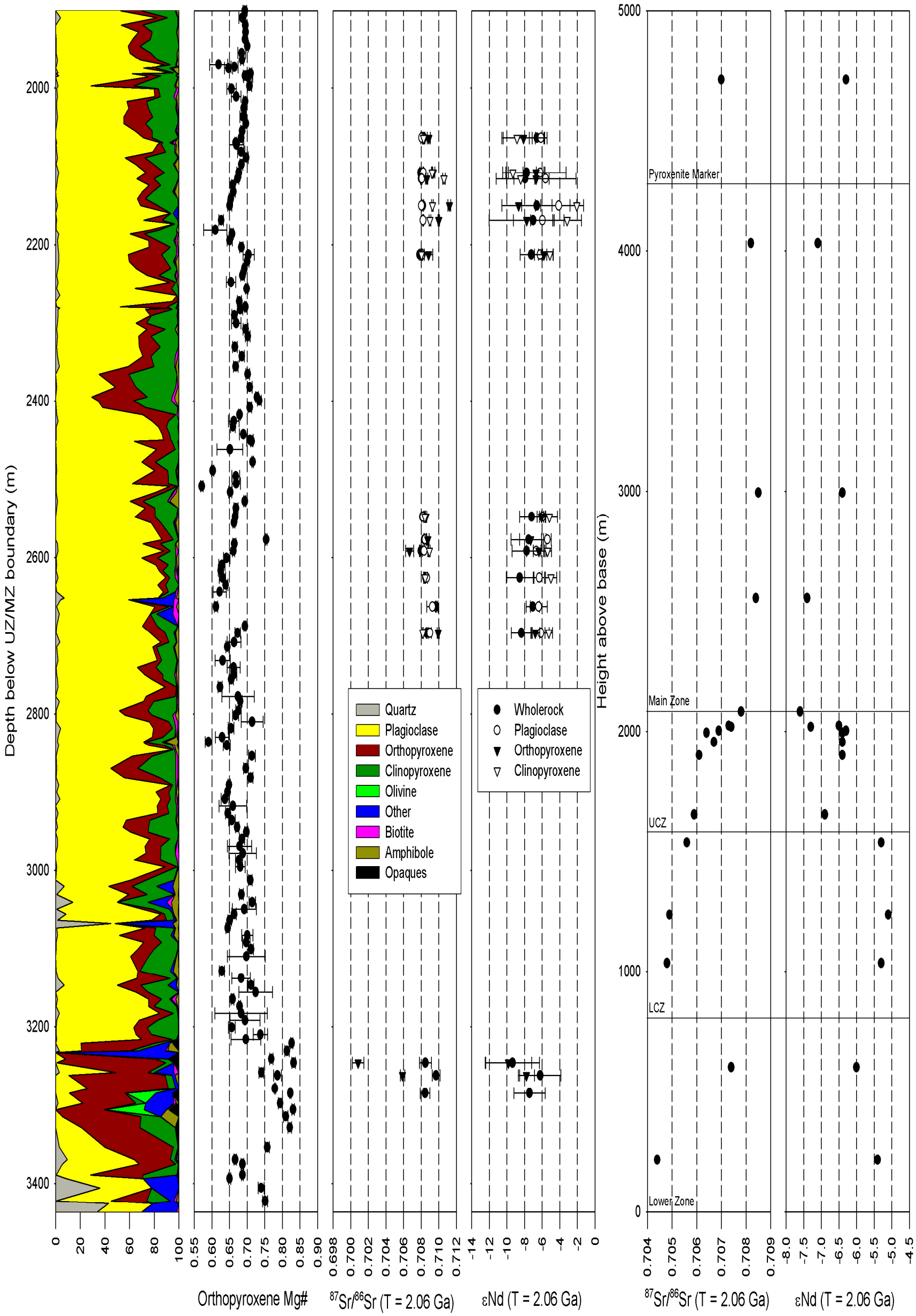

Figure 54: Variation in initial $^{87}Sr/^{86}Sr$ ratio and εNd in the rocks and mineral separates of the MO-1 drill core with depth.The two plots on the right show the variation in initial $^{87}Sr/^{86}Sr$ ratio and εNd for rocks from the main body of the Bushveld Complex as presented by Maier et al. (2000).

Plagioclase and whole-rocks from the upper part of the Main Zone exhibit an approximate isochron relationship for the Rb-Sr system with an implied age of 1752 ± 240 Ma and initial $^{87}Sr/^{86}Sr$ ratio (hereinafter referred to as Sr_i) of ~0.7084, with Sr_i values for co-existing ortho- and clinopyroxenes scattered between ~0.7080 and ~0.7112. For the Sm-Nd system, whole-rocks, plagioclase and the pyroxenes over this interval generally all exhibit an approximate isochron relationship with an implied age of 2011 ± 130 Ma and εNd of -5.3.

Plagioclase and whole-rocks from the deeper part of the Main Zone (viz. 2547.91 m to 2696.44 m) exhibit an approximate isochron relationship for the Rb-Sr system with an implied age of 2311 ± 300 Ma and Sr_i of ~0.7082, with Sr_i for co-existing ortho- and clinopyroxenes scattered between ~0.7067 and ~0.7100. For the Sm-Nd system, whole-rocks, plagioclase and the pyroxenes over this interval generally all exhibit an approximate isochron relationship with an implied age of 2062 ± 78 Ma and εNd of -7.3.

The Platreef has whole-rocks with Sr_i ranging between 0.7084 and 0.7097 and orthopyroxene with Sr_i ranging between 0.7008 and 0.7059, with no samples defining an approximate isochron relationship. For the Nd isotopes, however, the samples define an approximate isochron relationship with an implied age of 1830 ± 270 Ma and εNd of -3.3, with calculated εNd for individual whole-rocks and orthopyroxenes from the Platreef ranging between -6.2 and -9.8.

In the upper part of the Main Zone, over the depth interval 2063.66 m to 2212.63 m, whole-rocks and co-existing plagioclase have fairly constant Sr_i of between 0.7078 and 0.7083. Significant Sr isotopic disequilibrium is however apparent in co-existing ortho- and clinopyroxene when compared to plagioclase or whole-rocks, the magnitude of which is greatest towards the middle of this interval (with orthopyroxene Sr_i of up to 0.7112) and which diminishes towards the top and bottom of the interval. Nd isotopic disequilibrium between co-existing silicates and whole-rocks is not apparent over this interval, with εNd ranging between -2.1 and -9.3.

For the lower interval, Nd also does not show significant disequilibrium, with εNd for whole-rocks and their constituent minerals ranging between -5.0 and -8.5, which falls within the range of εNd values seen in the upper part of the Main Zone. In terms of Sr_i, however, plagioclase and whole-rocks show considerable variation over this interval, with Sr_i varying between 0.7080 and 0.7097 but with Sr_i for whole-rocks and constituent plagioclase generally overlapping at the 2-σ error level. For most samples, there appears to be little or no Sr isotopic disequilibrium between co-existing plagioclase and pyroxenes, although some do exhibit notable disequilibrium, e.g. the sample from depth 2591.7 m has orthopyroxene with Sr_i of 0.7067 co-existing with plagioclase and clinopyroxene with Sr_i of 0.7083 and 0.7089, respectively, and the sample from depth 2696.44 m which has orthopyroxene with Sr_i of 0.7100 co-existing with plagioclase and clinopyroxene with Sr_i of 0.7090 and 0.7082, respectively.

The existence of isotopic disequilibrium between co-existing plagioclase and pyroxene within the Main Zone necessitates a mechanism whereby plagioclase and pyroxene could crystallize from isotopically distinct magmas and then be incorporated into the same rock. The remainder of this thesis will be largely concerned with developing a model to account for this phenomenon, one which has not yet been described for the Main Zone of the Bushveld Complex.

4. DISCUSSION

4.1 The Main Zone

4.1.1. Stratigraphic positioning and comparison

Comparatively little is known about the layered rocks of the Northern Limb apart from the recent study by Ashwal et al. (2005), which concentrated on the Upper Zone and upper Main Zone. The Platreef has also been the subject of a considerable amount of research (Kruger, 2005). In the following exposition I will highlight the differences and similarities between the Main Zone as present in the Northern Limb and the main body of the intrusion.

The Bellevue drill core described by Ashwal et al. (2005) sampled the upper 1270 m of Main Zone rocks occurring to the west of the Moordkopje hole, with the core ending in a 204.4 m thick troctolitic horizon belonging to Van der Merwe's (1978) Plagioclase-clinopyroxene and olivine Subzone. This horizon was not sampled by the

Moordkopje hole and based on the thickness of Main Zone rocks sampled by the hole (~1352 m), the thickness of the Main Zone in the Northern Limb has to be at least ~2620 m. When correcting the thickness of Main Zone rocks sampled by the Moordkopje drill core for dip, assuming a mean dip of 17.5° as suggested by Ashwal et al. (2005), the thickness of the Main Zone sampled computes to ~1290 m, assuming a perfectly vertical borehole, in which case the thickness of the Main Zone would be ~2560 m. However, it is not uncommon for boreholes to follow a path roughly perpendicular to the layering, in which case no depth correction is necessary (Gordon Chunnett, pers. comm.). Furthermore, I estimate from surface geology that about 490 m of Main Zone stratigraphy is left unaccounted for between the end of the Bellevue drill core and the start of the Moordkopje drill core, in which case the Main Zone is estimated at ~3110 m thick, in comparison to thicknesses of 3940 m and 2860 m reported by Von Gruenewaldt (1971) and Molyneux (1970), respectively, for the Eastern Limb and 2380 m by Van der Merwe (1978) for the Northern Limb (see Folder 1).

Van der Merwe (1978) noted a "reasonable petrographic resemblance" between the Main Zone of the Northern Limb and that of the main body of the intrusion, but also noted that the "sequence of rocks constituting the Main Zone at Potgietersrus differs from that of the rest of the Bushveld Complex". Well-known marker horizons from the Eastern and Western Limbs such as the Porphyritic Gabbro Marker, the Main and Upper Mottled Anorthosites and the Pyroxenite Marker do not appear to have correlates in the Northern Limb. The troctolite described by Ashwal et al. (2005), similarly does not have correlates within the Eastern and Western Limbs, although Kruger (2005) is of the opinion that the trocolite represents the "proximal part" of the Pyroxenite Marker as developed elsewhere. Kruger (2005) also suggests, solely based on isotopic constraints, that the troctolite represents the top of the Main Zone within the Northern Limb, a suggestion which is unsupported by mineralogical criteria.

Changes in the mineralogy of low-Ca pyroxene in the Eastern and Western Limbs correlate fairly well, with the basal parts of the Main Zone in these limbs generally containing orthopyroxene as the sole low-Ca pyroxene (Mitchell, 1986; Molyneux, 1970; Von Gruenewaldt, 1971). Higher up in the succession, inverted pigeonite co-exists with primary orthopyroxene until the former becomes the dominant or sole low-

Ca pyroxene up to the level of the Pyroxenite Marker, where inverted pigeonite is replaced again by primary orthopyroxene. At Union Section, inverted pigeonite joins orthopyroxene as a low-Ca pyroxene at ~850 m below the Pyroxenite Marker (Mitchell, 1986, 1990), i.e. at least ~1110 m below the Upper Zone – Main Zone boundary, whereas at Steelpoort and Roossenekal, inverted pigeonite first occurs in the succession at a level of ~1480 m and ~2700 m below the Upper Zone – Main Zone boundary (Molyneux, 1970; Von Gruenewaldt, 1971). The lower Main Zone as exposed in the Moordkopje drill core is practically devoid of inverted pigeonite, with inverted pigeonite only becoming important at ~590 m below the Upper Zone – Main Zone boundary (see Folder 1).

In terms of its En-An relations between co-existing plagioclase and orthopyroxene, the lower Main Zone of the Northern Limb is situated roughly where expected, i.e. at plagioclase compositions more calcic and orthopyroxene compositions more magnesian than the upper Main Zone as studied by Ashwal et al. (2005) (Figure 55). Its plagioclase An content and orthopyroxene Mg# is also shifted towards the high end of the fields for Main Zone rocks from the Eastern Limb (Molyneux, 1970; Von Gruenewaldt, 1971) and corresponds fairly well with the lower Main Zone at Union Section in the Western Limb (Mitchell, 1986) (Figure 56).

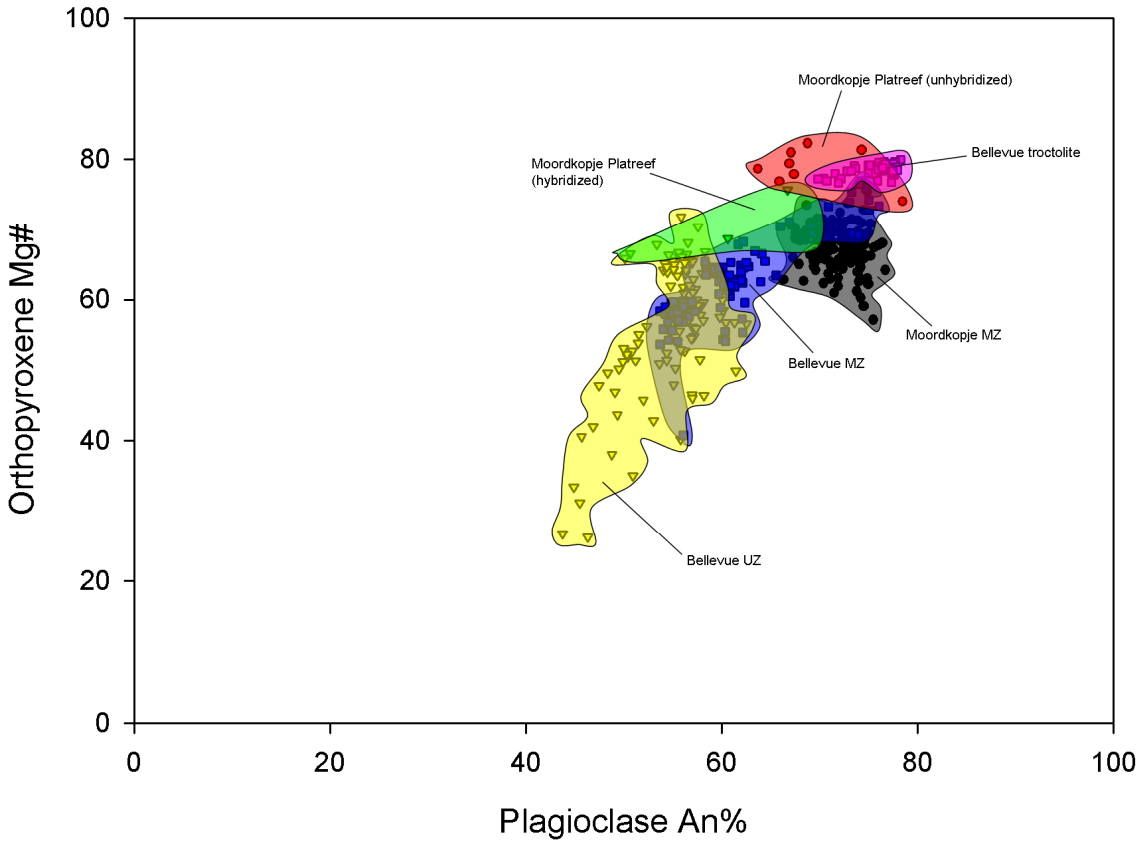

Figure 55: En-An relations amongst co-existing plagioclase and orthopyroxene for rocks from the Northern Limb as intersected by the Moordkopje and Bellevue drill holes.

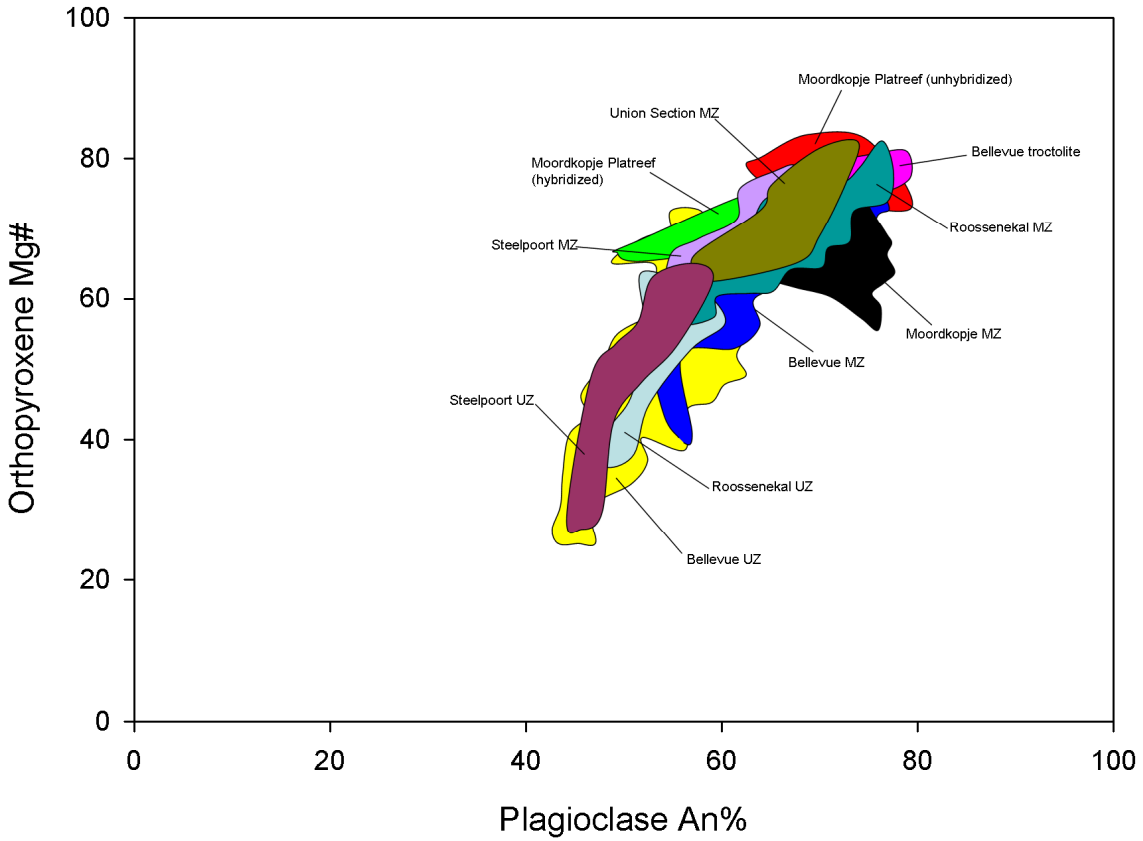

Figure 56: En-An relations amongst co-existing plagioclase and orthopyroxene for rocks from the Northern Limb compared with rocks from the Eastern and Western limbs.

Cr in orthopyroxene and Sr in plagioclase have been used successfully to discriminate between different magma lineages within the main body of the intrusion, with Sr in plagioclase generally <400 ppm in lower Main Zone rocks and >400 ppm for Upper Critical Zone rocks (Kinnaird, 2004), and Cr in orthopyroxene being considerably lower than 1000 ppm within the Main Zone, whereas the Critical and Lower zones typically have Cr in orthopyroxene in excess of ~3000 ppm (Cawthorn, 2007). In the Moordkopje hole, Cr in orthopyroxene down to depth ~2764 m was typically below the detection limit (i.e. less than ~340 ppm), with values increasing to as high as ~1400 ppm towards the Platreef. A similar situation of decreasing Cr in orthopyroxene is evident in the lower Main Zone of the Eastern and Western Limbs, where the base of the lower Main Zone has Cr in orthopyroxene of ~900 ppm, decreasing upward over ~750 m of stratigraphy to values <350 ppm (Cawthorn's (2007) figure 3a).

Sr in plagioclase in the lower Main Zone of the Northern Limb, calculated using the equation $Sr_{Plag} = Sr_{WR}(Al_2O_{3_{Plag}} / Al_2O_{3_{WR}})$ (Cawthorn, 2007) varies between 200 ppm and 413 ppm, with an average of 342 ppm, with measured Sr values in Main Zone plagioclase samples selected for isotopic study ranging between 326 ppm and 399 ppm (Appendix M), which is consistent with lower Main Zone values from the main body of the intrusion.

Whole-rock Ce/Sm and Th/Sm ratios were used by Maier & Barnes (1998) to discriminate between Lower + Lower Critical Zone lithologies and Main Zone lithologies at Union Section in the northwestern Bushveld Complex, with Ce/Sm for the former between 10 and 25 and for the latter generally less than 10 and with Th/Sm for the former generally more than 1 and for the latter less than 1. For the lower Main Zone as exposed by the Moordkopje hole, Ce/Sm varies between 7.5 and 13.4, with an average of 10.9 and Th/Sm between 0.6 and 2.0 with an average of 1.1, which is broadly in agreement with the values reported for the Main Zone by Maier & Barnes (1998).

A striking dissimilarity is apparent between the lower Main Zone in the Northern Limb and the main body of the intrusion, in that in the Northern Limb, the lower Main

Zone appears to be largely undifferentiated (see Folder 1). MO-1 records over the ~1350 m of Main Zone stratigraphy sampled virtually no large-scale fractionation in terms of either plagioclase An% or pyroxene Mg#, the former being on average 71.7 ± 2.2% and the latter 0.67 ± 0.03 for orthopyroxene, with plagioclase An% at the top and bottom of the core being 71.1% and 73.9%, respectively, and with orthopyroxene Mg# of 0.69 and 0.70, respectively. At Union Section, a corresponding stratigraphic interval shows an upward decline in plagioclase An% from ~72% to ~60% and orthopyroxene Mg# from ~0.81 to ~0.67 (Mitchell, 1986). At Steelpoort, the lower 1350 m of Main Zone rocks record an upward decline in plagioclase An% from ~71% to ~67% and orthopyroxene Mg# from ~0.78 to ~0.70 (Molyneux, 1970) and at Roossenekal, the corresponding values are from ~76% to ~62% and ~0.75 to ~0.67 (Von Gruenewaldt, 1971). The lack of differentiation in the lower Main Zone of the Northern Limb is also evident when considering the modified differentiation index (Figure 57). In the lower Main Zone of the Northern Limb, MDI values are scattered about ~31, whereas a corresponding thickness of the lower Main Zone in the Eastern Limb reflects a gradual upward increase from ~24 to 33.

From the above discussion it would suffice to say that the Main Zone of the Northern Limb shares a number of resemblances with that of the main body of the intrusion, but differs in a number of salient points, all of which are summarized in Table 6.

Table 6: Comparison between the Main Zone of the Northern Limb and that of the main body of the intrusion.

	Northern Limb	**Main Body**
Thickness	3110 m	3940 m / 2860 m
Marker Horizons	Present, but different from Main body	Present, but different from Northern Limb
Depth below Upper Zone at which inverted pigeonite becomes important	~590 m	>1110 m (Western Limb) 1480-2700 m (Eastern Limb)
Cr in orthopyroxene	<1400 ppm (typically <340 ppm)	900 ppm to less than 350 ppm
Sr in plagioclase	200-413 ppm	370-400 ppm (lower Main Zone)
Degree of differentiation	"Undifferentiated"	"Differentiated"

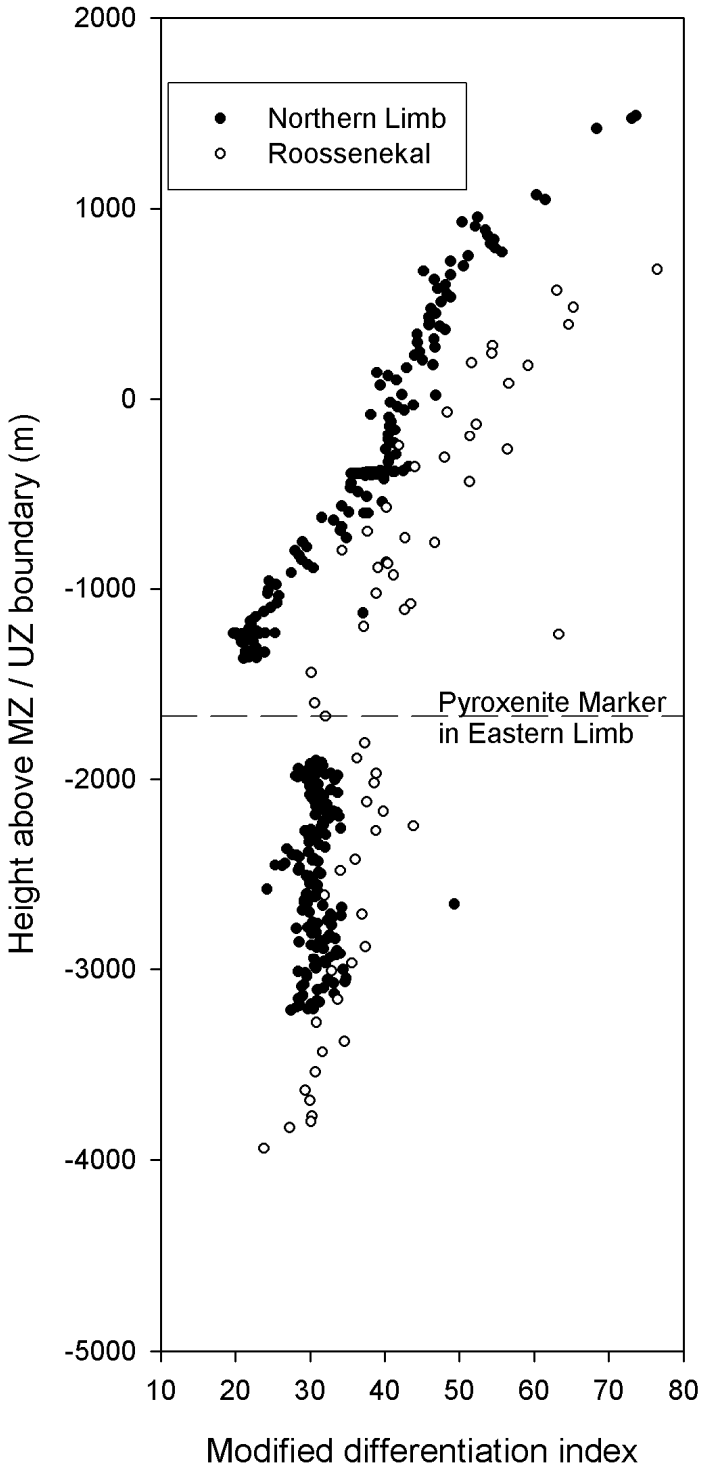

Figure 57: Modified differentiation index versus stratigraphic height in the intrusion. Data for Northern Limb from present study and unpublished data from the Bellevue drill core. Data for Roossenekal from Von Gruenewaldt (1971).

4.1.2 Isotope systematics

One of the most useful tools of discriminating between different parental magmas to the Bushveld Complex is isotope ratios, particularly following the 1994 paper by Kruger highlighting the Sr-isotopic stratigraphy of the western Bushveld Complex (Figure 58). Kruger's reconstruction of the isotope stratigraphy made use either of whole-rocks or plagioclase mineral separates in samples with high whole-rock Rb/Sr. In essence, Kruger divided the Rustenburg Layered Suite into a so-called Integration Stage, encompassing the Lower, Critical and lower Main zones, and a Differentiation Stage that included the upper Main and Upper zones. The integration stage records an irregular upward increase in Sr_i from ~0.7047 in the Lower Zone up to ~0.7091 in the lower Main Zone, which is followed by near- constant Sr_i of ~0.7085 up to the level of the Pyroxenite Marker, where Sr_i decreases to ~0.7073, a value that is retained to the top of the intrusion.

Although Kruger's model is probably correct in attributing changing Sr_i in the Rustenburg Layered Suite to progressive replenishment of the chamber with magmas with differing Sr_i, his probable assumption of co-existing minerals being in Sr-isotopic equilibrium failed to provide a comprehensive reconstruction of magma chamber processes other than straightforward magma mixing or bulk assimilation. The realization that co-existing minerals might be in isotopic disequilibrium is of particular importance in those areas of the intrusion where apparently no replenishment took place such as the upper Main and Upper zones (i.e. the Differentiation Stage), where specifically for Sr, whole-rocks may have near constant Sr_i (dominated by the very large contribution of Sr to whole-rock by plagioclase), but with pyroxene being in disequilibrium with plagioclase. This is exactly the case for the upper Main Zone interval characterized isotopically in this study. It is clear that such a situation requires a re-assessment of magma chamber processes over thus affected intervals, which would, when only considering whole-rock Sr_i be interpreted as an interval merely undergoing normal differentiation.

The realization that co-existing minerals in layered intrusions may not be in isotopic equilibrium is not an entirely new one, having been described for both Sr and Nd isotopes from whole-rocks and constituent plagioclase and pyroxene from the Skaergaard intrusion (McBirney & Creaser, 2003) and for Sr within single plagioclase

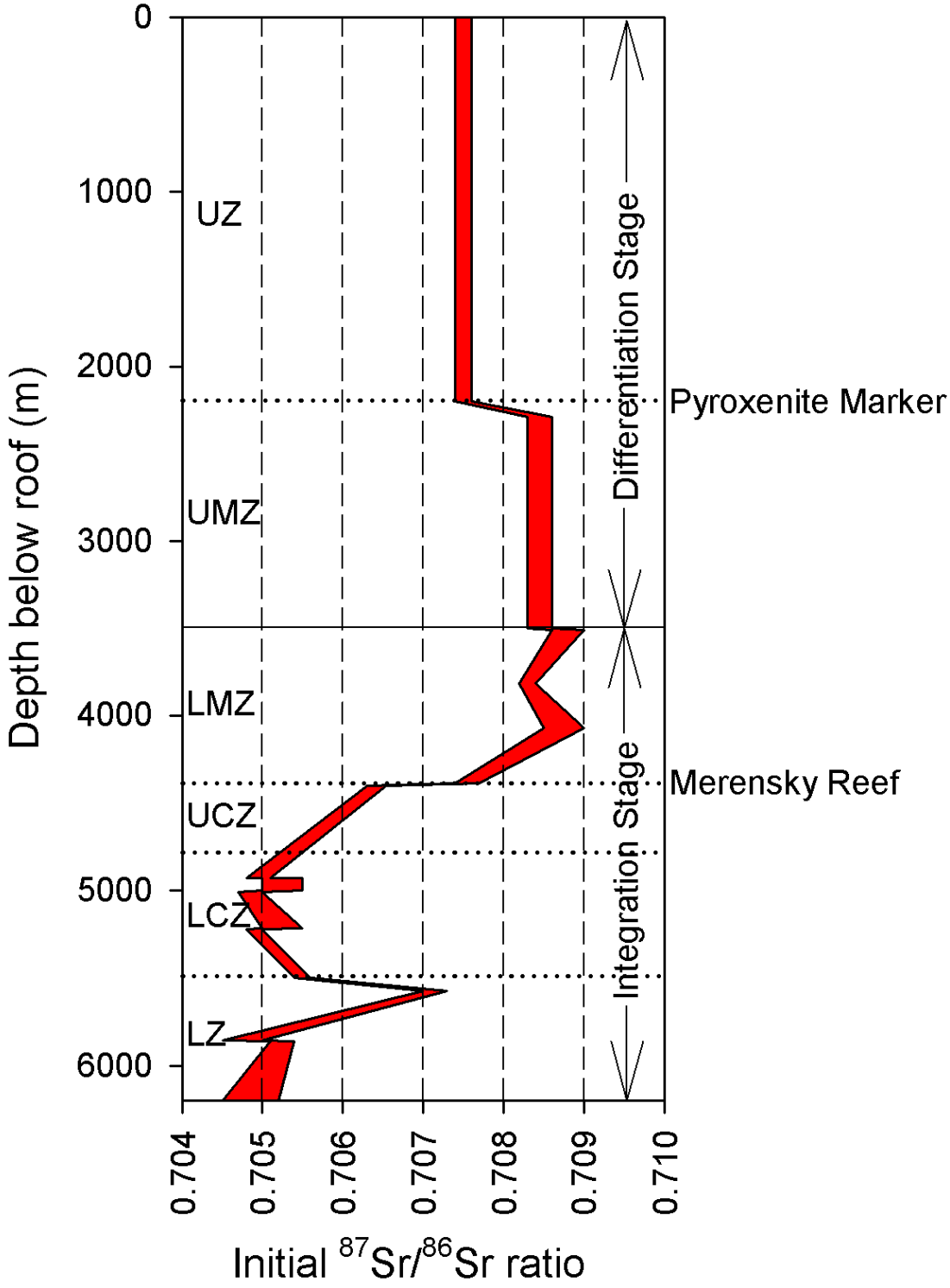

Figure 58: Sr-isotope stratigraphy of the Western Limb of the Bushveld Complex, after Kruger (1994).

crystals from the Rum layered intrusion (Tepley & Davidson, 2003). Geochemical and isotopic disequilibrium has additionally been described for the Bushveld Complex, albeit from the Upper Critical Zone, where co-existing plagioclase and pyroxene over the Merensky interval exhibit compositions (Seabrook et al., 2005) and Nd isotopes (Prevec et al., 2005) suggestive of crystallization from different parental magmas.

From a comparative viewpoint, Main Zone whole-rocks and plagioclase from the Moordkopje drill core have Sr_i (0.7078 to 0.7097, average 0.7084) and εNd (-4.1 to -8.5, average -6.7) not significantly different from that of the Main Zone from the main body of the intrusion, i.e. ~0.708 to 0.709 for Sr_i and -6.4 to -7.9 for εNd (Maier et al., 2000), the latter being the range exhibited by only four Main Zone samples, however. This taken at face value would suggest that the Main Zone of the Northern Limb may have a similar parental magma or magmas to that of the main body of the intrusion, a fact also highlighted by similarities in mineralogy, mineral compositions and geochemical parameters as discussed above.

4.1.3 A model for the origin of the Main Zone

A model for the origin of the lower Main Zone in the Northern Limb of the Bushveld Complex has to take into account several factors, including the fact that the sequence shows very little evidence for overall differentiation in terms of mineral compositions, the contrasting behaviour in differentiation trends as exhibited by plagioclase and pyroxene (see Section 3.1.2.1, page 47 above), the paucity of inverted pigeonite within the succession, and probably most importantly, the existence of isotopic disequilibrium between co-existing minerals. In the pages to follow, a model will be developed that I believe may explain many of the features of the lower Main Zone of the Northern Limb.

The model that will be developed here assumes the existence of a sub-Bushveld staging chamber, a feature that has been postulated by various researchers. Ashwal et al. (2005) postulated the existence of a sub-Bushveld magma staging chamber from whence new magma additions entered the chamber to blend with the pre-existing cumulate pile in an attempt to explain upward density increases, some of which are

coupled with reversals in differentiation trends in rocks from the Bellevue drill core. The existence of a staging chamber from whence 'crystal-charged magma batches' entered the Bushveld chamber was also proposed by Eales (2002) to account for the presence of excess olivine and chromium in the cumulates of the Lower and Lower Critical zones. McDonald & Holwell (2007) proposed a staging chamber that harbored sulfides from early Lower Zone magmas that were later supplied to the Platreef magma in order to account for the fact that Platreef sulfides were most probably not derived from the overlying Main Zone (Holwell et al., 2005), a theme elaborated upon by McDonald et al. (2009). A similar model was proposed by Barnes et al. (2009) to explain the lower than expected sulfur content of Lower and Critical Zone rocks, which assumed not only the existence of a sub-Bushveld magma chamber, but also the intrusion of crystal mushes into the main Bushveld magma chamber with the retention of sulfides within embayments present within the feeder system of the main chamber. The absence of changing $\delta^{18}O$ values with stratigraphic height in the Bushveld Complex also led Harris et al. (2005) to believe that contamination of the magmas parental to the Bushveld Complex took place in a staging chamber. The presence of a sub-Bushveld magma staging chamber was also implied by Maier et al. (2000), who suggested that Bushveld magmas were progressively contaminated by upper crustal partial melts and their restites.

The second tenet on which the model to be presented here is based is that the lower Main Zone in the Northern Limb is the product of a series of crystal mushes intruded into the chamber from the postulated staging chamber. This also is not an entirely new concept as is also evident from the discussion above. In addition, Maier & Barnes (1998) suggested on the basis of the similarity in REE compositions between Main Zone cumulates and the postulated parental magma thereto, that the Main Zone was intruded not as a liquid, but rather as a crystal mush, a theme elaborated upon by Maier et al. (2001) to account amongst other features for the "poorly developed cryptic variation observed in large parts of the Main Zone". Barnes et al. (2004) similarly suggested intrusion of crystal mushes in order to explain the enrichment in compatible elements and depletion in incompatible elements in Bushveld cumulate rocks relative to the marginal rocks of the Bushveld Complex.

Similar thinking is not confined only to the Bushveld Complex. Czamanske & Bohlen (1990) interpreted the thick anorthosite horizons within the Middle Banded series of the Stillwater intrusion as crystal mushes intruded from a staging chamber located at the crust/mantle interface. Ashwal & Wiebe (1989) similarly postulated that Proterozoic anorthosite massifs may have formed by intrusion of plagioclase-charged crystal mushes, wherein the accompanying residual liquids were progressively contaminated during ascent, with the result that co-existing plagioclase and mafic silicates are in isotopic disequilibrium. De Waal et al. (2004), based in part on the limited variation of olivine compositions (which is analogous to the limited variation in mineral compositions of the lower Main Zone of the Northern Limb of the Bushveld Complex) postulated that the Jinchuan ultramafic intrusion in China was the product of intrusion by crystal mushes from an underlying staging chamber. Although occurring on a significantly smaller scale, Bedard et al. (2007) interpreted anorthosite schlieren occurring in thick sills in Antarctica as having formed from locally derived crystal mushes. Finally, porphyritic lavas are in essence nothing more than crystal mushes in which the proportion of interstitial melt is still relatively large.

The morphology of a sub-Bushveld staging chamber that I believe may explain many of the features of the lower Main Zone in the Norhtern Limb is depicted schematically in Figure 59. It is postulated that the two sub-chambers, which were initially filled by magma of a similar composition (both chemically and isotopically) had wall rocks differing in the proportion of radiogenic Sr, but with relatively similar Nd-isotopic compositions. The evolution of the magmas present in both chambers would therefore proceed in a similar fashion, although the resident magmas would become progressively more isotopically distinct as assimilation of wall rocks proceeded. Although there exists considerable debate regarding the question whether plagioclase will be positively or negatively buoyant (a topic succinctly dealt with by Cawthorn & Ashwal (2009)) within basaltic magmas, it does not seem sufficiently exotic to suggest that plagioclase may have accumulated at the tops of the two sub-chambers whereas mafic silicates would have settled to the bottoms. Experimental work by Kushiro and Fujii (1977) for instance suggests that plagioclase with An content 65-90% would be positively buoyant in an olivine tholeiitic magma at pressures between ~2 kb and 9 kb, corresponding to depths of ~7-33 km. In addition, olivine may also have accumulated at the bottoms of both chambers at an early stage, an argument that

will be used to explain the anomalous troctolite layer occurring towards the bottom of the Bellevue drill core.

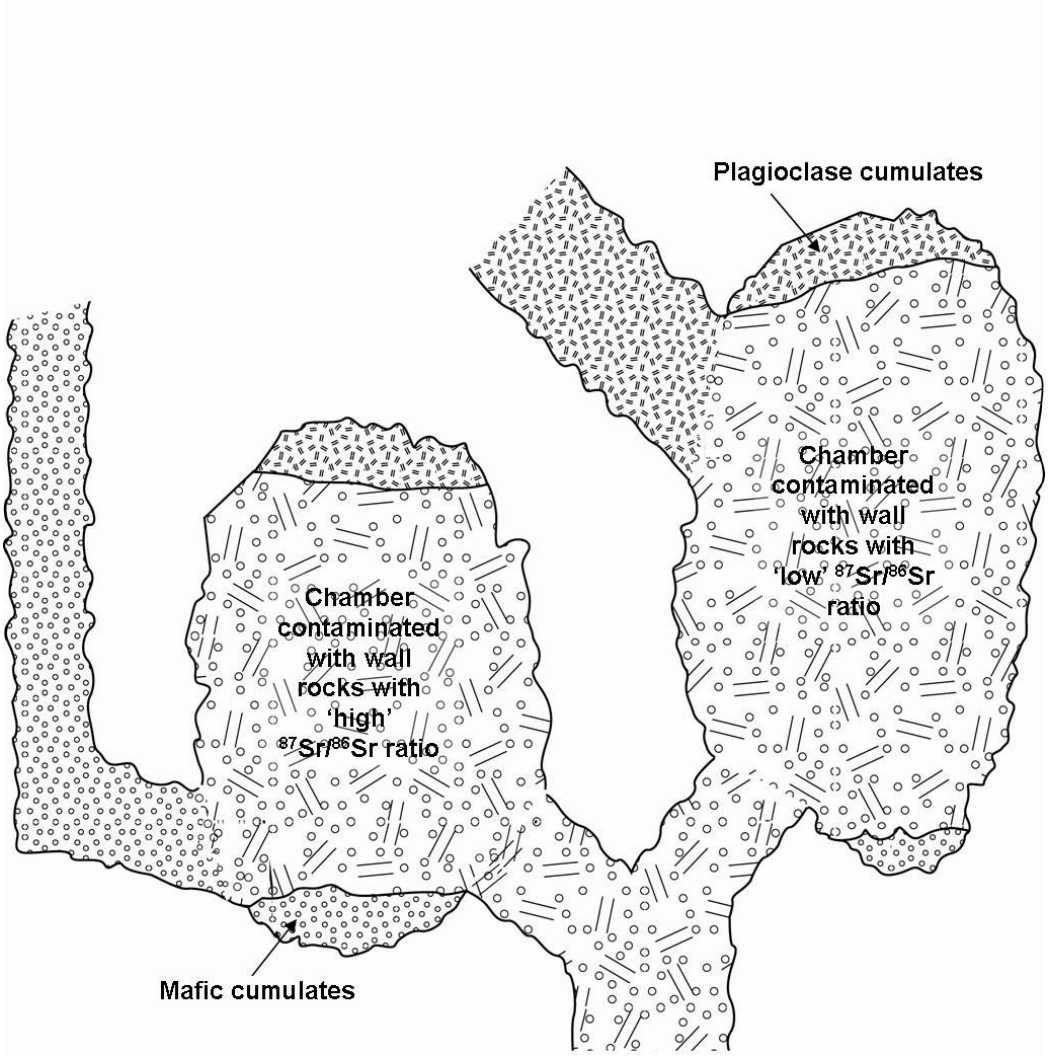

Figure 59: Schematic representation of the envisaged morphology of the staging chamber hosting parental magmas that gave rise to the Main Zone in the Northern Limb. Sub-chamber A and B on left and right, respectively. See text for details.

The apparent differentiation trend of pyroxene in the lower part of the Main Zone, as exemplified by decreasing Cr contents may be explained by emplacement of early-formed pyroxene from sub-chamber A, mixed with early formed plagioclase from sub-chamber B. Although isotopic data are lacking for this part of the layered sequence, it is postulated that isotopic disequilibrium between co-existing minerals in this part of the sequence will be absent or less significant than higher up in the lower

Main Zone due to the possible lack of significant wall rock assimilation during the early history of the staging chamber, a hypothesis that may be independently tested, and which appears to hold true for the deeper of the two intervals subjected to isotopic analysis. Subsequent influxes of magma into the Northern Limb would produce rocks bearing plagioclase and pyroxenes that are apparently in major element equilibrium, but which may differ significantly in terms of their Sr-isotopic compositions.

Of significance to the subsequent evolution of the Main Zone in the Northern Limb is the FeO content of plagioclase (see Figure 33), which is fairly constant (~0.23%) in the lower Main Zone up to a depth of ~2293.7 m, but then shows a sudden increase in FeO content (~0.36%) that is retained to the top of MO-1. In Bellevue, FeO in plagioclase ranges between 0.45% and 0.25%, with a somewhat poorly defined trend towards lower FeO contents with decreasing depth (Ashwal et al., 2005), with the Upper Main Zone in the western Bushveld Complex similarly showing upwards decreasing FeO in plagioclase, from 0.45% to 0.40% (Tegner & Cawthorn, in press).

One of the main factors influencing the FeO_T content of plagioclase is the oxygen fugacity (fO_2) (Phinney, 1992; Lundgaard & Tegner, 2004). Kress & Carmichael (1991) have shown that in a melt where the oxygen content is fixed by the composition of the melt (i.e. a closed system), fO_2 will increase with increasing pressure. Voluminous magma addition with a composition similar to that already present in the staging chamber and a concomitant increase in pressure may therefore feasibly have increased the fO_2 of the magma to such an extent that subsequent crystal mushes intruded into the Northern Limb may have contained plagioclase with higher FeO contents than those occurring deeper in the lower Main Zone. This voluminous magma addition may also have dislodged early formed olivine from the bases of the staging chambers giving rise to the troctolite horizon occurring within otherwise 'normal' Main Zone rocks.

Examination of the Bellevue data (Ashwal et al., 2005) shows that mineral compositions in the troctolite horizon remain fairly constant, which would be in agreement with it being intruded as a crystal mush. Only some distance above the troctolite horizon do plagioclase and pyroxene compositions start changing towards

lower An% and Mg# in a manner consistent with 'normal' differentiation as also seen for the Main Zone in the main body of the intrusion.

The appearance of inverted pigeonite for the first time in the evolving magma chamber approximately 550 m above the troctolite layer is further evidence of the lower Main Zone being intruded as crystal mushes, with significant iron enrichment culminating in the precipitation of pigeonite only being achieved in the upper Main Zone once differentiation started in-situ from the last voluminous influx of magma. If this postulate is correct, then minimal isotopic disequilibrium between co-existing minerals would be expected for the upper Main Zone of the Northern Limb, a fact that may be independently tested.

Non-cotectic proportions of plagioclase and pyroxene (Figure 60) in the Main Zone may also adequately be explained by the rocks having formed from crystal mushes as opposed to having crystallized from a liquid (Cawthorn & Ashwal, 2009). So too may rock sequences showing all possible combinations of vertical increases, decreases or unchanging values in terms of plagioclase An% and pyroxene Mg#.

4.1.4 Arguments against an in-situ origin for the lower Main Zone

There are undoubtedly researchers on the Bushveld Complex that would try to explain the genesis of the lower Main Zone by solely invoking processes that may have been operable within the Bushveld magma chamber itself. In the next few paragraphs a number of points will be highlighted in favour of the present model as opposed to models trying to explain the lower Main Zone by in-situ processes.

The distinct lack of differentiation in the lower Main Zone of the Northern Limb may perhaps be cited as being the result of differentiation from a comparatively larger body of magma than that which is preserved in the Northern Limb today, associated with the expulsion of more evolved liquids from the chamber. Similar arguments have been put forward by Cawthorn & Walraven (1998) to account for the so-called Cr paradox of the Bushveld Complex (Eales, 2002) and by Barnes et al. (2004) to account for differences between compatible and incompatible elements between Bushveld Complex cumulates and marginal rocks. Field evidence for such extrusives has, however, proven elusive (Eales, 2002; Kruger, 2005), favouring a model in which

more evolved liquids were perhaps retained in a staging chamber rather than being erupted as volcanics.

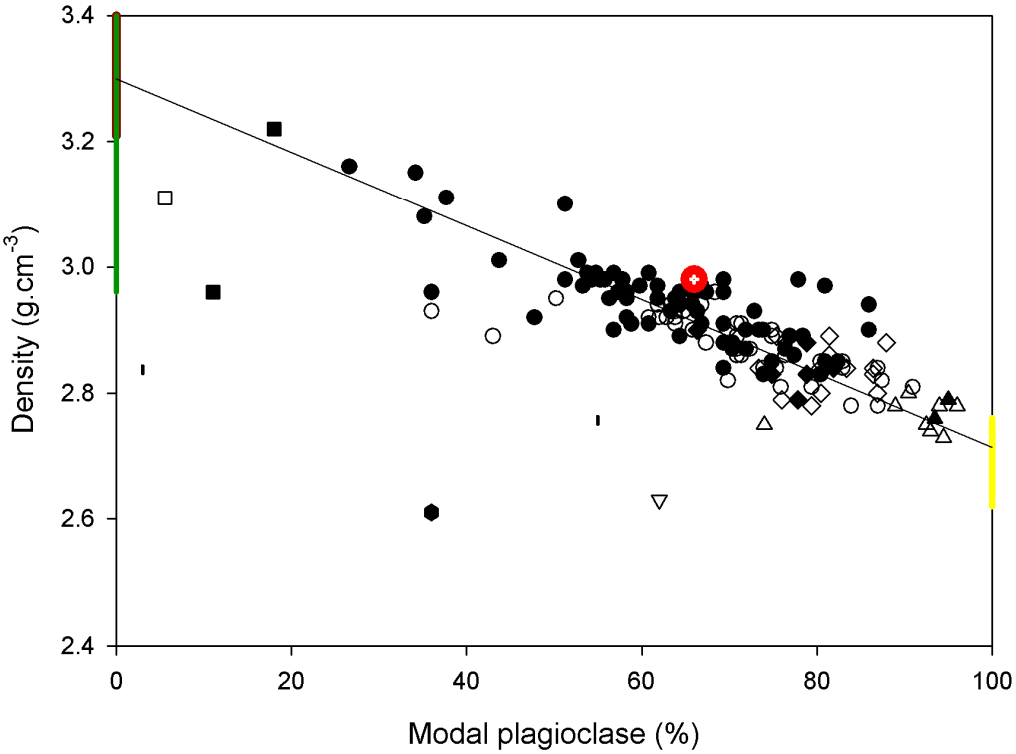

Figure 60: Variation in rock density with modal plagioclase content for rocks of the Moordkopje drill core. See Figure 33 for explanation of symbols used. Yellow, green and dark red lines on the ordinates show density ranges for plagioclase, augite and orthopyroxene, respectively, from Deer et al. (1980). Large red circle shows approximate cotectic proportion of plagioclase : pyroxene (Cawthorn & Ashwal, 2009).

Non-cotectic proportions of plagioclase to pyroxene in the Bushveld Complex have been reported by various authors (e.g. Cawthorn & Spies, 2003; Cawthorn & Ashwal, 2009). Cawthorn & Spies (2003) advocated a model to account for excess plagioclase in the Merensky and Bastard cyclic units in which magmas saturated in plagioclase were emplaced as a basal flow underneath the resident magma with plagioclase accumulation from both the new magma influx and the displaced resident magma, whereas Cawthorn & Ashwal (2009), based on the data of Ashwal et al. (2005), suggested that anorthosite layers were the result of a complex interplay between

rhythmically pulsed crystallization, pressure changes and mineral settling and sorting. It becomes difficult, however, to envisage how a process such as the latter will result in isotopic disequilibrium amongst co-existing phases as seen in the present data.

Studies on isotopic disequilbrium between co-existing minerals in the Bushveld Complex have been largely focused on the Upper Critical Zone, with various models being proposed to account for this. Eales et al. (1990) suggested pulsatory injection of more primitive liquid (with higher Sr_i) into a column of depleted residual liquids crystallizing plagioclase and orthopyroxene (with lower Sr_i) to account for plagioclase exhibiting a mixed population of Sr_i in the footwall to the UG1 chromitite. Prevec et al. (2005) suggested a model whereby contaminated orthopyroxenes (ε_{Nd} = -7.5) from a newly intruded magma settled into a layer of uncontaminated plagioclase (ε_{Nd} = -2.2) to account for Nd-isotopic disequilibrium within the Merensky Reef and its footwall. Seabrook et al. (2005) preferred a model in which Main Zone magma intruded at the level of the Merensky unit, displacing the resident Critical Zone magma upwards, with orthopyroxene and cumulus plagioclase settling through the newly intruded layer in order to account for the presence of minerals possessing Critical Zone and Main Zone affinities, respectively, within the Merensky Unit. Such a process is indeed conceivable at the level of the Merensky Unit, where interaction between two geochemically distinct magmas (i.e. Critical Zone and Main Zone magma) with distinctly different densities is indicated. A similar argument to explain isotopic disequilibrium within the Main Zone appears untenable, unless new magma additions into the Main Zone had distinctly different densities in comparison to the resident magma. Where density differences are absent, magma mixing would have resulted, with the effect that all minerals crystallizing from such hybrid magma would be in isotopic equilibrium.

In the model by Prevec et al. (2005), the authors contemplated whether contaminated plagioclase derived from their postulated magma pulse would also be preserved, concluding that “contaminated plagioclase is not precluded from this model, but would be expected to occur higher in the sequence”. Similarly, if isotopic disequilbrium in the present dataset is to be explained by mixing of minerals between a new magma influx and magma resident within the Bushveld magma chamber, it is

conceivable that one may expect to find layers in which plagioclase too is enriched in radiogenic Sr as is the case for orthopyroxene of the upper interval subjected to isotopic analysis. Plagioclase derived from the magma from which orthopyroxene of this interval crystallized would have to have a Sr_i of at least 0.711 taking into account the possible contamination of orthopyroxene mineral separates by co-existing plagioclase with lower Sr_i. Furthermore, significant Sr-isotopic disequilibrium is apparent over a stratigraphic interval of nearly 150 m, so that it becomes likely that layers enriched in plagioclase with $Sr_i > 0.711$ must be somewhere preserved within the succession. It is of course also possible that the Sr_i of plagioclase mineral separates represent the average of two populations of plagioclase exhibiting differing Sr_i and the need is therefore clearly indicated for in-situ isotopic analyses of Bushveld plagioclases similar to that performed by Tepley & Davidson (2003) for the Rum layered intrusion. Also, because rhythmic units within the Main Zone are not as clearly defined as for the Upper Critical Zone, a larger isotopic dataset is needed in order to elucidate possible mechanisms for successions exhibiting isotopic disequilibrium between co-existing minerals.

4.1.5 Modelling of crustal contaminants

Supracrustals and basement rocks of the Kaapvaal craton at 2.06 Ga exhibit a wide range of $^{87}Sr/^{86}Sr$ and εNd values, providing for a variety of possible contamination scenarios with mantle-derived melts (Figure 61, Table 7). From Figure 61 it is immediately apparent that the isotopic data for the Main Zone cannot be explained by mixing of a mantle-derived melt (εNd = +2.0; $^{87}Sr/^{86}Sr = 0.702$; Maier et al., 2000) and melts derived from the supracrustals of the Transvaal Supergroup or from the rocks of the Ancient Gneiss Complex, the Johannesburg Dome tonalites or the Rooiberg Group, primarily because of significant overlap in terms of the Nd-isotopic compositions of these units and Main Zone cumulates. The most likely contaminants therefore appear to be upper and lower crust of the Vredefort dome, as represented by the Outer Granite Gneiss (OGG) and Inlandsee Leucogranofels (ILG), respectively. Data for the Main Zone whole-rocks and mineral separates analysed in this study are shown along with the average compositions of OGG and ILG in Figure 62, providing better resolution in comparison to Figure 61.

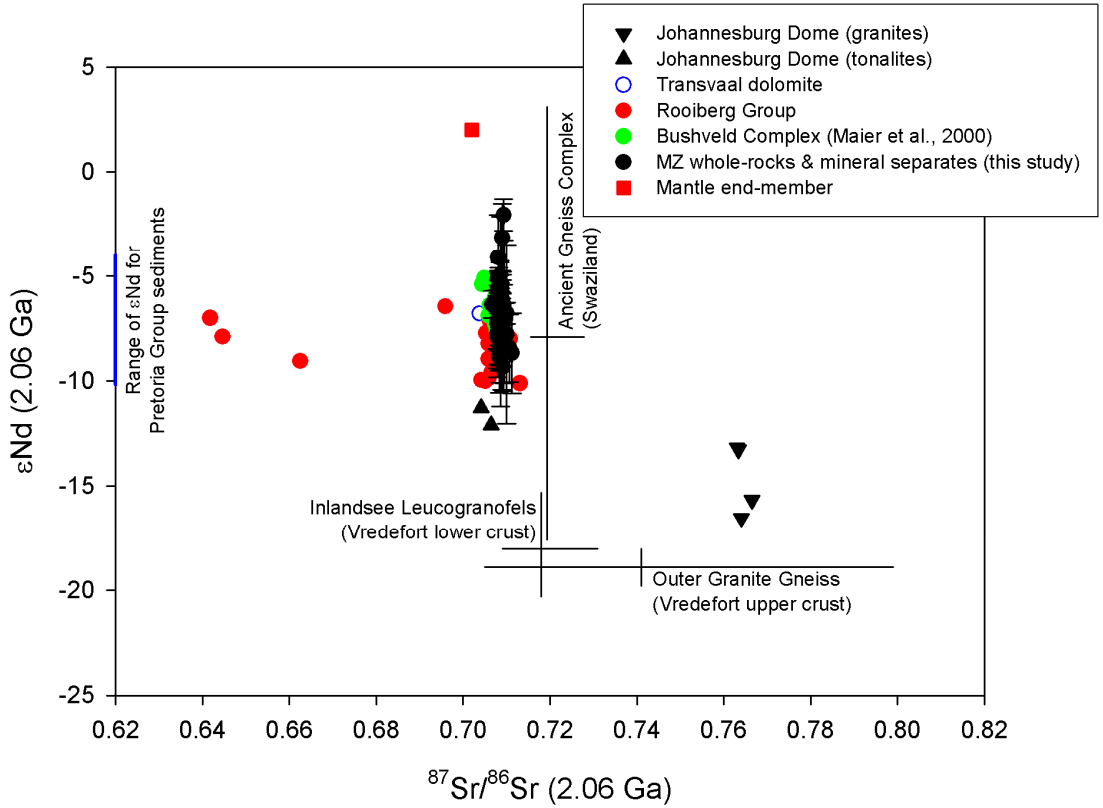

Figure 61: Plot of εNd vs. $^{87}Sr/^{86}Sr$ (2.06 Ga) for supracrustals and basement rocks of the Kaapvaal craton. Also shown are data for the Rooiberg Group, data for the Rustenburg Layered Suite (Maier et al., 2000), the results of the present study and a mantle melt with εNd = +2.0 and $^{87}Sr/^{86}Sr$ = 0.702. Rooiberg Group rocks with $^{87}Sr/^{86}Sr$ <0.70 are proposed to have been affected by post-crystallization alteration (Buchanan et al., 2004).

Table 7: Average Rb, Sr, Sm and Nd concentrations, $^{87}Sr/^{86}Sr$ ratios and εNd values for Kaapvaal supracrustals and basement rocks recalculated to an age of 2.06 Ga.

Entity	Rb, ppm	Sr, ppm	$^{87}Sr/^{86}Sr$ (2.06 Ga)	Sm, ppm	Nd, ppm	εNd (2.06 Ga)	Reference
Ancient Gneiss Complex (Swaziland)	84	276	0.7193	3.3	16.2	-7.9	Barton et al. (1980); Carlson et al. (1983)
Johannesburg Dome (Granites)	210	142	0.7643	5.0	24.0	-14.7	Barton et al. (1999)
Johannesburg Dome (Tonalites)	79.4	890	0.7053	5.7	29.1	-11.7	Barton et al. (1999)
Outer Granite Gneiss (Vredefort)	94.3	405	0.7415	4.3	31.0	-18.9	Hart et al. (1990), Hart et al., (1981)
Inlandsee Leucogranofels (Vredefort)	102	302	0.7179	2.4	20.7	-18.0	Hart et al. (1990), Hart et al. (1981)
Transvaal dolomite	2.4	687	0.7038	1.3	6.7	-6.8	Pronost et al. (2008)
Pretoria Group sediments	-	-	-	6.8	37.5	-5.7	Jahn & Condie (1995)
Rooiberg Group	-	-	0.7003	-	-	-8.4	Buchanan et al. (2004)

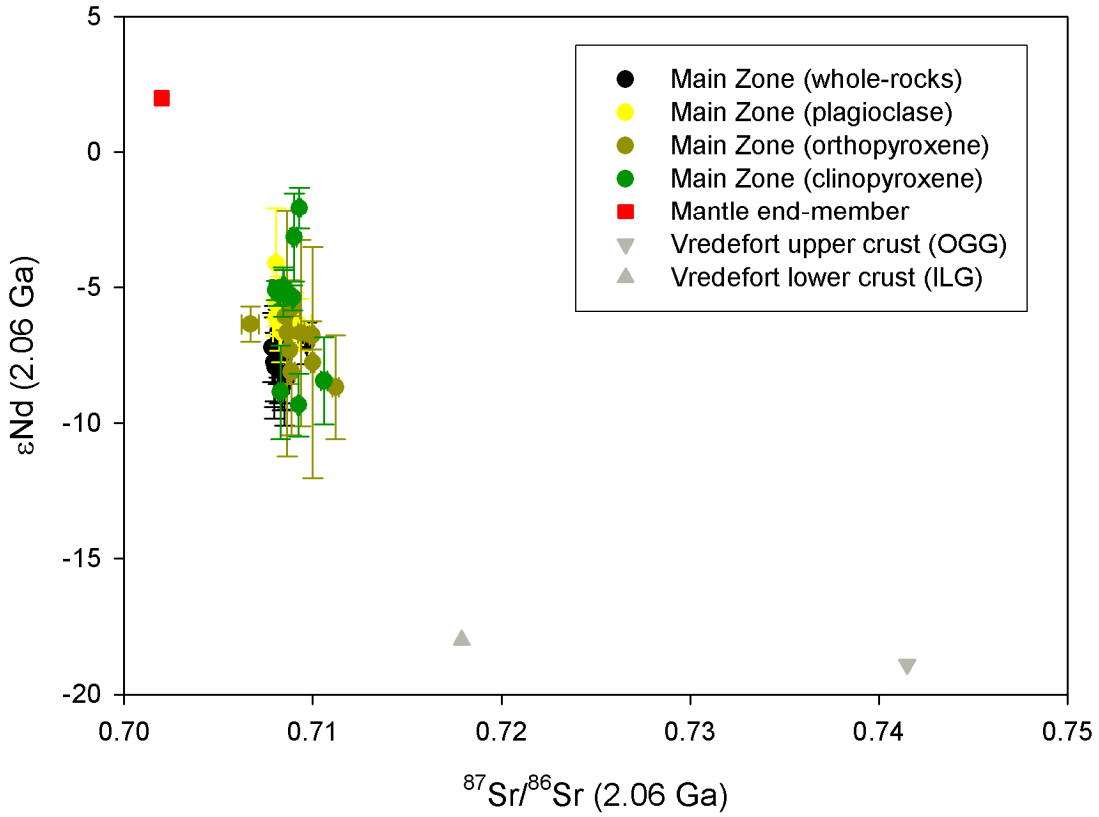

Figure 62: Plot of εNd vs. $^{87}Sr/^{86}Sr$ (2.06 Ga) showing data for Vredefort upper and lower crust, Main Zone whole-rocks and mineral separates, and a mantle melt with εNd = +2.0 and $^{87}Sr/^{86}Sr$ = 0.702.

For the purpose of the isotopic models that will be developed here, the mantle at 2.06 Ga was assumed to have εNd of +2.0 and $^{87}Sr/^{86}Sr$ of 0.702, in line with the recommendations of Maier et al. (2000). Maier et al.'s choice of Sr (52 ppm) and Nd (3.4 ppm) concentrations for their mantle end-member was, however, based on a 35% partial melt composition reported by Arndt et al. (1993) which intuitively appears unreasonably large for the case of the Bushveld Complex. The only other Sr (289 ppm) and Nd (16 ppm) concentrations reported by Arndt et al. (1993) were for the case of a 5% partial melt.

In order to gain an understanding of the variation of Sr and Nd concentrations in mantle having undergone different degrees of partial melting, modeling was performed using the pMELTS software package of Ghiorso et al. (2002). Calculations were performed using the pMELTS web-applet at a pressure of 20 kbar and temperatures of between 1380°C and 1580°C, using as a starting composition that of spinel peridotite as reported by McDonough (1990). The results of the calculations are presented in Table 8. The mineralogical compositions of the refractory restites at the different temperature increments allowed the calculation of bulk partition coefficients using the equations of Shaw (1970) for the case of equilibrium melting and the partition coefficients for Sr and Nd as reported by Arndt et al. (1993). This in turn allowed me to calculate the Sr and Nd concentrations in melts generated by different degrees of partial melting, using Sr and Nd concentrations of primitive mantle as presented by Hoffmann (1988). The Sr and Nd concentrations thus calculated are presented in Table 8. The results are encouraging when compared to the Sr and Nd concentrations of 5% and 35% partial melts reported by Arndt et al. (1993).

For the generation of partial melts of the Vredefort crustal end-members, a different approach, largely based on that used by Maier et al. (2000), had to be employed. Sr and Nd concentrations in 5%, 10%, 15% and 20% equilibrium partial melts of the ILG and OGG were calculated following a similar approach to that used for the case of mantle melting as discussed in the preceding paragraph by utilizing the results of Patino Douce & Beard (1995) on the isobaric melting behaviour of synthetic biotite-gneiss at a pressure of 10 kbar.

Table 8: Melting relations and liquid compositions of spinel peridotite (McDonnough, 1990) at P = 20 kbar and at temperatures ranging between 1380°C and 1580°C as obtained using the pMELTS web-applet of Ghiorso et al. (2002). Also shown are the Sr and Nd concentrations of liquids calculated according to the method outlined in the text.

Temperature (°C)	1380	1400	1420	1440	1460	1480	1500	1520	1540	1560	1580
Liquid	0.95	1.34	2.00	3.03	4.73	7.72	12.38	15.60	19.89	25.98	35.31
Spinel	1.73	1.71	1.68	1.62	1.51	1.33	1.09	0.94	0.79	0.64	0.47
Clinopyroxene	10.18	10.01	9.69	9.13	7.91	5.10	0.00	0.00	0.00	0.00	0.00
Orthopyroxene	19.25	19.26	19.27	19.27	19.46	20.43	22.58	20.74	18.36	15.06	10.01
Olivine	67.97	67.79	67.51	67.13	66.56	65.60	64.11	62.89	61.12	58.49	54.37
TOTAL	100.08	100.11	100.15	100.18	100.17	100.18	100.16	100.17	100.16	100.17	100.16
Liquid composition											
SiO_2	49.9	47.5	45.0	43.6	43.2	43.0	43.3	43.6	44.1	44.8	45.6
TiO_2	0.9	0.9	0.9	0.9	0.8	0.7	0.6	0.5	0.4	0.3	0.2
Al_2O_3	16.1	15.1	13.9	12.9	12.1	11.2	10.1	9.2	8.2	7.0	5.7
Fe_2O_3	0.2	0.3	0.5	0.6	0.8	0.9	0.9	0.8	0.7	0.6	0.5
Cr_2O_3	0.1	0.1	0.1	0.1	0.1	0.2	0.2	0.2	0.3	0.3	0.4
FeO	4.2	5.7	7.3	8.8	10.1	10.9	11.3	11.6	11.8	11.8	11.3
MnO	0.0	0.0	0.0	0.0	0.0	0.0	0.0	0.0	0.0	0.1	0.1
MgO	7.9	10.5	13.2	15.7	17.7	19.3	20.7	22.7	24.8	27.2	29.9
CaO	4.5	6.0	7.4	8.3	8.9	9.7	10.3	9.1	7.8	6.5	5.2
Na_2O	9.1	8.1	6.7	5.2	3.8	2.7	1.8	1.5	1.2	0.9	0.7
K_2O	5.7	4.0	2.7	1.8	1.1	0.7	0.4	0.3	0.3	0.2	0.2
P_2O_5	1.4	1.8	2.1	1.8	1.2	0.7	0.5	0.4	0.3	0.2	0.2
TOTAL	100.0	100.0	99.8	99.7	99.8	100.0	100.1	99.9	99.9	99.9	100.0
Sr, ppm	867	735	585	445	320	216	144	115	90	69	51
Nd, ppm	38.5	34.5	29.4	24.0	18.5	13.5	9.5	7.6	6.0	4.6	3.4

Bulk partition coefficients were calculated for each degree of partial melting using the restite compositions of Patino Douce & Beard (1995) and the mineral / melt partition coefficients of Bacon & Druitt (1988) and Nash & Crecraft (1985). The calculated Sr and Nd concentrations of the ILG and OGG derived partial melts were found to be remarkably constant for the different degrees of partial melting, with Sr and Nd in ILG derived partial melts (5-20%) ranging between 211 ppm and 209 ppm, and 21.2 ppm and 26.2 ppm, respectively, and for OGG derived partial melts between 280 ppm and 286 ppm and, 31.1 ppm and 38.6 ppm, respectively. For comparison, Maier et al. (2000) calculated Nd and Sr concentrations of 39 ppm and 189 ppm, respectively, for a 15% partial melt of ILG generated at 10 kbar. The discrepancy is most likely the result of a different set of partition coefficients used by Maier et al. (2000).

Because of the existence of significant Sr isotopic disequilibrium between co-existing plagioclase and orthopyroxene within the Main Zone, the isotopic compositions of these two minerals were used as proxies for the magmas from which they crystallized. The requirement of a feasible isotopic mixing model would therefore be not only to recreate the isotopic compositions of the plagioclase and orthopyroxene mineral separates, but also to provide a feasible bulk magma composition capable of crystallizing orthopyroxene and plagioclase exhibiting Sr and Nd concentrations similar to those actually observed within orthopyroxene and plagioclase mineral separates. One such model is presented in Figure 63. The model was generated assuming an 8% mantle-derived partial melt and the mixing of small degree (<20%) partial melts derived from Vredefort upper (OGG) and lower (ILG) crust. The model suggests that the magma chamber from which plagioclase crystallized was contaminated by ~25% of small degree partial melts predominantly derived from the Vredefort lower crust (~70-80%) with a smaller contribution from the Vredefort upper crust (~20-30%), whereas the magma chamber from which orthopyroxene crystallized was contaminated by roughly similar amounts of small degree partial melts with a higher contribution of Vredefort upper crust (30-40%).

Calculations show that the Sr and Nd concentrations of both magma chambers would have been on the order of 220 ppm and 17 ppm, respectively. The distribution coefficient for Sr into plagioclase (An% = 72%) at a nominal crystallization

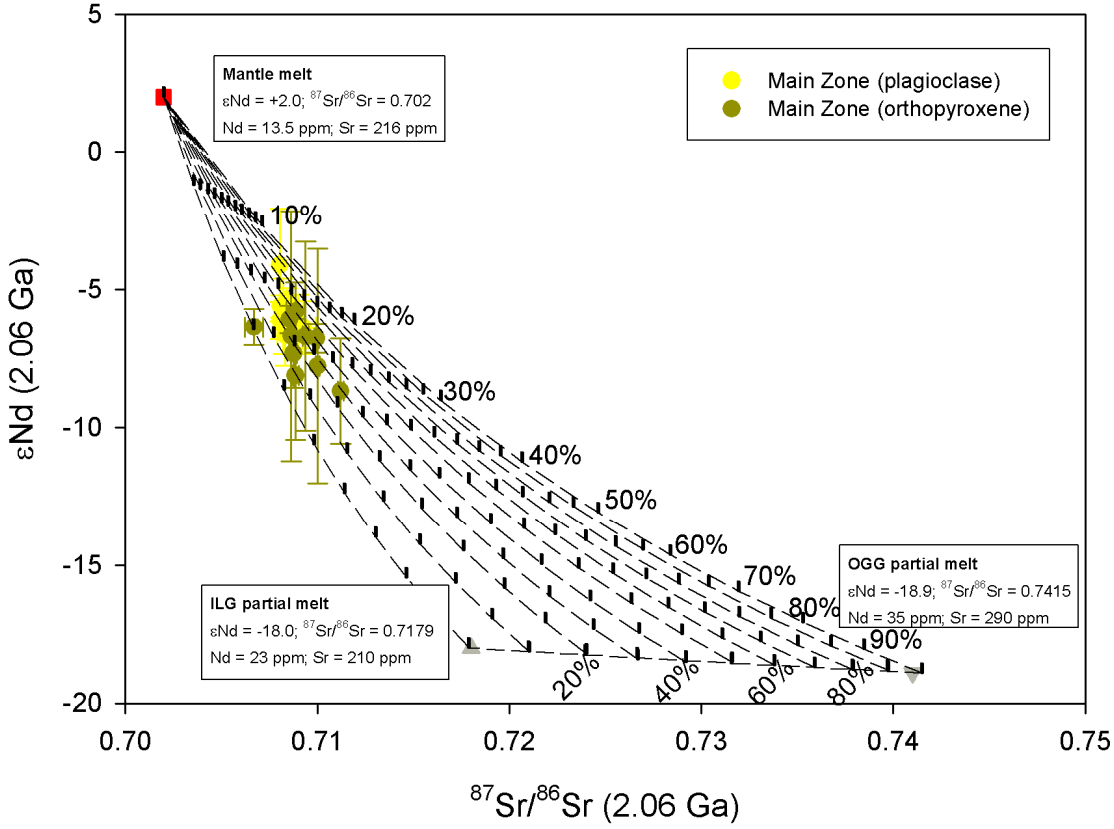

Figure 63: Isotopic mixing model showing how the isotopic compositions of plagioclase and orthopyroxene in the Main Zone can be explained by interaction between a primary mantle melt and partial melts of Vredefort upper and lower crust.

temperature of 1200°C to 1300°C is estimated to be on the order of 1.86 (Blundy & Wood, 1991), so that plagioclase crystallizing from these chambers would contain on the order of 409 ppm Sr, a value not significantly different from that actually observed for plagioclase within the Main Zone. Similarly, using $D_{Sr}^{Opx} = 0.007$ (McKenzie & O'Nions, 1991), it can be shown that orthopyroxene crystallizing from these chambers should contain on the order of 1.5 ppm Sr, whereas the average Sr content of orthopyroxenes as measured in this study amounts to 8.5 ppm. This feature suggests that orthopyroxene mineral separates may have been contaminated by up to 10% plagioclase and that pure orthopyroxene mineral separates would have exhibited even larger degrees of isotopic disequilibrium relative to plagioclase than those actually measured.

Using $D_{Nd}^{Plag} = 0.14$ and $D_{Nd}^{Opx} = 0.0068$ (McKenzie & O'Nions, 1991), plagioclase and orthopyroxene crystallizing from a magma with a Nd content of 17 ppm should contain ~2.4 ppm and ~0.1 ppm Nd, respectively. The value for plagioclase compares well with those actually measured for plagioclase, being on average 2.2 ppm for plagioclase separates from the Main Zone. The calculated Nd content of orthopyroxene, however, compares less favourably, with measured Nd contents in Main Zone orthopyroxenes being 1.2 ppm. Using a higher D_{Nd}^{Opx} of 0.02 (Irving & Frey, 1984) only marginally lessens the discrepancy, with orthopyroxene then expected to contain 0.34 ppm Nd.

The above approach, unfortunately, does not allow one to calculate the major element compositions of the hybrid magmas produced through crustal contamination of primary mantle melts due to the uncertainties involved with respect to the major element compositions of the ILG and OGG derived partial melts. However, it is expected that due to the similarity in both the major and trace element compositions of the ILG and OGG (Figure 64), that partial melts derived from them would have had relatively similar compositions, such that both postulated magma chambers would have evolved in broadly similar terms from a major (and to a lesser extent also a trace) element perspective.

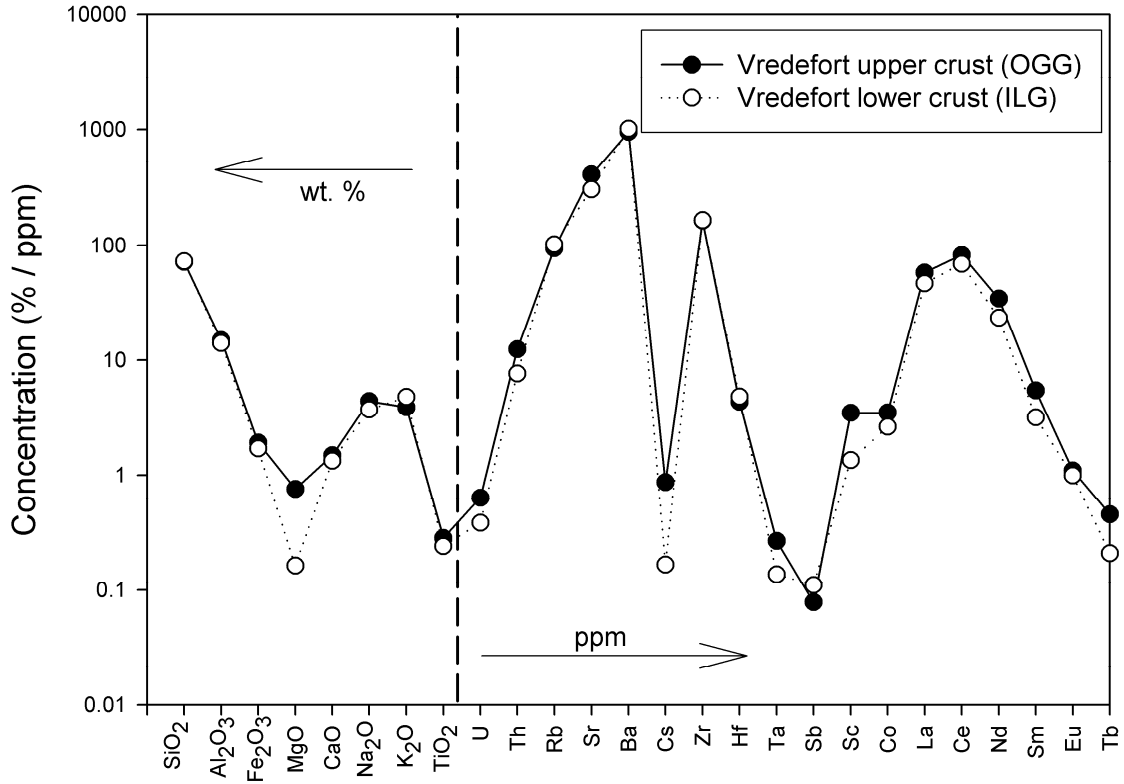

Figure 64: Average major and trace element composition of the Vredefort upper and lower crust. Data from Hart et al. (1990). Major elements expressed as oxides (in wt. %) and trace elements in parts per million.

The above calculations allow refinement of the staging chamber morphology presented in Figure 59 above, taking into account the relative contributions of upper and lower crustal contaminants, with the newly proposed staging chamber morphology presented in Figure 65.

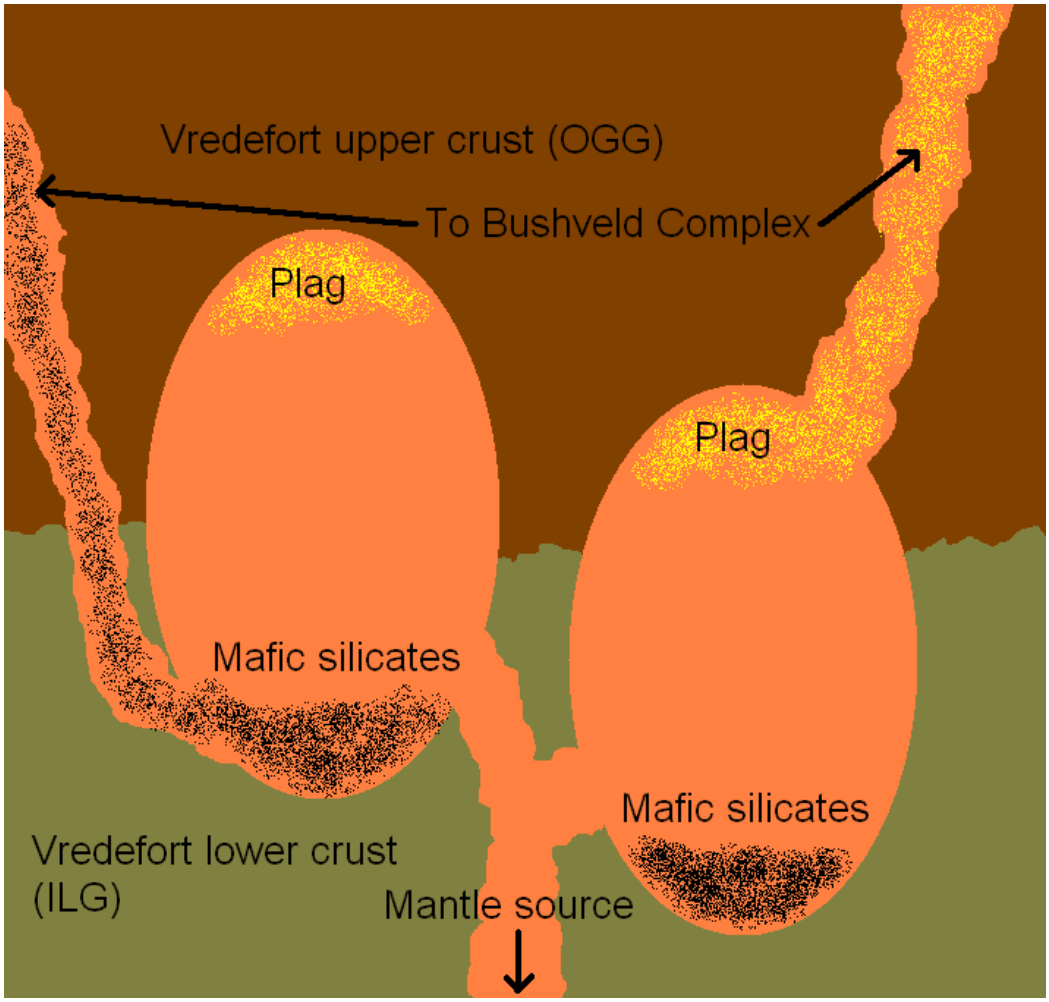

Figure 65: Schematic representation of the refined staging chamber morphology for the Main Zone of the Northern Limb taking into account the isotopic models presented above.

It is realized that 25% contamination of mantle-derived melts by crustal rocks may be cited as an unrealistically high figure. Large degrees (20-40%) of crustal contamination of Bushveld magmas are, however, also suggested by Harris et al. (2005), to account for the oxygen isotopic composition of Bushveld rocks. Marginally lower degrees of contamination may be modeled if higher degrees of partial melting

of the mantle are assumed. In these scenarios, mantle-derived melts have lower Sr and Nd concentrations (see Table 8), however, which quickly become problematic when having to account for the envisaged Sr and Nd concentrations of the contaminated melts from which plagioclase and orthopyroxene are proposed to have crystallized from.

4.2 The Platreef

4.2.1 Overview

From a petrogenetic viewpoint, the Platreef remains an enigmatic entity in that a clear correlation with the main Bushveld Complex is lacking (Kinnaird, 2004). Not considering the added complexities resultant from the existence of isotopic disequilibrium amongst co-existing minerals, Critical Zone rocks are normally assumed to have Sr_i of <0.707, whereas Main Zone rocks have Sr_i >0.707 (Kruger, 1990). The use of isotope ratios in discriminating the magma(s) parental to the Platreef is confounded by the severe contamination of the Platreef by its footwall (Cawthorn et al., 1985). Barton et al. (1986) suggests that the parental magma to the Platreef had a Sr_i comparable to that of the Merensky Reef (0.7066-0.7074, Kruger & Marsh, 1982), with the Platreef rocks overlying dolomite in the Southern Sector (Sr_i = 0.7054) and early formed orthopyroxene (Sr_i = 0.7079) representing the closest approximates for the isotopic composition of the "truly magmatic" Platreef magma, with footwall interaction having resulted in whole-rock Sr_i of up to 0.7226. For the Moordkopje drill core, whole-rock Sr_i for the unhybridized Platreef varies between 0.7084 and 0.7097, with two orthopyroxenes exhibiting values of 0.7008 and 0.7059, respectively, the former value probably being the result of late changes to the Rb/Sr ratio rather than being a reflection of the initial Sr ratio of the magma from which it crystallized. The present results are therefore in partial agreement with the results and interpretation of Barton et al. (1986) in that orthopyroxene within the unhybridized Platreef probably provides the closest approximation of the Sr_i of the "uncontaminated" Platreef magma, with whole-rock values reflecting interaction between the Platreef magma and footwall-derived granitic melts. Initial Sr ratios would therefore suggest a genetic relationship with Lower / Critical Zone magmas.

Nd isotopic data for the Platreef from the Moordkopje drill core is consistent also with the above interpretation. Whole-rock εNd for the three unhybridized Platreef samples

analysed cover the range -6.2 to -9.4, with the two orthopyroxene separates having values of -7.8 and -9.8, respectively. The fact that whole-rocks and the orthopyroxene that they host have similar initial Nd isotope ratios despite significant felsic contamination of intercumulus liquids as indicated by initial Sr ratios is explained by the similarity in the εNd values of the intruding magma and likely contaminants (εNd 9.42 to -20.7, Pronost et al., 2008). Comparison of the initial Nd isotope ratio for orthopyroxene from the Platreef with published Nd isotope data from Union Section (Maier et al., 2000) suggests that the "uncontaminated" Platreef magma from which orthopyroxene crystallized prior to significant contamination with footwall-derived felsic contaminants had a Nd isotopic signature comparable to Upper Critical Zone / Main Zone rocks, which is in contrast with the picture emerging when considering initial Sr ratios (Figure 66).

Other geochemical parameters also do not provide an unequivocal answer. According to Kinnaird (2004), the Sr content of Platreef plagioclase (<373 ppm) suggests affiliations with the Main Zone (<400 ppm) rather than with the Critical Zone (>400 ppm), whereas whole-rock $Cr_{(ppm)}/MgO_{(\%)}$ values suggest the opposite, with Cr/MgO for the Main Zone typically <50 and for the Critical Zone typically >100. The unhybridized Platreef in the Moordkopje drill core has an average whole-rock Cr/MgO of 94, with values ranging between 1.6 and 245, the former value obtained for the altered ultramafic from depth 1369 m, whereas the hybridized Platreef has an average whole-rock Cr/MgO of 77, with values ranging between 24 and 118. For comparison, Main Zone samples from the Moordkopje drill core exhibit average whole-rock Cr/MgO of 20 with values ranging between 5 and 62.

The interpretation by McDonald et al. (2005) takes cognizance of the apparently contradicting geochemical character of the Platreef as highlighted above and equates it with the so-called GNPA (Grasvally norite pyroxenite anorthosite) member of the Northern Limb, suggesting that both the Platreef and GNPA member formed in a series of mixing events involving geochemically distinct Lower Zone and Main Zone magmas.

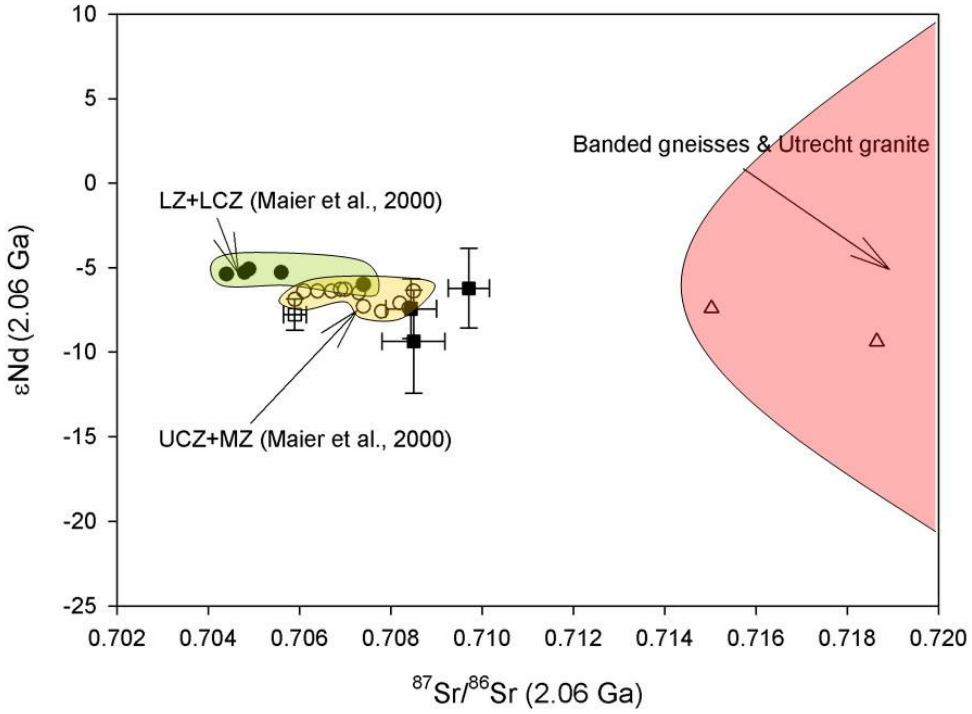

Figure 66: Binary variation diagram of ε_{Nd} versus initial Sr ratio showing data for Platreef whole-rocks (solid squares) and Platreef orthopyroxene (open square). Also shown are data for the Lower Zone, Lower Critical Zone, Upper Critical Zone and Main Zone from Union Section (Maier et al., 2000) and data for banded gneisses & Utrecht granite from the footwall to the Platreef (Pronost et al., 2008; Cawthorn et al., 1985).

4.2.4 Isotopes as tracers of footwall contamination of the unhybridized Platreef

A crude approximation of the amount of contamination underwent by the unhybridized Platreef as a result of footwall-derived partial melts can be made using the isotopic data as obtained on orthopyroxene and whole-rocks from the unhybridized Platreef. If it is assumed that the isotopic composition of cumulates produced by the Platreef magma was similar to that exhibited by orthopyroxene within the Platreef (using sample from depth 3261.7 m as proxy), then using $D_{Sr}^{Opx} = 0.007$ and $D_{Nd}^{Opx} = 0.0068$ (McKenzie & O'Nions, 1991) it can be shown that the Platreef magma had to contain 581 ppm Sr and 104 ppm Nd. A rock with modal composition similar to that from depth 3261.7 m (~9% plagioclase, 85% orthopyroxene and 6% clinopyroxene) can then be shown, using appropriate partition

coefficients for Sr and Nd into plagioclase and clinopyroxene, to have contained 105 ppm Sr and 3.2 ppm Nd when ignoring the effects of a trapped liquid fraction.

To determine the Sr and Nd concentrations of the footwall-derived partial melt, a procedure similar to that described above for the generation of partial melts from the Vredefort upper and lower crust was employed based on the experimental data of Patino Douce & Beard (1995) on the melting behaviour of synthetic biotite gneiss at a pressure of 5 kbar and for the production of a 20% equilibrium partial melt. These calculations indicate Sr and Nd contents in the melt of 96 ppm and 8.3 ppm, respectively, when using the average Sr and Nd contents of the Utrecht granite as reported by Cawthorn et al. (1985) and Pronost et al. (2008). The Utrecht granite (at T = 2.06 Ga) exhibits very variable isotopic compositions, with εNd ranging between -20.7 and 9.42 (Pronost et al., 2008) and $^{87}Sr/^{86}Sr$ ratios of between 0.7316 and 0.7906 (Cawthorn et al., 1985). In the model calculations, average εNd and $^{87}Sr/^{86}Sr$ ratios of -5.6 and 0.7699, respectively, were employed. The modeled results are depicted graphically in Figure 67, which shows that the whole-rock isotopic compositions of the unhybridized Platreef may be explained by small amounts (~5%) of contamination from partial melts derived from the Utrecht granite constituting the footwall. The model is based on the assumption that footwall-derived partial melts infiltrated the largely solidified Platreef along grain boundaries, resulting in the expulsion of the remaining interstitial melt, the presence of which would invalidate the model.

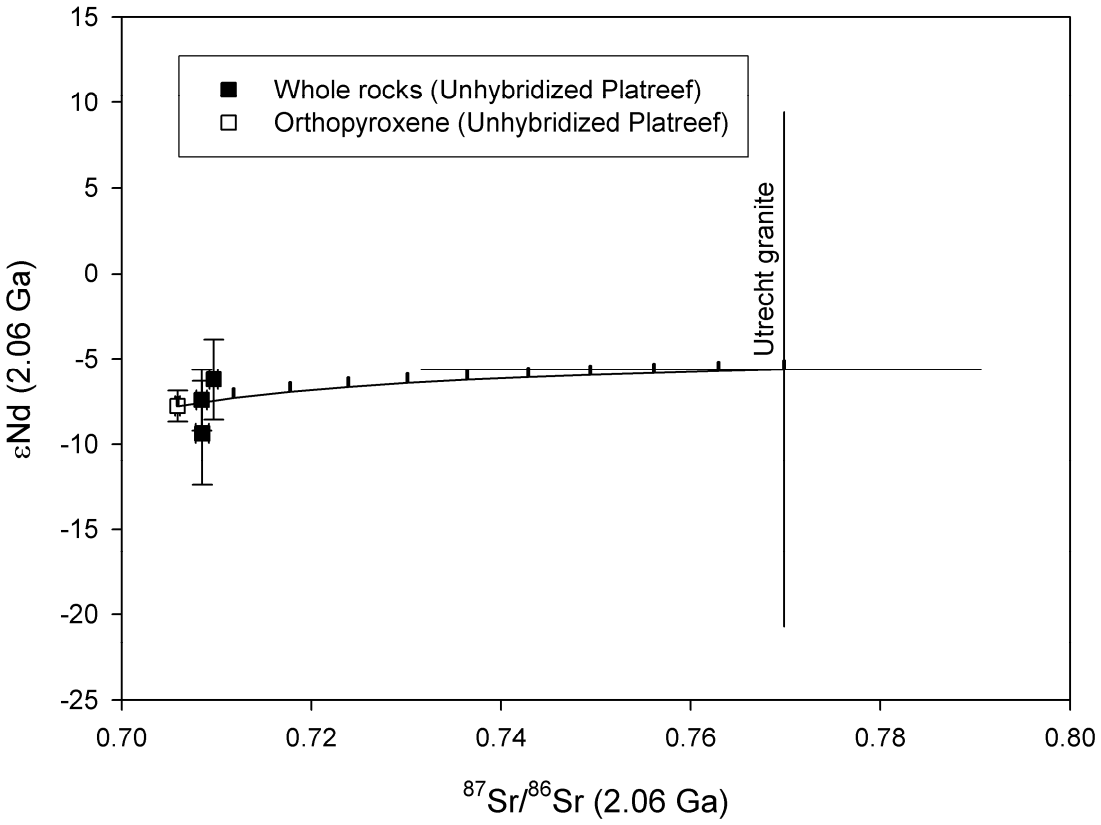

Figure 67: Isotopic mixing model showing how the isotopic compositions of whole-rocks from the unhybridized Platreef may be explained by contamination of the Platreef by small amounts of footwall-derived partial melts.

4.2.3 Rare-earth elements as indicators of footwall contamination and magmatic lineage

Sharman-Harris & Kinnaird (2004) and Sharman-Harris et al. (2005) showed that the sulfur isotopic composition of Platreef sulfides varies according to the type of footwall lithology, suggesting footwall control on sulfide mineralization within the Platreef. In this section a brief comparison will be made of the rare-earth element geochemistry of the Platreef compared to that of the footwall to the Platreef along strike in an effort to arrive at the average rare-earth element composition of Platreef cumulates least affected / unaffected by footwall interaction.

As shown above (Figure 46), unhybridized Platreef rocks have REE concentrations covering the range 1.4 to 12.6 times chondrites, whereas hybridized Platreef lithologies cover the range 2.8 to 58 times chondrites, a range intermediate between that of the unhybridized Platreef and the granitic footwall, which exhibit REE concentrations covering the range 5 to 86 times chondrites. At Overysel, the farm adjoining Moordkopje to the east, the REE concentrations of feldspathic pyroxenites of the Platreef cover the range 1.8 to 32.2 times chondrites, whereas that of quartzo-feldspathic pyroxenites cover the range 2.2 to 22.8 times chondrites (Holwell & McDonald, 2006). The footwall banded gneisses and granites cover the range 1.6 to 69 and 1.2 to 29.7 times chondrites, respectively (Figure 68).

The reef feldspathic pyroxenites at Overysel (Figure 68) exhibit Ce/Sm_N and Tb/Yb_N ratios of 1.0 to 3.0 and 0.6 to 1.4, respectively, which compares well with ratios of 1.2 to 2.7 and 0.8 to 1.7 for the unhybridized Platreef at Moordkopje. The quartzo-feldspathic pyroxenites at Overysel generally exhibit a distinct trough shaped REE profile and positive europium anomalies (Eu/Eu^* 1.2 to 1.5) that is dissimilar from that observed for the bulk of both the feldspathic pyroxenites at Overysel and the unhybridized Platreef at Moordkopje, with the quartzo-feldspathic pyroxenites exhibiting Ce/Sm_N of 1.8 to 2.7 and Tb/Yb_N of 0.6 to 1.1.

At Sandsloot, where the footwall is composed primarily of calc silicates and siliceous dolomite (McDonald et al., 2005), there is extensive overlap between the REE profiles of the primary reef, the replaced reef, including footwall hybrids and the footwall itself (Figure 69).

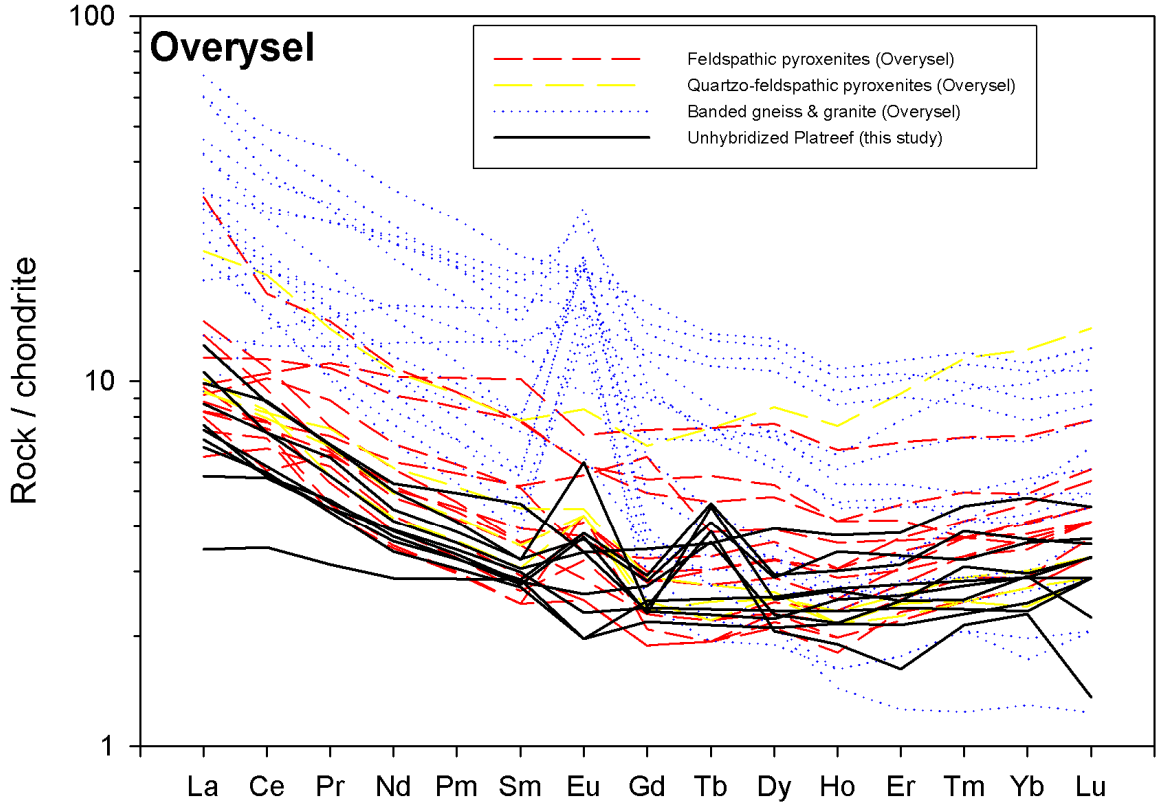

Figure 68: Chondrite normalized REE abundances in rocks of the Platreef and its footwall on Overysel (Holwell & McDonald, 2006) compared with that of the unhybridized Platreef from the Moordkopje drill core.

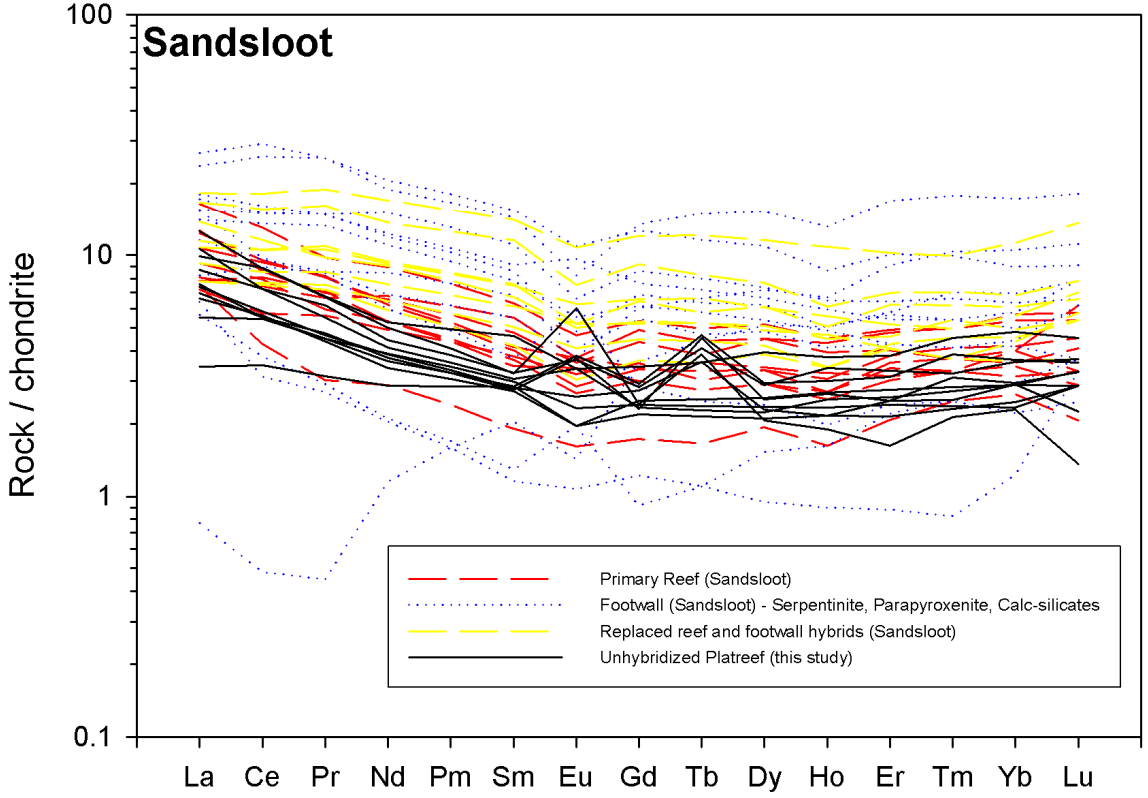

Figure 69: Chondrite normalized REE abundances in rocks of the Platreef and its footwall on Sandsloot (McDonald et al., 2005) compared with that of the unhybridized Platreef from the Moordkopje drill core.

REE concentrations for the primary reef cover the range 1.6 to 16.4 times chondrites, whereas those in the replaced reef, including footwall hybrids, and those in the footwall itself cover the range 3.0 to 18.7 and 0.5 to 29.1 times chondrites, respectively. Primary reef samples generally exhibit negative Eu anomalies, with Eu/Eu^* ranging between 0.7 and 1.1 with an average of 0.9. Ce/Sm_N ratios for the primary reef at Sandsloot range between 1.3 and 2.3 with Tb/Yb_N of between 0.6 and 1.1, compared with values of 1.2 to 2.7 and 0.8 to 1.7 for the unhybridized Platreef at Moordkopje, respectively. REE patterns for replaced reef and footwall hybrids at Sandsloot show considerably less LREE:HREE fractionation compared to both the primary reef at Sandsloot and the unhybridized Platreef at Moordkopje, with Ce/Sm_N and Tb/Yb_N covering the ranges 1.3 to 1.8 and 0.8 to 1.2, respectively.

At Townlands, the Platreef appears to be intrusive into metasediments of the Silverton Formation (Transvaal Supergroup) and occurs as three sills termed the Lower, Middle and Upper Platreef that are separated from one another by hornfels horizons (Manyeruke et al., 2005). The presence of more primitive orthopyroxene compositions in the higher reefs and decreasing whole-rock concentrations of incompatible trace elements with height are suggestive of enhanced crustal contamination of the lower reefs, with the Upper Reef therefore representing the reef least affected by crustal contamination. In terms of its REE geochemistry, it is the Upper Reef at Townlands that is most similar to the unhybridized Platreef at Moordkopje (Figure 70). The Upper Reef has REE covering the range 1.7 to 31.7 times chondrites with Ce/Sm_N and Tb/Yb_N of 1.9 to 3.2 and 0.6 to 1.5, respectively. The Middle and Lower reefs are progressively more enriched in REE with REE for the former covering the range 2.8 to 51.3 times chondrites and for the latter 5.3 to 54.0 times chondrites. The rocks of all three reefs do not show an europium anomaly. The hornfelses at Townlands are by far the most REE enriched country rocks known for the Platreef localities that have been described in literature, with REE concentrations covering the range 0.6 to 988.8 times chondrites. Ce/Sm_N and Tb/Yb_N for the hornfelses range between 1.9 to 11.4 and 0.5 to 29.1, respectively.

From the above comparison it is clear that the unhybridized Platreef at Moordkopje, along with the feldspathic pyroxenites at Overysel, the primary reef at Sandsloot and the Upper Platreef at Townlands, represent good candidates for Platreef cumulates

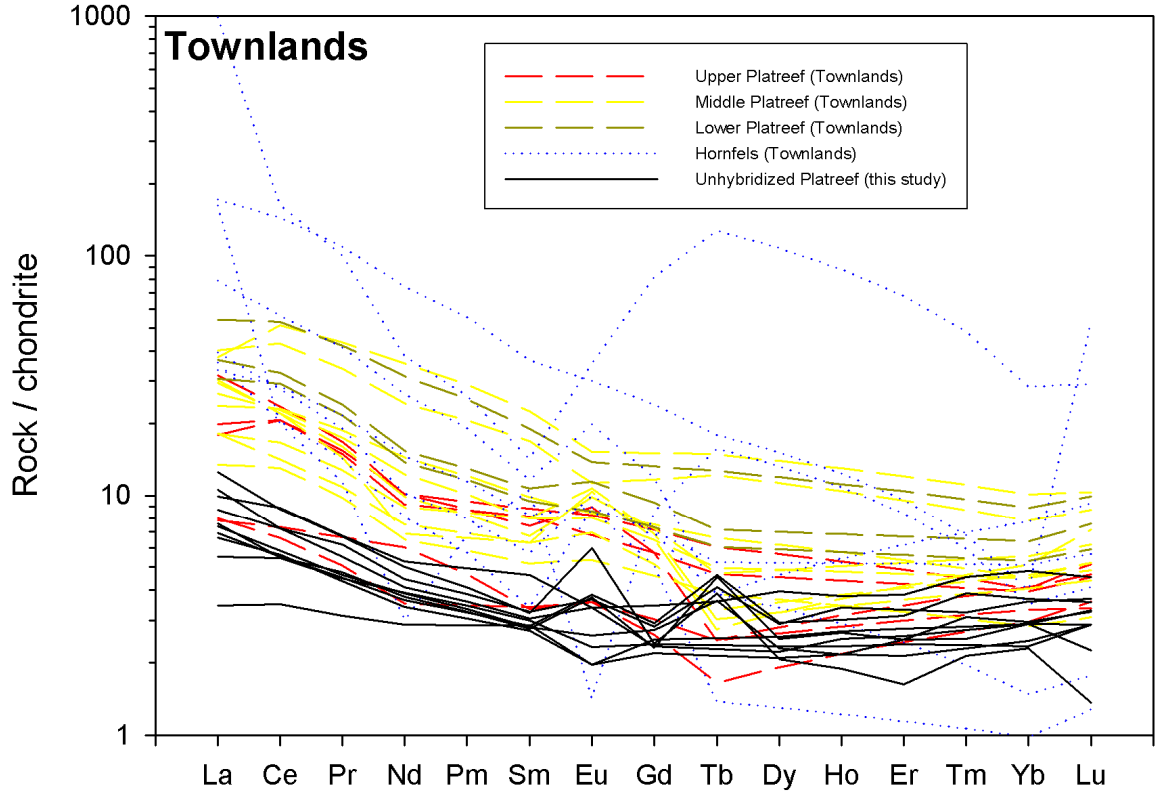

Figure 70: Chondrite normalized REE abundances in rocks of the Upper, Middle and Lower reefs at Townlands, including local hornfels (Manyeruke et al., 2005) compared with that of the unhybridized Platreef from the Moordkopje drill core.

that have experienced the minimum of interaction between the intruding Platreef magma(s) and footwall lithologies. In all instances, these units represent the stratigraphically highest horizons within the Platreef and it follows that these units would most likely show less evidence for footwall interaction than the stratigraphically lower horizons, as indeed appears to be the case when considering their REE geochemistry. On average, therefore, the Platreef cumulates showing the least amount of footwall contamination have REE concentrations covering the range 1.5 to 30 times chondrites and Ce/Sm_N and Tb/Yb_N ratios 1.0 to 3.0 and 0.6 to 1.5, respectively, with variable europium anomalies.

At Moordkopje, footwall interaction resulted in an increase in the REE content of hybridized Platreef lithologies and a concomitant increase in the Ce/Sm_N ratio of hybrid rocks as a result of the enriched REE content of the footwall granite and its significant LREE:HREE fractionation profile. At Overysel, footwall interaction with the banded gneisses did not significantly alter the REE geochemistry of the resultant quartzo-feldspathic pyroxenites due to significant overlap in the REE profiles of the former and latter, apart from perhaps a slight decrease in the Tb/Yb_N ratio of the quartzo-feldspathic pyroxenites and the generation of positive europium anomalies in these rocks as a result of interaction with the gneisses which also have distinct positive europium anomalies.

At Sandsloot, overlap between the REE profiles of the primary reef and its footwall (serpentinites, calc-silicates & parapyroxenites) is the most pronounced for all four Platreef localities compared above. Footwall interaction at Sandsloot, apart from resulting in a generalized increase in the REE contents of contaminated rocks, also resulted in a slight decrease in the Ce/Sm_N ratio of these rocks as a result of the fairly low Ce/Sm_N ratios of the footwall lithologies (0.2 to 2.9), whereas at Townlands, footwall interaction primarily resulted in an increase in the REE contents of the Lower and Middle reefs as a result of the very high REE contents of the hornfels country rocks.

The identification of Platreef cumulates showing limited evidence for footwall interaction along the strike of the Northern Limb allows one to use the incompatible trace element characteristics (including those of the REEs) of these cumulates in order

to assess the likely magmatic lineage of the Platreef. A broadly similar approach, albeit aided by the availability of REE data for mineral separates, was used by Charlier et al. (2005) to constrain the composition of the parental magma to the Bjerkreim-Sokndal layered intrusion in Norway. Two magmas are generally proposed as being parental to the Bushveld Complex Lower, Critical and Main Zones:

- A so-called B-1 magma believed to be parental to the Lower and Lower Critical zones, and;
- A so-called B-3 magma believed to be parental to the Upper Critical and Main zones (Harmer & Sharpe, 1985).

Sr-isotopic, Mg#, REE and incompatible trace element data for the Lower and Lower Critical zones are compatible with crystallization from the putative B-1 magma, whereas the same cannot be said of the B-3 magma for the Upper Critical and Main zones (Eales, 2002). It would therefore appear from the literature that the B-1 magma was certainly involved in the genesis of the Bushveld Complex, but that the B-3 magma may not have been important in the genesis of the Bushveld Complex at all.

Binary variation diagrams of P_2O_5, Rb and Zr versus total REE and for Zr/Rb versus Ce/Sm for the Platreef least affected or unaffected by footwall contamination (as exemplified by the unhybridized Platreef in the Moordkopje drillcore, by the Primary Reef at Sandsloot and by the feldspathic pyroxenites at Overysel) are presented in Figures 71 to 74, where the data are compared to that of the proposed B-1 and B-3 magmas. The diagrams clearly illustrate the fact that B-3 magma was not involved in the genesis of the Platreef, whereas B-1 magma may explain the trace element characteristics of the Platreef on the assumption that the bulk of the incompatible trace elements within Platreef cumulates are hosted within a trapped liquid fraction.

Modelling of the amount of footwall contamination underwent by the hybridized Platreef in the Moordkopje rocks is complicated by uncertainty as to the composition of possible footwall-derived partial melts and by the fact that the Platreef rocks probably represent cumulates and not liquids. However, if it is assumed that contamination of the unhybridized Platreef was achieved through interaction with a melt having the same bulk composition as that of the footwall, and that such melt

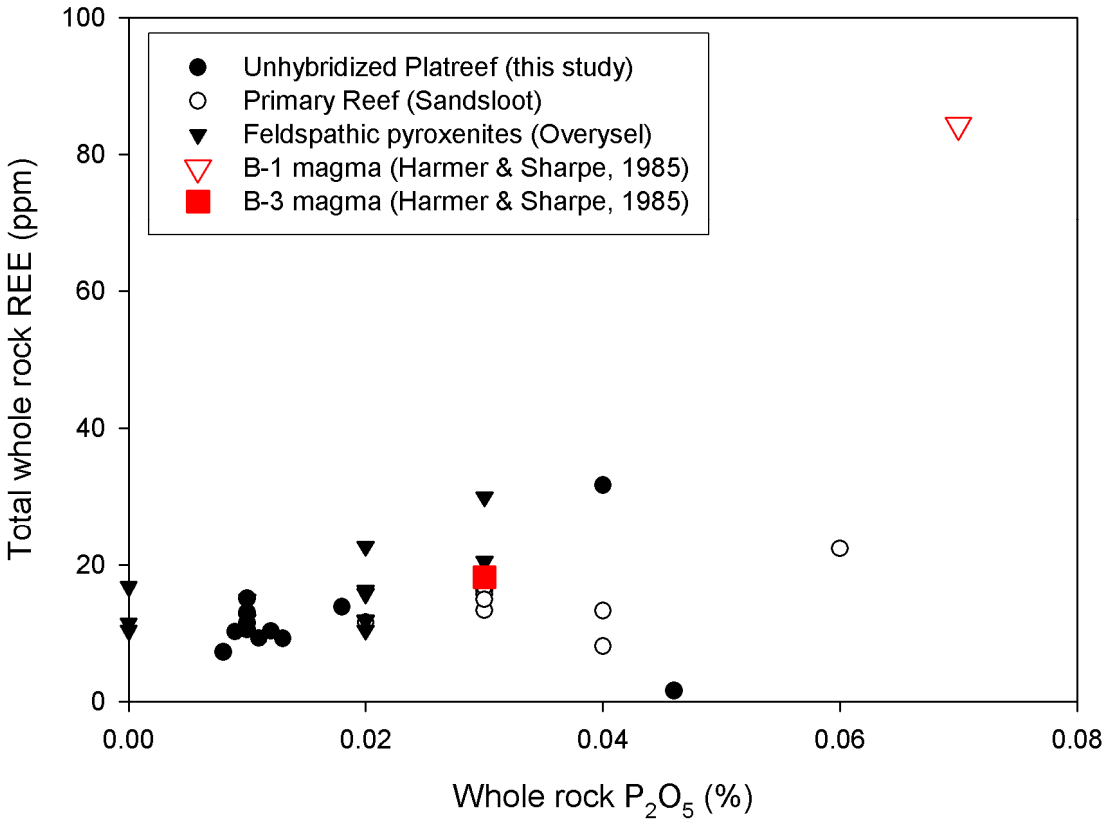

Figure 71: Binary variation diagram of P_2O_5 versus total REE for Platreef rocks least affected or unaffected by footwall contamination. Data for the B-1 and B-3 magma of Harmer & Sharpe (1985) shown for comparison.

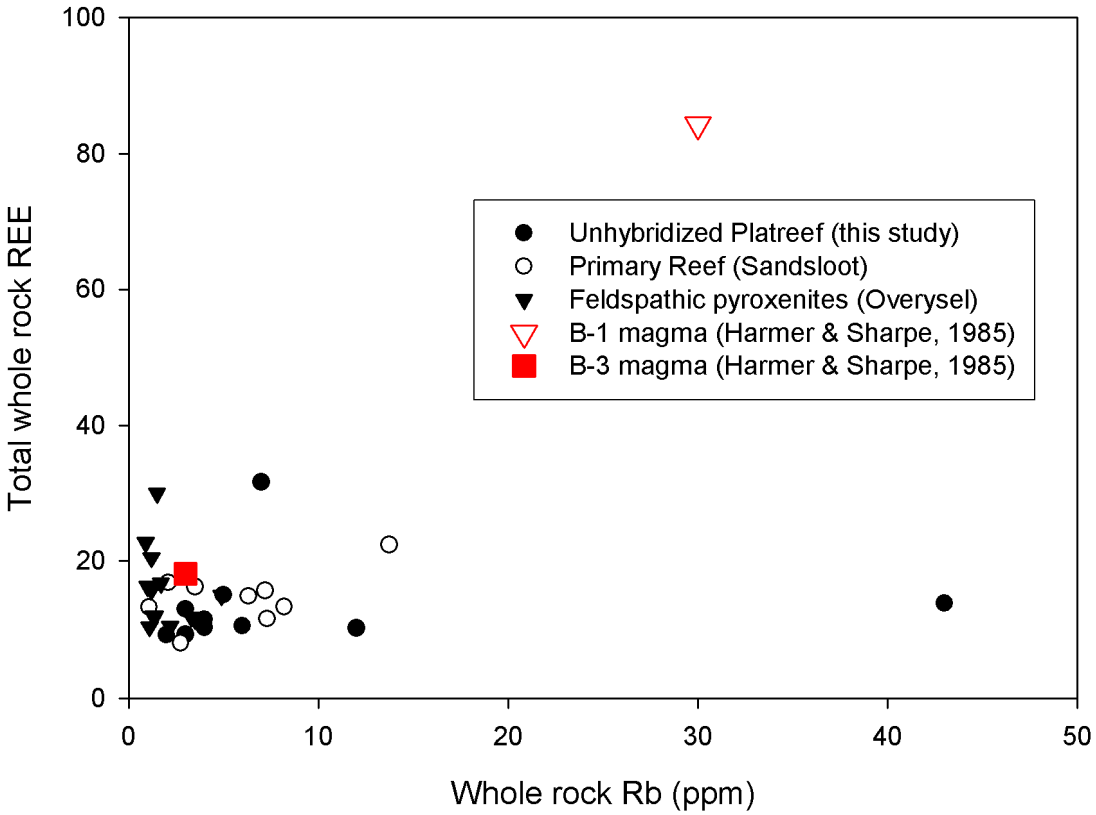

Figure 72: Binary variation diagram of Rb versus total REE for Platreef rocks least affected or unaffected by footwall contamination. Data for the B-1 and B-3 magma of Harmer & Sharpe (1985) shown for comparison.

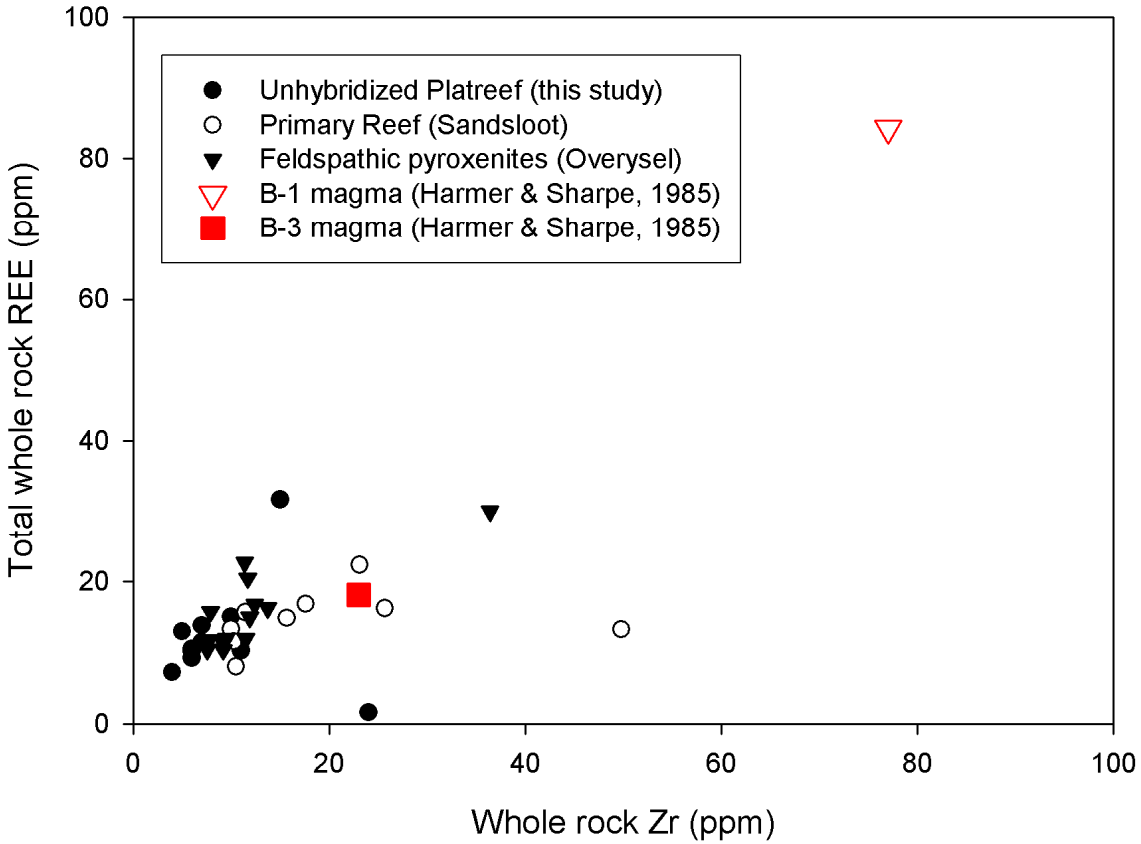

Figure 73: Binary variation diagram of Zr versus total REE for Platreef rocks least affected or unaffected by footwall contamination. Data for the B-1 and B-3 magma of Harmer & Sharpe (1985) shown for comparison.

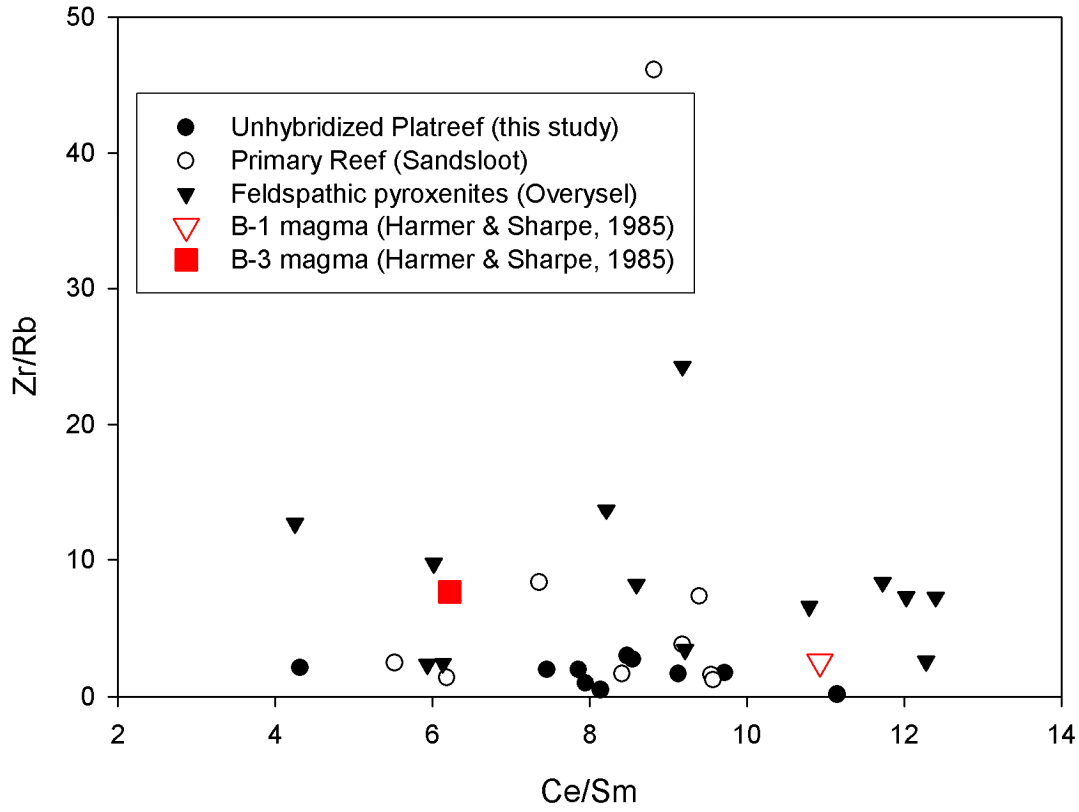

Figure 74: Binary variation diagram of Zr/Rb versus Ce/Sm for Platreef rocks least affected or unaffected by footwall contamination. Data for the B-1 and B-3 magma of Harmer & Sharpe (1985) shown for comparison.

infiltrated the partially solidified Platreef where it mixed with the remaining interstitial liquid, a reasonable approximation of the amount of contamination underwent by the hybridized Platreef can be made by considering the incompatible trace element ratios of the unhyridized Platreef, the hybridized Platreef and the granitic footwall (Figure 75 and 76). Consideration of Th/Nd versus Ce/Sm suggests 10% to 40% contamination of the unhybridized Platreef by footwall-derived melts, with similar amounts of contamination indicated when considering Zr/Rb versus Ce/Sm. These values may be cited as being arrived at in an overly simplistic manner, but are supported by the modal amount of quartz-feldspar graphic intergrowths in the rocks of the hybridized Platreef which is typically present in quantities in excess of ~10%.

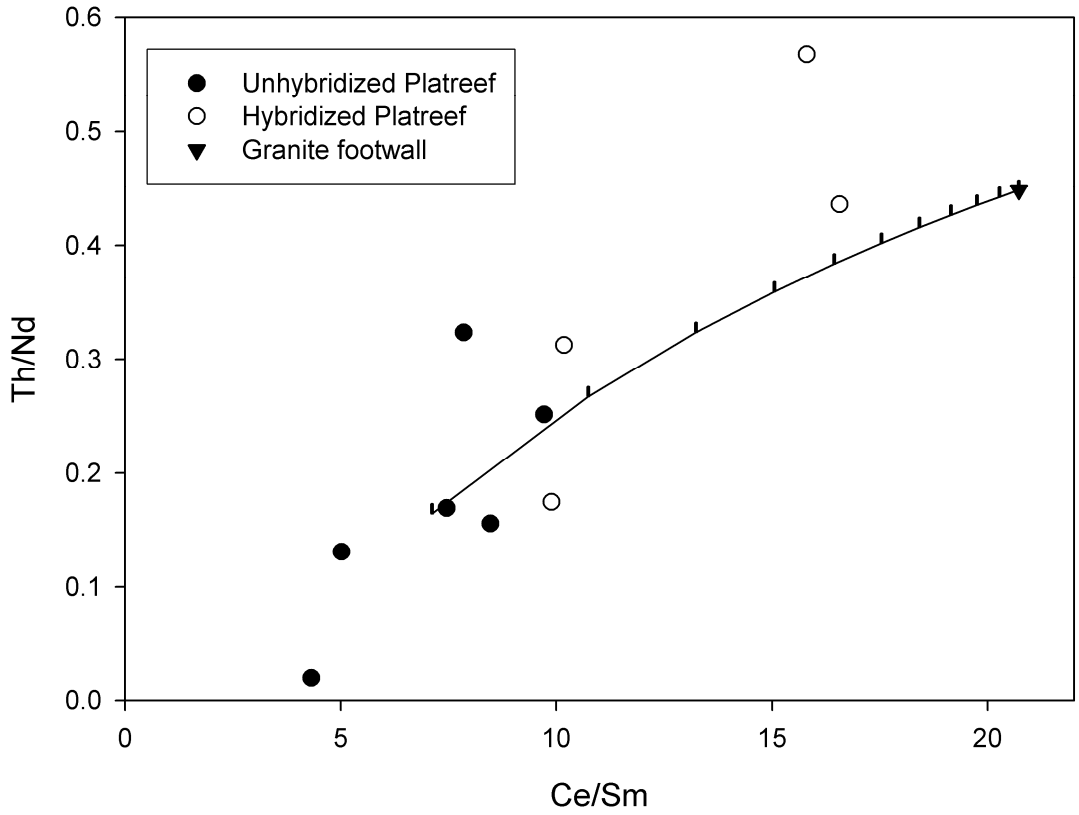

Figure 75: Whole-rock Th/Nd versus Ce/Sm for the unhybridized Platreef, the hybridized Platreef and the granite footwall.

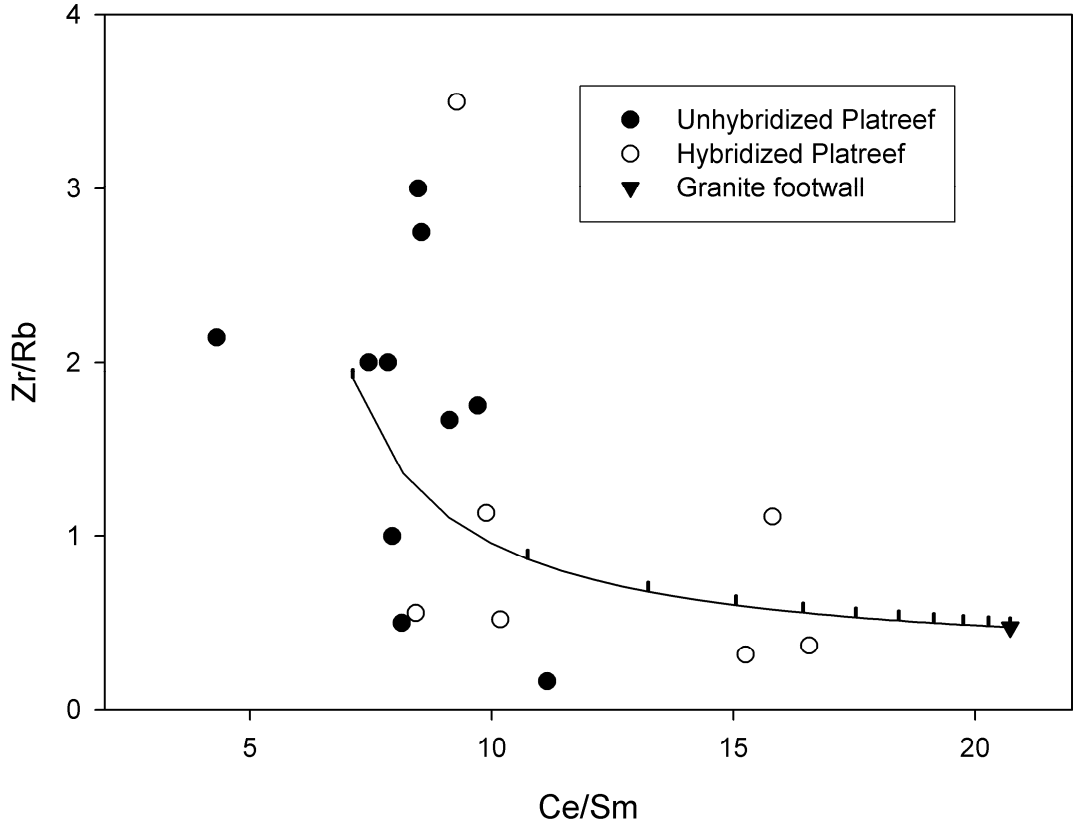

Figure 76: Whole-rock Zr/Rb versus Ce/Sm for the unhybridized Platreef, the hybridized Platreef and the granite footwall.

4.3 Bulk composition of the Bushveld Complex

The current whole-rock geochemical dataset allows calculation of an estimated bulk composition for the Bushveld Complex and a comparison with previous estimates and postulated parental magma compositions. Eales (2002) highlighted the difficulties associated with attempts to model the bulk composition of the Bushveld Complex and the reader should therefore take heed of the limitations of such an exercise. The main difficulties summarized by Eales (2002) are:

- Uncertainty with respect to the shape of the Bushveld Complex magma chamber.
- The notion that chilled margins taken to represent parental magma compositions may be different from the calculated bulk composition as a result of the intrusion of crystal charged slurries rather than aphyric liquids.
- The lack of knowledge regarding lateral variations within the layered sequence of the Bushveld Complex.
- The possible expulsion of residual liquids from the Bushveld magma chamber.

Table 9 contains the results of the calculations using the present dataset in addition to unpublished whole-rock data for the Bellevue drill core compared to published estimates and postulated parental magma compositions. The calculation procedure employed entailed calculation of the arithmetic mean of all samples belonging to a specific stratigraphic unit (viz. Upper Zone, Main Zone, the Bellevue troctolite horizon and Platreef), with the weighted mean then calculated based on the thickness of each unit.

All calculation methods (columns 2-5, Table 9) indicate that the cumulates of the Main Zone are typically enriched in components associated with feldspar (Al_2O_3, CaO, Na_2O & K_2O) and depleted in mafic components (FeO, MgO, TiO_2, Cr_2O_3, MnO), relative to postulated parental magma compositions for the Main Zone. For SiO_2 the results are ambiguous. At first glance, the results appear to be in agreement with the suggestion by Maier et al. (2001, 2001) that the Main Zone was intruded as plagioclase-rich crystal mushes that formed as a result of mixing of Bushveld mantle-derived magma(s) with plagioclase-rich residues of partial melting of upper crustal material. However, if such upper crustal residues were indeed entrained by Bushveld

Table 9:Estimated bulk compositions of the Main and Upper zones compared with similar estimates from other localities and proposed parental magma compositions.

	Present dataset combined with unpublished data from the BV1 drill core							
	MZ (excl. Platreef & troctolite)	**MZ (incl. troctolite excl. Platreef)**	**MZ (incl. Platreef excl. troctolite)**	**MZ (incl. Platreef & troctolite)**	**MZ + UZ (incl. Platreef & troctolite)**	**MZ (Mitchell, 1986)[a]**	**B3 (Harmer & Sharpe, 1985)[a]**	**B3 (Maier et al., 2000)**
n	*220*	*248*	*233*	*261*	*307*	*23*		
SiO_2	51.21	50.88	51.14	50.83	48.79	51.85	50.8	51.58
Al_2O_3	20.23	20.28	19.64	19.74	19.36	18.89	16.1	16.04
Fe_2O_3 (tot)	6.34	6.41	6.55	6.60	10.82	6.57	9.79	10.62
MnO	0.11	0.11	0.12	0.12	0.13	0.12	0.16	0.19
MgO	6.19	6.66	6.86	7.26	5.85	7.87	8.26	7.57
CaO	12.57	12.47	12.29	12.22	11.25	11.93	11.5	10.95
Na_2O	2.36	2.30	2.28	2.22	2.47	2.23	2.32	1.85
K_2O	0.33	0.31	0.32	0.31	0.36	0.20	0.2	-
TiO_2	0.21	0.19	0.20	0.19	1.04	0.14	0.39	0.46
P_2O_5	0.02	0.02	0.02	0.02	0.09	-	-	0.05
Cr_2O_3	0.02	0.03	0.04	0.04	0.03	0.03	0.06	0.07
Total	**99.58**	**99.66**	**99.47**	**99.55**	**100.20**	**99.83**	**99.58**	**99.38**
Mg#	0.66	0.67	0.68	0.69	0.52	0.71	0.63	0.59

a: As cited by Maier & Barnes (1998)

magmas as they intruded the main chamber of the Bushveld Complex as is suggested by Maier et al. (2001), it may be expected of plagioclase within the Main Zone to have isotopic compositions akin to those modeled for the restites by Maier et al. (2000). These authors have shown the restites to have ε_{Nd} and Sr_i of -17 and 0.716, respectively, which are considerably different from the values obtained for plagioclase separates in the present study. Although I concur with the fact that the Main Zone probably was intruded as crystal mushes, they most probably did not originate in the fashion suggested by Maier et al. (2000, 2001), as is also indicated by the isotopic models developed above (see section 4.1.5). In-situ isotopic determinations on Main Zone plagioclases will be useful in determining whether the Main Zone contains plagioclase sharing the isotopic characteristics suggested by Maier et al. (2001).

The present dataset also allowed calculation of the bulk composition of the Main and Upper zones taken collectively, the results of which are presented in column 6 of Table 9. The bulk composition of the combined Main and Upper Zones are richer in FeO, Na_2O, K_2O, TiO_2 and P_2O_5 and poorer in SiO_2, Al_2O_3, MgO and CaO relative to that of the Main Zone considered alone, which is largely a reflection of the mafic minerals becoming more iron-rich and the feldspars becoming less calcic as differentiation proceeded. The lower silica content of the combined Main and Upper zones relative to the Main Zone alone may be a consequence of a variety of factors, including: a) the presence of abundant non-silicates within the Upper Zone, including titano-magnetite and apatite (and their possible over-representation in the suite of analysed rocks); b) the presence of iron-rich silicates containing less silica by mass compared to their more magnesian counterparts, which offsets the expected increase in silica associated with the presence of less calcic feldspars; c) the possible loss of liquids enriched in silica as volcanics; and d) the possibility that the Upper Zone crystallized from a fundamentally different parental magma than that parental to the Main Zone (cf. Davies & Cawthorn, 1984).

A major point related to the calculations presented in Table 9 above, is the fact that the calculated bulk compositions do not reflect viable melt compositions. Modelling using the MELTS software package of Ghiorso & Sack (1995) at a nominal pressure of 3 kbar and a melt composition similar to that given in column 2 of Table 9 shows

that the first mineral to crystallize from such a magma will be plagioclase (An% = 83%) at a temperature on the order of 1290°C. Clinopyroxene (Mg# = 0.81) joins plagioclase in the crystallizing assemblage only at a temperature of ~1240°C, when the fraction of remaining liquid equals ~72%. It is therefore clear that a magma of this composition cannot give rise to cumulates dominated by plagioclase + 2 pyroxenes. Melt with a composition similar to that given in column 6 of Table 9 also has plagioclase (An% = 82%) as liquidus mineral at a temperature of ~1270°C. Small amounts of spinel join the crystallizing assemblage at a temperature of ~1260°C and only at a temperature of ~1220°C does orthopyroxene (Mg# = 0.81) start to crystallize, when the fraction of remaining liquid equals ~77%. A magma of such a composition is therefore also not a viable melt composition to produce cumulates dominated by plagioclase + 2 pyroxenes.

A conclusion consistent with that arrived at in the preceding paragraph is reached when considering the CIPW normative mineralogy of the calculated bulk compositions when plotted in the system Opx-Cpx-Plag as presented by Nex et al. (2002) and containing the postulated eutectic compositions of Cawthorn & Davies (1983) and Irvine (1970) at pressures of 3 kbar and 4.5 kbar, respectively (Figure 77). All compositions plot well within the plagioclase field, which would suggest that magmas with such compositions will crystallize significant quantities of plagioclase before becoming saturated in one or both pyroxenes.

Possible solutions to this apparent contradiction could entail either the loss of liquids from the Bushveld Complex magma chamber as volcanics (cf. Cawthorn & Walraven, 1998; Barnes et al., 2004) or perhaps the retention of liquids within a staging chamber and hence, the fact that the Bushveld Complex "cumulates" do not represent cumulates formed within the Bushveld Complex itself, but rather within a staging chamber underlying the complex, as also suggested above. The latter option is favoured by the lack of suitably aged volcanics within the Bushveld Complex igneous province (Eales, 2002; Kruger, 2005), with the removal of such volcanics by erosion also seeming unlikely taking into account the small age difference between the Bushveld Complex and somewhat younger supracrustals (e.g. Waterberg and Soutpansberg Groups) (Dorland et al., 2006).

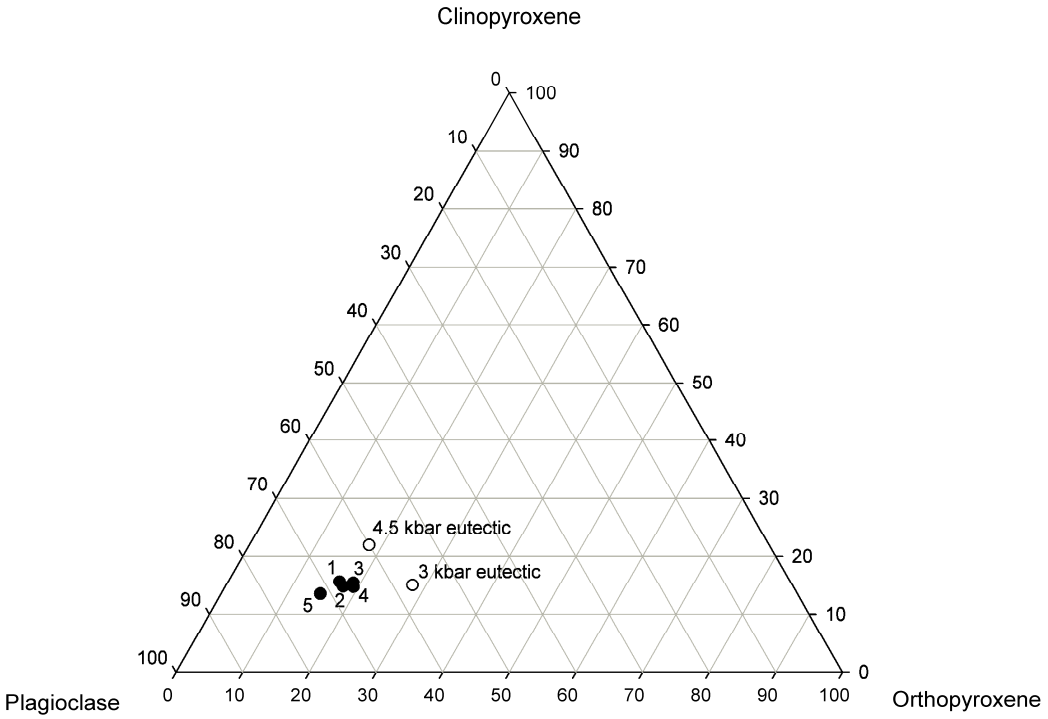

Figure 77: Triangular diagram of CIPW normative mineralogy in the system Opx-Cpx-Plag after Nex et al. (2002). Positions of postulated eutectic compositions after Cawthorn & Davies (1983) and Irvine (1970), at 3 kbar and 4.5 kbar, respectively. Numbers 1-5 refer to bulk compositions in columns 2-6 of Table 9. All calculated compositions lie well within the plagioclase field.

5. SUMMARY & CONCLUSIONS

The Main Zone of the Northern Limb, apart from sharing petrographic features with the Main Zone as known from the Eastern and Western limbs, differs in a number of respects with the latter. These differences include:

- The absence of well-known marker horizons of the Eastern and Western limbs (e.g Pyroxenite Marker, Giant Mottled Anorthosite etc).
- The presence of an anomalous troctolite layer not present within the Eastern and Western limbs.
- The relative paucity of inverted pigeonite within the Northern Limb compared to both the Eastern and Western limbs.

- The virtual lack of differentiation in the lower Main Zone of the Northern Limb as exemplified by parameters such as the An content of plagioclase, the Mg# of mafic silicates and the modified differentiation index.
- The existence of isotopic disequilibrium between co-existing minerals within the lower Main Zone, a feature that has not been described for the Main Zone as present in the other limbs of the Bushveld Complex.
- Decoupling of the differentiation trends of plagioclase and pyroxene in the lower Main Zone of the Northern Limb, a feature only locally observed elsewhere in the Bushveld Complex.

Many of these differences may be explained if the lower Main Zone of the Northern Limb formed not by in-situ fractional crystallization of magma within the Bushveld Complex magma chamber, but instead by the intrusion of crystal mushes from a deep-seated staging chamber straddling the boundary between the upper and lower crust. As such, the petrogenesis of the Main Zone of the Northern Limb is thought to have involved the intrusion of crystal mushes of plagioclase and pyroxene from a sub-Bushveld staging chamber. The staging chamber itself is proposed to have consisted of two sub-compartments connected at depth, with the wall rocks of the sub-compartments differing in terms of their radiogenic Sr contents. Plagioclase crystallized within the staging chamber is proposed to have floated to the tops of the sub-compartments with mafic minerals settling to their bases. The morphology of the chamber may have been such that magma pulses entering the main Bushveld magma chamber contained floated plagioclase from one of the sub-compartments mixed with mafic silicates settled onto the floor of the other sub-compartment. Continued residence of magma within the staging chamber and intermittent replenishment thereof is thought to be responsible for the apparent major element equilibrium seen in the Main Zone coupled with isotopic disequilibrium amongst co-existing phases.

Isotopic models suggest that the sub-compartment that contributed mostly plagioclase to the Bushveld Complex may have been contaminated by ~25% of a melt dominated by lower crustal material (70-80%) with a smaller contribution from upper crustal material (20-30%), whereas the sub-compartment from which the mafic silicates were derived, was contaminated by similar amounts of a melt richer in upper crustal

material (30-40%) and poorer in lower crustal material (60-70%) in comparison to that which contaminated the sub-compartment from which plagioclase was derived. It should be noted that the models developed in this regard do not provide conclusive answers, but that significant crustal isotopic heterogeneity of the Kaapvaal craton at 2.06 Ga provided a backdrop against which mantle-derived melts could have acquired significantly different isotopic compositions.

The abrupt increase in the FeO content of plagioclase some distance below the troctolite horizon of the Main Zone is thought to be the result of a sudden increase in the pressure prevalent within the staging chamber, perhaps as a result of a large addition of magma. Such a pressure increase may have resulted in an increase in the oxygen fugacity of the magma and a concomitant increase in the partition coefficient for FeO_T into plagioclase. Early formed mafic cumulates may subsequently have been ripped from the floor of the staging chamber as a result of voluminous magma input into the main Bushveld magma chamber giving rise to the anomalous troctolite layer occurring within otherwise 'normal' Main Zone cumulates. This last voluminous pulse of magma then proceeded to crystallize within the main magma chamber, with the result that rocks above the troctolite layer show a clear differentiation trend towards lower An content of plagioclase and lower Mg# of pyroxene. Only at a height of ~550 m above the troctolite layer did the magma differentiate to such an extent as to allow for the crystallization of inverted pigeonite.

A number of aspects related to the proposed model may be independently tested, including:

- whether the basal parts of the lower Main Zone exhibit lesser isotopic disequilibrium in comparison to the higher parts as will be expected if the initial magma pulses did not dwell within the staging chamber for extended time periods and therefore did not experience sufficient wall rock assimilation to result in significant isotopic disequilibrium. The results of the present study, although limited in this regard, suggest that this may indeed be the case;
- whether the troctolite horizon exhibits isotopic disequilibrium or not. However, either possibility may be accommodated by the present model. Because the troctolite is thought to represent early formed cumulates ripped

from the floors and roofs of the staging chamber, it may be possible that isotopic disequilibrium is absent as a result of the fact that the magmas from which these cumulates were derived did not undergo extensive contamination within the staging chamber at such an early stage of the staging chamber's evolution;

- whether the Main Zone above the troctolite layer exhibits isotopic disequilibrium or not, with the latter to be expected if the present model has merit.

In support of a model whereby the lower Main Zone was formed by the intrusion of crystal mushes rather than by in-situ fractional crystallization, is the fact that the bulk compositions of the cumulates of the Main and Upper zones of the Northern Limb do not appear to be of a suitable composition to allow for the crystallization of plagioclase + 2 pyroxenes. Supporters of an in-situ origin for the Main Zone will suggest that the missing component required for a bulk magma composition capable of crystallizing plagioclase + 2 pyroxenes may have been lost from the Bushveld magma chamber as a result of volcanic acitivity. Such an argument is, however, confounded by the lack of suitably aged volcanics within the Bushveld Complex magmatic province and by recognition of the fact that complete removal of such volcanics by erosion appears to be unlikely when taking into account the short time interval between the age of the Bushveld Complex and somewhat younger supracrustals (e.g. Waterberg and Soutpansberg Groups). It therefore becomes much more likely that the missing component may have been retained within a staging chamber at depth.

The recognition of isotopic disequilibrium within the Main Zone casts doubt on the significance of conclusions drawn based only on the isotopic data for whole-rocks or single mineral separates, as is frequently encountered within literature. There is therefore a clear need for more isotope data on the Bushveld Complex, and specifically so for isotope data on mineral separates. Taking into account the vastness of the Bushveld Complex and the isotopic heterogeneity of the Kaapvaal crust into which the Bushveld Complex was emplaced, it also appears feasible and indeed likely, that isotopic disequilibrium may not only exist between co-existing minerals, but also on the scale of an individual mineral grain or between different grains of the

same mineral. In such a case, the isotopic analysis of mineral separates may in itself be insufficient. Ideally, therefore, isotopic analyses should be performed at the scale of single crystals, a technique which has only been recently developed for strontium isotopes (Charlier et al., 2006).

The number of Platreef samples studied during the present investigation was probably insufficient for such a heterogeneous body of rocks, but the resultant data nevertheless allowed for a comparison to be drawn between the Platreef as exposed in the Moordkopje drill core and the Platreef as exposed at other localities along the strike of the Northern Limb. In particular, comparison of the REE data for Platreef samples along the strike of the Northern Limb allowed for the identification of those Platreef cumulates least affected or unaffected by footwall interaction, typically being those rocks occurring in the vicinity of the hangingwall contact of the Platreef, as would intuitively be expected. Incompatible trace element abundances and ratios suggest a B-1 magmatic lineage for the Platreef, which would equate the Platreef with the Lower and Lower Critical zones of the remainder of the Bushveld Complex. Such a conclusion is also arrived at when considering the initial $^{87}Sr/^{86}Sr$ ratio of orthopyroxene within the Platreef, which is deemed to have crystallized from the Platreef magma before significant contamination by footwall-derived melts took place.

Two modest contributions pertaining to the geology of the Northern Limb, although not forming part of the study as originally planned, were also made in the course of this study. The first was the description of a rare form of exsolution texture known as symplectitic augite, occurring within the Platreef, that was proposed to be indicative of fluid / rock interaction and an associated increase in grain boundary mobility of augite within the Platreef. The second was the description of a texture occurring within the hangingwall to the Platreef, in which orthopyroxene exsolution lamellae within clinopyroxene protrude into adjacent plagioclase crystals. The texture was probably formed during late-stage infiltration of a more primitive magma into the nearly solidified crystal mush of the Main Zone, with concomitant displacement of the last dregs of intercumulus melt. The realization that cumulate rocks may be affected by melt migration of this sort has important implications for the way in which such

rocks are studied and calls for a re-assessment of the well established dogmas pertaining to the study of layered intrusions.

6. REFERENCES

Anders, E. & Grevesse, N. (1989) *Abundances of the elements: Meteoritic and solar.* Geochimica et Cosmochimica Acta 53: 197-214

Arndt, N.T., Czamanske, G.K., Wooden, J.L., Fedorenko, V.A. (1993) *Mantle and crustal contributions to continental flood volcanism.* Tectonophysics 223: 39-52

Ashwal, L.D., Webb, S.J., Knoper, M.W. (2005) *Magmatic stratigraphy in the Bushveld Northern Lobe: continuous geophysical and mineralogical data from the 2950m Bellevue drill core.* South African Journal of Geology 108: 199-232

Ashwal, L.D. & Wiebe, R.A. (1989) *Isotopic disequilibrium in the internal Sm-Nd and Rb-Sr systematics of Proterozoic anorthosites.* EOS Transactions of the American Geophysical Union 70: 486

Bacon, C.R. & Druitt, T.H. (1988) *Compositional evolution of zoned calcalkaline magma chamber of Mount-Mazama, Crater Lake, Oregon.* Contributions to Mineralogy and Petrology 98: 224-256

Barnes, S-J., Maier, W.D., Ashwal, L.D. (2004) *Platinum-group element distribution in the Main Zone and Upper Zone of the Bushveld Complex, South Africa.* Chemical Geology 208: 293-317

Barnes, S-J., Savard, D., Bédard, L.P., Maier, W.D. (2009) *Selenium and sulfur concentrations in the Bushveld Complex of South Africa and implications for formation of the platinum-group element deposits.* Mineralium Deposita 44: 647-663

Barton, J.M., Barton, E.S., Kröner, A. (1999) *Age and isotopic evidence for the origin of the Archaean granitoid intrusives of the Johannesburg Dome, South Africa.* Journal of African Earth Sciences 28: 693-702

Barton, J.M. Cawthorn, R.G., White, J. (1986) *The role of contamination in the evolution of the Platreef of the Bushveld Complex.* Economic Geology 81: 1096-1104

Barton, J.M., Hunter, D.R., Jackson, M.P.A., Wilson, A.C. (1980) *Rb-Sr age and source of the Bimodal Suite of the Ancient Gneiss Complex, Swaziland.* Nature 283: 756-758

Beattie, P. (1993) *The effect of partial melting of spinel peridotite on uranium series disequilibria: constraints from partitioning studies.* Earth and Planetary Science Letters 177: 379-391

Bédard, J.H.J., Marsh, B.D., Hersum, T.G., Naslund, H.R., Mukasa, S.B. (2007) *Large-scale mechanical redistribution of orthopyroxene and plagioclase in the Basement Sill, Ferrar Dolerites, McMurdo Dry Valleys, Antarctica. Petrological, mineral-chemical and field evidence for channelized movement of crystals and melt.* Journal of Petrology 48: 2389-2326

Begemann, F., Ludwig, K.R., Lugmair, G.W., Min, K., Nyquist, L.E., Patchett, P.J., Renne, P.R., Shih, Y., Villa, I.M., Walker, R.J. (2001) *Call for an improved set of decay constants for geochrnological use.* Geochimica et Cosmochimica Acta 65: 111-121.

Biesheuvel, K. (1970) *An interpretation of a gravimetric survey in the area west of the Pilanesberg in the Western Transvaal* in Symposium on the Bushveld Igneous Complex and other Layered Intrusions (Visser, DJL, Von Gruenewaldt, G, eds.) Geological Society of South Africa Special Publication 1, 266-282

Bindeman, I.N., Davis, A.M., Drake, M.J. (1998) *Ion microprobe study of plagioclase-basalt partition experiments at natural concentration levels of trace elements.* Geochimica et Cosmochimica Acta 62: 1175-1193

Blundy, J.D. & Wood, B.J. (1991) *Crystal-chemical controls on the partitioning of Sr and Ba between plagioclase feldspar, silicate melts, and hydrothermal solutions.* Geochimica et Cosmochimica Acta 55: 193-209

Bougault, H. & Hekinian, R. (1974) *Rift valley in the Atlantic Ocean near 36°50'N; petrology and geochemistry of basaltic rocks.* Earth and Planetary Science Letters 24: 249-261

Buchanan, P.C., Reimold, W.U., Koeberl, C., Kruger, F.J. (2004) *Rb-Sr and Sm-Nd isotopic compositions of the Rooiberg Group, South Africa: early Bushveld-related volcanism.* Lithos 29: 373-388

Buick, I.S., Maas, R., Gibson, R. (2001) *Precise U-Pb titanite age constraints on the emplacement of the Bushveld Complex, South Africa.* Journal of the Geological Society of London 158: 3-6

Canil, D. (1999) *Vanadium partitioning between orthopyroxene, spinel and silicate melt and the redox states of mantle source regions for primary magmas.* Geochimica et Cosmochimica Acta 63: 557-572

Carlson, R.W., Hunter, D.R., Barker, F. (1983) *Sm-Nd age and isotopic systematics of the bimodal suite, ancient gneiss complex, Swaziland.* Nature 305: 701-704

Cawthorn, R.G. (2005) *Contrasting sulphide contents of the Bushveld and Sudbury Igneous Complexes.* Mineralium Deposita 40: 1-12

Cawthorn, R.G. (2007) *Cr and Sr: keys to parental magmas and processes in the Bushveld Complex, South Africa.* Lithos 95: 381-398

Cawthorn, R.G. & Ashwal, L.D. (2009) *Origin of anorthosite and magnetitite layers in the Bushveld Complex constrained by major element compositions of plagioclase.* Journal of Petrology 50: 1607-1637

Cawthorn, R.G., Barton, J.M., Viljoen, M.J. (1985) *Interaction of floor rocks with the Platreef on Overysel, Potgietersrus, Northern Transvaal.* Economic Geology 80: 988-1006

Cawthorn, R.G. & Davies, G. (1983) *Experimental data at 3 Kbars pressure on parental magma to the Bushveld Complex.* Contributions to Mineralogy and Petrology 83: 128-135

Cawthorn, R.G. & Spies, L. (2003) *Plagioclase content of cyclic units in the Bushveld Complex, South Africa.* Contributions to Mineralogy and Petrology 145: 47-60

Cawthorn, R.G. & Walraven, F (1998) *Emplacement and crystallization time for the Bushveld Complex.* Journal of Petrology 39: 1669-1687

Charlier, B.L.A., Ginibre, C., Morgan, D., Nowell, G.M., Pearson, D.G., Davidson, J.P., Ottley, C.J. (2006) *Methods for the microsampling and high-precision analysis of strontium and rubidium isotopes at single crystal scale for petrological and geochronological applications.* Chemical Geology 232: 114-133

Charlier, B., Vander Auwera, J., Duchesne, J-C. (2005) *Geochemistry of cumulates from the Bjerkreim-Sokndal layered intrusion (S. Norway) Part II. REE and the trapped liquid fraction.* Lithos 83: 255-276

Czamanske, G.K. & Bohlen, S.R. (1990) *The Stillwater Complex and its anorthosites: An accident of magmatic underplating?* American Mineralogist 75: 37-45

Davies, G. & Cawthorn, R.G. (1984) *Mineralogical data on a multiple intrusion in the Rustenburg Layered Suite of the Bushveld Complex.* Mineralogical Magazine 48: 469-480

Deer, W.A., Howie, R.A., Zussman, J. (1980) *An introduction to the rock-forming minerals.* Longman Group Limited, London, 528p

De Waal, S.A., Xu, Z., Li, C., Mouri, H. (2004) *Emplacement of viscous mushes in the Jinchuan ultramafic intrusion, western China.* The Canadian Mineralogist 42: 371-392

Dorland, H.C., Beukes, N.J., Gutzmer, J., Evans, D.A.D., Armstrong, R.A. (2006) *Precise SHRIMP U-Pb zircon age constraints on the lower Waterberg and Soutpansberg Groups, South Africa.* South African Journal of Geology 109: 139-156

Eales, H.V. (2002) *Caveats in defining the magmas parental to the mafic rocks of the Bushveld Complex, and the manner of their emplacement: review and commentary.* Mineralogical Magazine 66(6):815-832

Eales, H.V. & Cawthorn, R.G. (1996) *The Bushveld Complex,* in Layered Intrusions (Cawthorn, R.G., ed.) Developments in Petrology 15. Elsevier, Amsterdam, 181-230

Eales, H.V., De Klerk, W.J., Butcher, A.R., Kruger, F.J. (1990) *The cyclic unit beneath the UG1 chromitite (UG1FW unit) at RPM Union Section Platinum Mine – Rosetta Stone of the Bushveld Upper Critical Zone.* Mineralogical Magazine 54: 23-43

Ewart, A., Bryan, W.B., Gill, J.B. (1973) *Mineralogy and geochemistry of the younger volcanic islands of Tonga.* Journal of Petrology 14: 429-465

Frey, F.A., Green, D.H., Roy, S.D. (1978) *Integrated models of basalt petrogenesis: a study of quartz tholeiites to olivine melilites from South Eastern Australia utilizing geochemical and experimental petrological data.* Journal of Petrology 19: 463-513

Ghiorso, M.S., Hirschmann, M.M., Reiners, P.W., Kress, V.C. (2002) *The pMELTS: An revision of MELTS aimed at improving calculation of phase relations and major element partitioning involved in partial melting of the mantle at pressures up to 3 GPa.* Geochemistry, Geophysics, Geosystems 3: 5

Ghiorso, M.S. & Sack, R.O. (1995) *Chemical mass transfer in magmatic processes. IV. A revised and internally consistent thermodynamic model for the interpolation and extrapolation of liquid-solid equilibria in magmatic systems at elevated temperatures and pressures.* Contributions to Mineralogy and Petrology 119: 197-212.

Hall, A.L. (1932) *The Bushveld Igneous Complex of the central Transvaal*. Geological Survey Memoir 28. Government Printer, Pretoria, 530p

Harmer, R.E. & Sharpe, M.R. (1985) *Field relations and strontium isotope systematics of the marginal rocks of the Eastern Bushveld Complex.* Economic Geology 80:813-837

Harris, C., Pronost, J.J.M., Ashwal, L.D., Cawthorn, R.G. (2005) *Oxygen and hydrogen isotope stratigraphy of the Rustenburg Layered Suite, Bushveld Complex: Constraints on crustal contamination*. Journal of Petrology 46: 579-601

Hart, R.J., Andreoli, M.A.G., Tredoux, M., De Wit, M.J. (1990) *Geochemistry across an exposed section of the Archaean crust at Vredefort, South Africa: with implications for mid-crustal discontinuities.* Chemical Geology 82: 21-50

Hart, R.J., Welke, H.J., Nicolaysen, L.O. (1981) *Geochronology of the deep profile through Archean basement at Vredefort, with implications for early crustal evolution.* Journal of Geophysical Research 86: B10663-10680

Hart, S.R. & Dunn, T. (1993) *Experimental cpx/melt partitioning of 24 trace elements*. Contributions to Mineralogy and Petrology 113: 1-8

Hatch, F.H. & Corstorphine, G.S. (1905) *The geology of South Africa.* 2nd edition., MacMillan and Co., London, 394p

Hofmann, A.W. (1988) *Chemical differentiation of the Earth: the relationship between mantle, continental crust and oceanic crust.* Earth and Planetary Science Letters 90: 297-314

Holwell, D.A., Armitage, P.E.B., McDonald, I. (2005) *Observations on the relationship between the Platreef and its hanging wall.* Applied Earth Science (Transactions of the Institute of Mining and Metallurgy B) 114:199-207

Holwell, D.A. & McDonald, I. (2006) *Petrology, geochemistry and the mechanisms determining the distribution of platinum-group element and base metal sulphide mineralisation in the Platreef at Overysel, northern Bushveld Complex, South Africa.* Mineralium Deposita 41:575-598

Holwell, D.A. & Jordaan, A. (2006) *Three-dimensional mapping of the Platreef at the Zwartfontein South mine : implications for the timing of magmatic events in the northern limb of the Bushveld Complex, South Africa.* Applied Earth Science (Transactions of the Institute of Mining and Metallurgy B) 115:41-48

Hulbert, L.J. (1983) *A petrographical investigation of the Rustenburg Layered Suite and associated mineralisation south of Potgietersrus.* Unpublished D.Sc Thesis, University of Pretoria, Pretoria

Irvine, T.N. (1970) *Crystallization sequences in the Muskox intrusion and other layered intrusions.* Geological Society of South Africa Special Publication 1: 441-476

Jahn, B. & Condie, K.C. (1995) *Evolution of the Kaapvaal craton as viewed from geochemical and Sm-Nd isotopic analyses of intracratonic pelites.* Geochimica et Cosmochimica Acta 59: 2239-2258

Jarosewich, E., Nelen, J.A., Norberg, J.A. (1980) *Reference standards for electron microprobe analysis.* Geostandards Newsletter 4(1):43-47

Keleman, P.B. & Dunn, J.T. (1992) *Depletion of Nb relative to other highly incompatible elements by melt/rock reaction in the upper mantle.* EOS, Transactions of the American Geophysical Union 73: 656-657

Kinnaird, J.A. (2004) *An overview of the Platreef.* Geoscience Africa 2004, Abstract Volume, University of the Witwatersrand, Johannesburg, South Africa: 345-346

Kinnaird, J.A., Hutchinson, D., Schurmann, L., Nex, P.A.M., De Lange, R. (2005) *Petrology and mineralisation of the southern Platreef : northern limb of the Bushveld Complex, South Africa.* Mineralium Deposita 40: 576-597

Kress, V.C. & Carmichael, I.S.E. (1991) *The compressibility of silicate liquids containing Fe_2O_3 and the effect of composition, temperature, oxygen fugacity and pressure on their redox states.* Contributions to Mineralogy and Petrology 108: 82-92

Kruger, F.J. (1990) *The stratigraphy of the Bushveld Complex: a reappraisal and the relocation of the Main Zone Boundaries.* South African Journal of Geology 93(2):376-381

Kruger, F.J. (1994) *The Sr-isotopic stratigraphy of the western Bushveld Complex.* South African Journal of Geology 97(4):393-398

Kruger, F.J. (2005) *Filling the Bushveld Complex magma chamber: lateral expansion, roof and floor interaction , magmatic unconformities, and the formation of giant chromitite, PGE and Ti-V-magnetitite deposits.* Mineralium Deposita 40: 451-472

Kruger, F.J., Cawthorn, R.G., Walsh, K.L. (1987) *Strontium isotopic evidence against magma addition in the Upper Zone of the Bushveld Complex*. Earth and Planetary Science Letters 84(1):51-58

Kruger, F.J. & Marsh, J.S. (1982) *Significance of $^{87}Sr/^{86}Sr$ ratios in the Merensky cyclic unit of the Bushveld Complex.* Nature 298: 53-55

Kushiro, I. & Fujii, T. (1977) *Floatation of plagioclase in magma at high pressures and its bearing on the origin of anorthosite.* Proceedings of the Japanese Academy 53B: 262-266

Le Maitre, R.W. (ed.) (1989) *A classification of igneous rocks and glossary of terms.* Blackwell Scientific Publications, Oxford, 193p

Lundgaard, K.L. & Tegner, C. (2004) *Partitioning of ferric and ferrous iron between plagioclase and silicate melt.* Contributions to Mineralogy and Petrology 147: 470-483

Maes, S.M., Ferré, E.C., Tikoff, B., Brown, P.E., Marsh, J.S. (2008) *Rock magnetic stratigraphy of a layered mafic sill: A key to the Karoo volcanics plumbing system.* Journal of Volcanology and Geothermal Research 172: 75-92

Maier, W.D., Arndt, N.T., Curl, E.A. (2000) *Progressive crustal contamination of the Bushveld Complex: evidence from Nd isotopic analyses of the cumulate rocks.* Contributions to Mineralogy and Petrology 140:316-327

Maier, W.D. & Barnes, S-J. (1998) *Concentrations of rare earth elements in silicate rocks of the Lower, Critical and Main zones of the Bushveld Complex*. Chemical Geology 150: 85-103

Maier, W.D., Barnes, S-J., Van der Merwe, M.J. (2001) *Platinum-group elements in the Pyroxenite Marker, Bushveld Complex: implications for the formation of the Main Zone.* South African Journal of Geology 104: 301-308

Manyeruke, T.D. (2007) *Compositional and lithological variation of the Platreef on the farm Nonnenwerth, northern lobe of the Bushveld Complex: Implications for the origin of Platinum-group elements (PGE) mineralization.* Unpublished Ph.D Thesis, University of Pretoria, Pretoria, 248p

Manyeruke, T.D., Maier, W.D., Barnes, S-J. (2005) *Major and trace element geochemistry of the Platreef on the farm Townlands, northern Bushveld Complex.* South African Journal of Geology 108:381-396

Markgraaf, J. (1973) *Die piroksene van die westelike Bosveldkompleks.* Unpublished M.Sc Dissertation, Potchefstroom University of Christian Higher Education, Potchefstroom, 125p

McBirney, A.R. & Creaser, R.A. (2003) *The Skaergaard Layered series, Part VII: Sr and Nd isotopes.* Journal of Petrology 44: 757-771

McDonald, I. & Holwell, D.A. (2007) *Did Lower Zone magma conduits store PGE-rich sulphides that were later supplied to the Platreef?* South African Journal of Geology 110: 611-616

McDonald, I., Holwell, D.A., Armitage, P.E.B. (2005) *Geochemistry and mineralogy of the Platreef and "Critical Zone" of the northern lobe of the Bushveld Complex, South Africa: implications for Bushveld stratigraphy and the development of PGE mineralization.* Mineralium Deposita 40: 526-549

McDonald, I., Holwell, D.A., Wesley, B. (2009) *Assessing the potential involvement of an early magma staging chamber in the generation of the Platreef Ni-Cu-PGE deposit in the northern limb of the Bushveld Complex: a pilot study of the Lower Zone Complex at Zwartfontein.* Applied Earth Science: IMM Transactions B 118: 5-20

McDonough, W.F. (1990) *Constraints on the composition of the continental lithospheric mantle.* Earth and Planetary Science Letters 101: 1-18

McKenzie, D. & O'Nions, R.K. (1991) *Partial melt distributions from inversion of rare earth element concentrations.* Journal of Petrology 32: 1021-1091

Mitchell, A.A. (1986) *The petrology, mineralogy and geochemistry of the Main Zone of the Bushveld Complex at Rustenburg Platinum Mines, Union Section.* Unpublished Ph.D Thesis, Rhodes University, Grahamstown, 122p

Mitchell, A.A. (1990) *The stratigraphy, petrography and mineralogy of the Main Zone of the northwestern Bushveld Complex.* South African Journal of Geology 93(5/6):818-831

Molyneux, T.G. (1970) *A geological investigation of the Bushveld Complex in Sekhukuneland and part of the Steelpoort Valley, Eastern Transvaal, with particular reference to the oxide minerals.* Unpublished D.Sc Thesis, University of Pretoria, Pretoria, 123p

Molyneux, T.G. (1974) *A geological investigation of the Bushveld Complex in Sekhukhuneland and part of the Steelpoort Valley.* Transactions of the Geological Society of South Africa 77:329-338

Mysen, B. (1978) *Experimental determination of nickel partition coefficients between liquid, pargasite and garnet peridotite minerals and concentration limits of behaviour according to Henry's Law at high pressure and temperature.* American Journal of Science 278: 217-243

Nash, W.P. & Crecraft, H.R. (1985) *Partition coefficients for trace elements in silicic magmas.* Geochimica et Cosmochimica Acta 49: 2309-2322

Nex, P.A.M., Cawthorn, R.G., Kinnaird, J.A. (2002) *Geochemical effects of magma addition: compositional reversals and decoupling of trends in the Main Zone of the western Bushveld Complex.* Mineralogical Magazine 66: 833-856

Paster, T.P., Schauwecker, D.S., Haskin, L.A. (1974) *The behavior of some trace elements during solidification of the Skaergaard layered series.* Geochimica et Cosmochimica Acta 38: 1549-1577

Patino Douce, A.E. & Beard, J.S. (1995) *Dehydration-melting of biotite gneiss and quartz amphibolite from 3 to 15 kbar.* Journal of Petrology 36: 707-738

Pederson, A.K. (1979) *Basaltic glass with high-temperature equilibrated immiscible sulfide bodies with native iron from Disko, Central West Greenland.* Contributions to Mineralogy and Petrology 69: 397-407

Phinney, W.C. (1992) *Partition coefficients for iron between plagioclase and basalt as a function of oxygen fugacity: Implications for Archean and lunar anorthosites.* Geochimica et Cosmochimica Acta 56: 1885-1895

Poldervaart, A. & Hess, H.H. (1951) *Pyroxenes in the crystallization of basaltic magma.* Journal of Geology 59:472-489

Poldervaart, A. & Parker, A.B. (1964) *The crystallization index as a parameter of igneous differentiation in binary variation diagrams.* American Journal of Science 262: 281-289

Pots, P.J., Tindle, A.G., Webb, P.C. (1992) *Geochemical reference material compositions.* Whittles Publishing, Caithness, 313p

Prevec, S.A., Ashwal, L.D., Mkaza, M.S. (2005) *Mineral disequilibrium in the Merensky Reef, western Bushveld Complex, South Africa : new Sm-Nd isotopic evidence.* Contributions to Mineralogy and Petrology 149:306-315

Pronost, J., Harris, C., Pin, C. (2008) *Relationship between footwall composition, crustal contamination, and fluid-rock interaction in the Platreef, Bushveld Complex, South Africa.* Mineralium Deposita 43(8):825-848

Roelofse, F. & Ashwal, L.D. (2008) *Symplectitic augite from the Platreef: textural evidence for fluid/rock interaction in the Northern Sector of the Northern Limb of the Bushveld Complex?* South African Journal of Geology 111: 21-26

Roelofse, F., Ashwal, L.D., Pineda-Vargas, C.A., Przybylowicz, W.J. (2009) *Enigmatic textures developed along plagioclase-augite grain boundaries at the base of the Main Zone, Northern Limb, Bushveld Complex – evidence for late stage melt infiltration into a nearly solidified crystal mush.* South African Journal of Geology 112: 39-46

Seabrook, C.L., Cawthorn, R.G., Kruger, F.J. (2005) *The Merensky Reef, Bushveld Complex: mixing of minerals not mixing of magmas.* Economic Geology 100: 1191-1206

Sharman-Harris, E.R. & Kinnaird, J.A. (2004) *Into the new millennium: Sulphur isotope studies of the Southern Platreef, Northern Limb, Bushveld Igneous Complex.* Geoscience Africa 2004. Abstract Volume, University of the Witwatersrand, Johannesburg, South Africa: 589-590

Sharman-Harris, E.R., Kinnaird, J.A., Harris, C., Horstmann, U.E. (2005) *A new look at sulphide mineralization of the northern limb, Bushveld Complex: a stable isotope study.* Applied Earth Science: IMM Transactions B 114: 252-263

Sharpe, M.R. (1985) *Strontium isotope evidence for preserved density stratification in the Main Zone of the Bushveld Complex, South Africa.* Nature 316:119-126

Shaw, D.M. (1970) *Trace element fractionation during anatexis.* Geochimica et Cosmochimica Acta 34: 237-243

South African Committee for Stratigraphy (SACS) (1980) *Stratigraphy of South Africa Part 1: Lithostratigraphy of the Republic of South Africa, South West Africa / Namibia and the Republics of Bophutatswana, Transkei and Venda.* (Kent, L.E., Compiler) Handbook of the Geological Survey of South Africa 8. Government Printer, Pretoria.

Steiger, R.H. & Jager, E. (1977) *Subcommission on geochronology: Convention on the use of decay constants in geo- and cosmochronology.*Earth and Planetary Science Letters 36: 359-362.

Tanaka, T., Togashi, S., Kamioka, H., Amakawa, H., Kagami, H., Hamamoto, T., Yuhara, M., Orihashi, Y., Yoneda, S., Shimizu, H., Kunimaru, T., Takahashi, K., Yanagi, T., Nakano, T., Fujimaki, H., Shinjo, R., Asahara, Y., Tanimizu, M., Dragusanu, C. (2000) *JNdi-1: a neodymium isotopic reference in consistency with LaJolla neodymium.* Chemical Geology 168: 279-281.

Tegner, C. & Cawthorn, R.G. (in press) *Iron in plagioclase in the Bushveld Complex and the Skaergaard intrusion: implications for iron contents in evolving basic magmas.* Contributions to Mineralogy and Petrology

Tepley, FJ. & Davidson, J.P. (2003) *Mineral-scale Sr-isotope constraints on magma evolution and chamber dynamics in the Rum layered intrusion, Scotland.* Contributions to Mineralogy and Petrology 145: 628-641

Thornton, C.P. & Tuttle, O.F. (1960) *Chemistry of igneous rocks, I. Differentiation index.* American Journal of Science 258: 664-684.

Van der Merwe, M.J. (1976) *The layered sequence of the Potgietersrus Limb of the Bushveld Complex*. Economic Geology 71:1337-1351

Van der Merwe, M.J. (1978) *The geology of the basic and ultramafic rocks of the Potgietersrus Limb of the Bushveld Complex.* Unpublished Ph.D Thesis, University of the Witwatersrand, Johannesburg, 176p

Van der Merwe, M.J. (1979) *An olivine bearing unit in the Main Zone of the Bushveld Complex, Potgietersrus.* Geological Survey Report 1979-0002, Pretoria, 3p

Von Gruenewaldt, G. (1971) *A petrographical and mineralogical investigation of the rocks of the Bushveld Igneous Complex in the Tauteshoogte-Roossenekal area of the Eastern Transvaal.* Unpublished D.Sc Thesis, University of Pretoria, Pretoria, 228p

Von Gruenewaldt, G., Hulbert, L.J., Naldrett, A.J. (1989) *Contrasting platinum-group concentration patterns in cumulates of the Bushveld Complex*. Mineralium Deposita 24: 219-229

Wager, L.R. & Brown, G.M. (1968) *Layered igneous rocks*. Oliver and Boyd Ltd., Edinburgh, 588p

Wagner, P.A. (1973) *Platinum deposits & mines of South Africa* (2nd impression). C. Struik (Pty) Ltd., Cape Town, 338p.

Waight, T., Baker, J., Peate, D.W. (2002) *Sr isotope ratio measurements by double-focusing MC-ICPMS: techniques, observations and pitfalls.* International Journal of Mass Spectrometry 221: 229-244

Webb, P.C., Thompson, M., Potts, P.J., Batjargal, B. (2006) *GEOPT19 – An international proficiency test for analytical geochemistry laboratories – Report on round 19 / July 2006 (Gabbro, MGR-N).* International Association of Geoanalysts, unpublished report

White, J.A. (1994) *The Potgietersrus prospect- Geology and exploration history.* XVth CMMI Congress, Johannesburg, SAIMM Volume 3:173-181

Willemse, J. (1964) *A brief outline of the geology of the Bushveld Igneous Complex* in The Geology of some ore deposits of Southern Africa 2. Geological Society of South Africa: 91-128

Willemse, J. (1969) *The geology of the Bushveld Igneous Complex, the largest repository of magmatic ore deposits in the world.* Economic Geology Monographs 4: 1-22